In presenting the dissertation as a partial fulfillment of the requirements for an advanced degree from the Georgia Institute of Technology, I agree that the Library of the Institute shall make it available for inspection and circulation in accordance with its regulations governing materials of this type. I agree that permission to copy from, or to publish from, this dissertation may be granted by the professor under whose direction it was written, or, in his absence, by the Dean of the Graduate Division when such copying or publication is solely for scholarly purposes and does not involve potential financial gain. It is understood that any copying from, or publication of, this dissertation which involves potential financial gain will not be allowed without written permission.

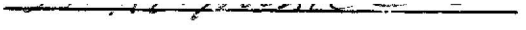

3/17/65
b

THE BEHAVIOR OF SAND UNDER PLANE STRAIN CONDITIONS

A THESIS

Presented to

The Faculty of the Graduate Division

by

Mosaid M. Al-Hussaini

In Partial Fulfillment

of the Requirements for the Degree

Doctor of Philosophy in the School of Civil Engineering

Georgia Institute of Technology

August, 1967

THE BEHAVIOR OF SAND UNDER PLANE STRAIN CONDITIONS

Approved:

Chairman

Date approved by Chairman: 15 April 1968

ACKNOWLEDGMENTS

The author wishes to express his sincere appreciation to all who assisted with the development of this thesis. Dr. N. H. Wade, his thesis advisor, deserves special thanks for his guidance, encouragement, and advice during the execution of this work. Gratitude is extended to Regents Professor G. F. Sowers and Dr. B. B. Mazanti, members of the reading committee, for their helpful comments on the text.

The author wishes to acknowledge the financial assistance provided by the National Science Foundation and the School of Civil Engineering during this study.

TABLE OF CONTENTS

TABLE OF CONTENTS (Continued)

LIST OF TABLES

LIST OF ILLUSTRATIONS

LIST OF ILLUSTRATIONS (Continued)

LIST OF ILLUSTRATIONS (Continued)

LIST OF ILLUSTRATIONS (Continued)

GLOSSARY OF SYMBOLS

Symbol	Definition
$\sigma_1\ \sigma_2\ \sigma_3$	Principal stresses
$\sigma'_1\ \sigma'_2\ \sigma'_3$	Principal effective stresses
σ_{oct}	Octahedral normal stress $\left[\frac{1}{3}(\sigma'_1 + \sigma'_2 + \sigma'_3)\right]$
τ_{oct}	Octahedral shearing stress $\left[\frac{1}{3}\sqrt{(\sigma_1 - \sigma_2)^2 + (\sigma_2 - \sigma_3)^2 + (\sigma_3 - \sigma_1)^2}\right]$
$\epsilon_1\ \epsilon_2\ \epsilon_3$	Principal unit strains
V_o	Initial volume of the specimens
V_c	Volume of the specimen at the end of consolidation
$\frac{\Delta V}{V_c}$	Volumetric strain
E	Young modulus of elasticity
E_c	Modulus of deformation
E_i	Initial tangent modulus
ν	Poisson's ratio
K_a	Coefficient of active earth pressure
K_p	Coefficient of passive earth pressure
K_o	Coefficient of earth pressure at rest
G_s	Specific gravity of the soil
e_o	Initial void ratio

Symbol	Definition
e_c	Void ratio at the end of consolidation
D_r	Relative density
w	Deflection of a point on the surface
R	Radius of circular footing
q	Unit pressure on a footing
ϕ	Mohr friction angle in terms of effective stresses

SUMMARY

In the majority of practical problems such as dams, retaining walls, and embankments, the shearing deformations can be approximated by plane strain. Because the results of soil tested in plane strain are different from that in triaxial, the strength measurement and stability analysis should be based on test data obtained under plane strain conditions.

With the advant of new technology in hydroelectric power and the demand to store or regulate large quantities of water, a need has arisen to build water retaining structures such as earth and rockfill dams of greater height than the previous ones. The magnitude of the stresses within a dam are largely influenced by its height. Some of the existing dams exceed a height of 500 feet and the soils within such a dam are subjected to a confining stress of 250 psi or more.

The available data on high pressure testing of soils are limited to the conventional triaxial apparatus and the direct shear apparatus. As far as is known, the published data on the behavior of sand under plane strain conditions (10,12) are limited to a confining pressure of 40 psi, which is far below the confining pressure which can be expected in large dams. The study of plane strain deformation of soil under confining pressures greater than previously investigated is important since earth and rockfill dams are continuously being constructed with greater height as knowledge is gained in their construction and performance.

The purpose of this research was to investigate the behavior of sand

under plane strain conditions with a confining pressure similar to that expected in high dams and with different relative densities. To fulfill this objective a special plane strain apparatus was constructed to test sand by applying three independent principal stresses. The apparatus was designed to allow the specimens to be consolidated under conditions of zero lateral strain. Three series of tests were conducted on sand, each series corresponding to a certain consolidation pressure. The consolidation pressures used were 70 psi, 110 psi, and 285 psi.

In the first two series the specimens were subjected to either isotropic or K_o consolidation. In the third series the specimens were consolidated under isotropic conditions only.

The bulk of the specimens were sheared under drained conditions, but a few specimens confined at 70 psi were sheared under consolidated undrained conditions. The nominal size of the plane strain specimens was 2" x 4" x 16". Three other series of tests with the same range of consolidation pressure were conducted in the standard triaxial apparatus on samples with different relative densities under the same consolidation stress conditions. The value of K_o was found to vary linearly with the relative density, becoming lower at the higher densities, and was not affected by the magnitude of the consolidation pressure or the shape of the specimens tested. The modulus of deformation of sand during isotropic compression was found to be intermediate between the initial tangent modulus of sand tested under conditions of axial symmetry and those tested under plane strain conditions. It was also found that both the modulus of deformation during isotropic compression varies linearly with the relative density of sand and exponentially with respect to the octahedral normal stress.

The relationships between the modulus of deformation and the confining pressure found in this test program are similar to those found by Sowers (28) for different types of sand, in that both suggest that the modulus of deformation increases exponentially with respect to the confining pressure.

During the shear stage of the plane strain test the variation of the intermediate principal effective stress with respect to axial strain is similar to, but less than the variation of the major principal effective stress. It was also found that the ratios $\frac{\sigma_2'}{\sigma_1'}$ and $\frac{\sigma_2'}{\sigma_1' + \sigma_3'}$ at failure were affected by initial relative density but not significantly by the consolidation pressure used. The values of $\frac{\sigma_2'}{\sigma_1'}$ and $\frac{\sigma_2'}{\sigma_1' + \sigma_3'}$ at failure may approximate the value of K_o and Poisson's ratio, respectively.

It was found in this test program that the axial failure strain of sand tested in the conventional triaxial apparatus is always higher than that in plane strain, which is in agreement with previous tests (10,12) on other types of sands. It was also found in this investigation that the ratio between the axial failure strain in the triaxial tests and that in plane strain tests decreases with increasing confining pressure. For both types of tests the failure strain decreases with the increase of relative density.

The Mohr-Coulomb angle of internal friction, ϕ', for sand in plane strain is higher than that for sand at the same relative density tested under triaxial conditions. The difference between the two angles was found to be as much as $3\frac{1}{2}$ degrees for dense sand and 1 degree for loose sand. This finding is in good agreement with the tests carried out at Imperial College (10,12) on different types of sand and at a consolidation

pressure of 40 psi. As reported herein an increase in the consolidation pressure produces a decrease in the value of ϕ' for dense sand, but does not significantly affect the value of ϕ' for loose sand. It was also found that the method of consolidation for both types of tests has no effect on the angle of internal friction.

The volumetric strain at failure for plane strain specimens is always lower than that of specimens tested in the triaxial apparatus. This suggests that higher pore pressures would be expected for consolidated plane strain tests, a fact that was substantiated by the consolidated undrained test series.

When the experimental data were plotted in principal stress space it was found that the failure points for plane strain tests fell in the region between the Mohr and Tresca failure surfaces.

CHAPTER I

INTRODUCTION

In the latter part of the eighteenth century and the early part of the nineteenth century, French military engineers established empirical equations for calculating earth pressures to be used in the design of earth retaining structures. They also contributed semi-analytical formulas based on somewhat arbitrary assumptions. In 1776 the first recorded scientific approach was introduced to the analysis of soils engineering problems. In that year Coulomb developed his analysis of the sliding wedge theory, formulating the concept of friction and cohesion in both solid bodies and granular material. This concept marked the beginning of a new period. It was characterized by the development of several theories pertaining to earth pressures and equilibrium of earth masses, known later as the classical theories of Soil Mechanics.

Modern soil mechanics started at the beginning of the twentieth century, when such early pioneers as Karl Terzaghi introduced a new approach in dealing with soil as a unique material. They recognized that the behavior of soil under load was influenced by such factors as density, moisture content, previous stress history, etc.

Although man used soil long before any other engineering material, soils did not receive the same attention as other building materials such as steel. The lack of understanding of the behavior of soil under applied load arises from the complex nature of soil. Soils consist of small mineral

grains of different sizes, shapes, and characteristics. The voids between the grains may be filled with either water or gases or both. For the sake of simplicity, it is generally assumed that the three components of soil (i.e., the solids, liquids, and gases) are uniformly distributed in the total mass.

In order to determine exactly the behavior of soil under given stress conditions the physical contributions of each of the components to the resistance of the total stress must be evaluated. However, it is difficult to formulate a general mathematical model to predict the exact behavior of soil under stress. Thus, as a result empirical methods are generally utilized. At the present time most soil engineers use the conventional triaxial cell to obtain the needed physical properties relating to stress, strain, and failure. In the conventional triaxial test the stresses applied to the soil and the resultant strains are characterized by axial symmetry. However, the stresses and strains are compatible with only a few real situations.

Many practical problems in the field of soil mechanics can be approximated by plane strain conditions. These conditions may develop with the soil existing in either the undisturbed state or in the compacted state necessary to the construction. Earth structures such as embankments, dams, retaining walls, etc., belong in this latter category.

Current design methods for plane strain problems commonly utilize the value of soil shearing resistance determined from the conventional triaxial test. This situation leads to the problem of soils in the laboratory being subjected to stress conditions which are quite different from those existing in the field. If, because of such conditions, the shearing re-

sistance of soil as found in the laboratory is lower than that which exists in the field, then the design of the structure based on the laboratory data may lead to unnecessary financial expenditure. In the conventional method of stability and bearing capacity analysis, it is ordinarily assumed that the Mohr failure envelope is a straight line. This assumption implies that the angle of shearing resistance does not vary within the range of the applied stresses. Several studies have been made to determine the effect of elevated pressure on the shearing resistance of soils at failure. These results have indicated (37,38,39) that Mohr failure envelopes are not always straight lines and that their curvature varies with the applied confining pressure. However, no attempt to date has been made to study the effect of pressure greater than 40 psi on the failure characteristics of soils subjected to plane strain deformation, a case which more closely simulates field conditions. The necessity of providing design engineers with information in connection with many practical problems such as the design of earth dams, some of which are planned to exceed a height of 1,000 feet, brings up the question--what is the behavior of soil under the combined conditions of plane strain and high confining pressure?

Thus, it is felt that there is a need to improve the current testing procedure by introducing more realistic testing techniques which more closely approximate field conditions. The purpose of this investigation was to study the influence of high confining pressure on the failure characteristics of sand when tested under plane strain conditions. Such study may bridge the gap between actual soil behavior and the current design procedures based on the conventional triaxial tests.

On the basis of the experience gained in the study of plane strain

deformation, a new plane strain apparatus was designed and built for the purpose of this investigation. Tests were conducted on a sand in this apparatus and the results were compared with similar data obtained from the conventional triaxial equipment. In this comparison the emphasis was on the stress-strain relationships, the effects of the intermediate principal stress, the relative density, and the maximum consolidation pressure on the strength parameters.

The failure strengths obtained from both the triaxial compression and plane strain tests are compared with existing theories of failure.

CHAPTER II

APPARATUS FOR THE MEASUREMENT OF SOIL STRENGTH

Soil is a complex material. Its complexity arises from the fact that it is a three-phase material and no single natural law governs or describes the strength parameters such as the internal friction and cohesion which is associated with each phase. However, reliable determination of soil strength may be obtained when the soil mass is considered as a single phased and homogeneous material.

At the present state of development in soil mechanics, the strength parameters are generally obtained by an experimental approach. In order for the data so collected to be an accurate representation of the soil strength, the experimental technique must meet two basic requirements; first, accuracy and care must be exercised in the sampling and measuring techniques, and secondly, the soil specimen should be tested under conditions similar to those in the field. Refined methods have been developed in sampling as well as in measuring techniques which satisfy the first requirement. In order to fulfill the second requirement, various test equipment has been developed. Apparatus currently in use for obtaining directly the physical properties of soil relating to stresses, strains, and failure may be placed in five groups. These five groups are as follows: the direct shear box, the conventional triaxial apparatus, torsional shear apparatus, vane shear apparatus, and plane strain apparatus. The various types of testing equipment which fall in the first four groups with their application, advantages,

and shortcomings are adequately described by Sowers (1) and will not be discussed.

Plane Strain Apparatus

As indicated previously, in many earth structures the actual deformation under load is essentially two-dimensional or representative of plane strain conditions. Under plane strain conditions, soil elements are subjected to three-dimensional stress and two-dimensional strain conditions, where the strains associated with the third dimension are zero. Many apparatus have been developed to simulate these phenomena. The first successful apparatus in which the three principal stresses and the three principal strains could be varied independently was developed in 1936 by Kjellman (2). The apparatus was built to test 62 mm cubical soil specimens. The specimen was placed inside a rubber membrane and pressure was applied on each side by means of 100 brass rods. Each rod was 6 x 6 x 32 mm with one end resting on the membrane while the other end reacted against a steel plate, as shown in Figure 1. The amount of stress applied on each surface of the soil specimen was calculated from the force applied on the brass rods acting on that surface, while the strain was measured by the amount of movement each steel plate moved from the original position.

The apparatus is not widely used, partly because of the difficulties involved in preparing the soil specimen, and partly because the strains are limited by the small gaps between the brass rods. Large deformation in one direction could occur but side friction would then be introduced when the rods come together.

Among the early plane strain apparatus was the one developed at the

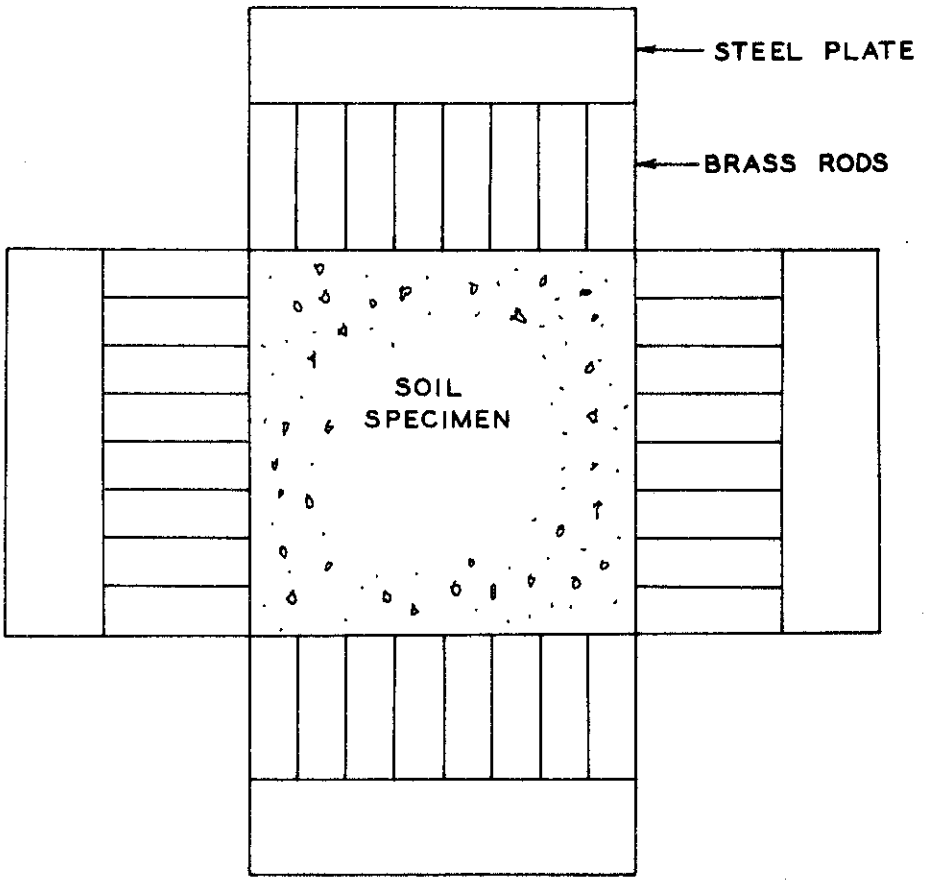

Figure 1. Triaxial Apparatus of Kjellman

Norwegian Geotechnical Institute by Bjerrum (3). This apparatus was used to test rectangular specimens 30 x 12 x 4 cm and 60 x 12 x 4 cm. It consists of an upper platen, lower platen, and a rubber membrane. The lower platen is provided with a filter for drainage purposes. Each specimen was first subjected to an internal vacuum to act as all-round pressure and subsequently was carried to failure by gradually increasing the axial stress.

No attempt was made to measure or to control the intermediate principal stress or the intermediate principal strain. It was simply assumed that the high ratio of length to width would create conditions similar to those of plane strain. This assumption may not be true since the ratio of length to width which creates the plane strain condition is not yet known. The apparatus is only used to test soil under low confining pressure.

At the Danish Geotechnical Institute, Christensen (4) conducted a series of tests on sand to evaluate the coefficient of earth pressure under no lateral deformation. The apparatus used consisted of a wooden box of 1.0 m x 1.0 m in cross-section, and 0.50 m high. The upper half of one side was made to rotate around a horizontal axis parallel to the wall and at a distance from it, as shown in Figure 2. The moveable wall is divided into three parts and only the central part was considered in the measurement simply to eliminate the effect of wall friction. Several electric resistance strain gage type proving rings were placed in the rotating walls to measure the pressure exerted by the sand. The test procedure consisted of filling the box with sand and rotating the wall slowly from the box until the sand failed. Pressure readings were taken during the progress of the test, the highest pressure being at the beginning of the test and the lowest occurring at failure. In this apparatus it is assumed that a plane state of deforma-

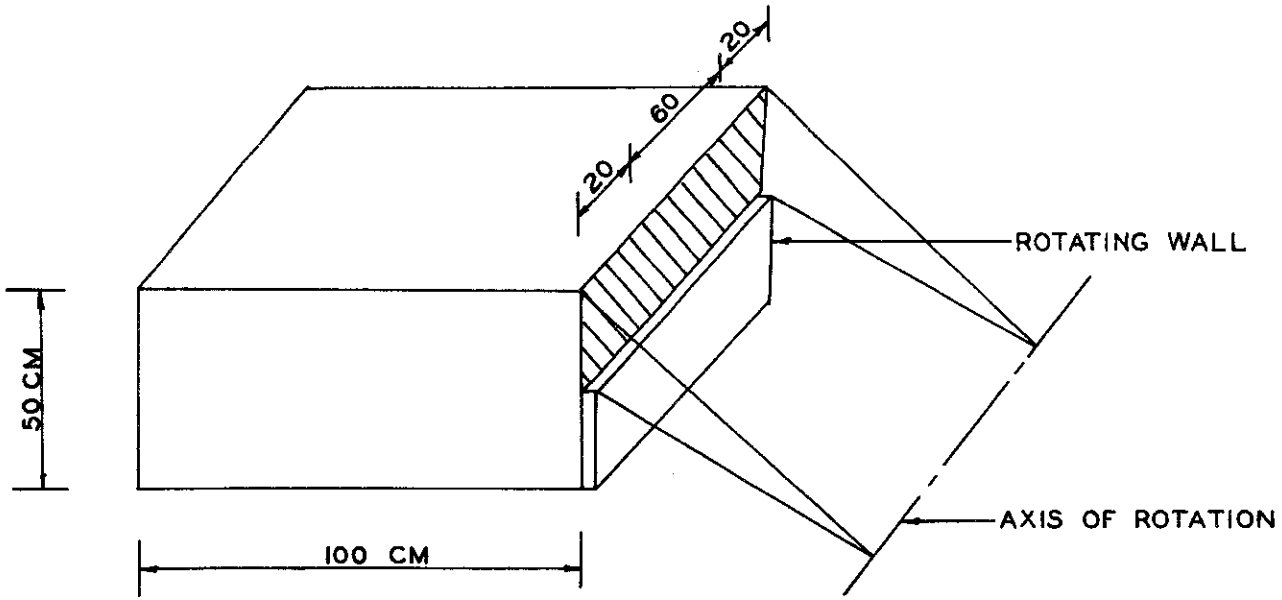

Figure 2. Plane Active Earth Pressure Apparatus of Christensen

tion exists in the sand since deformation in the direction perpendicular to the movement of the sand is prevented. However, the stress distribution in that direction is not known. The stresses and strains throughout the soil mass are not known and are more than likely non-uniform.

Another plane strain apparatus in which the major and minor principal stresses can be varied independently was developed by Whitman (5). The soil specimen consisted of a thick-walled cylinder placed between two rubber membranes and covered with a sealing cap. The whole assembly was contained in a pressure chamber similar to that of the conventional triaxial cell. The sealing cap shown in Figure 3 consists of a special arrangement to hold the outside and inside membrane in place. It is also connected with a central steel rod to prevent axial displacement, thus allowing the sand to fail under no deformation in the axial direction. Since the axial stress in this type of test represents the intermediate principal stress, the sand failed under plane strain conditions. The loading system used in the tests consisted of inside pressure which is called bore pressure, and outside pressure which is represented by the cell pressure. The bore pressure and the surrounding pressure can be varied independently during the test. If the bore pressure is different from the surrounding pressure then each element in the soil specimen will be acted upon by a radial stress, a tangential stress, and an axial stress, which represent the three principal stresses. Although the major and minor principal stresses can be varied independently, the distribution of stresses throughout the specimen is not uniform. In this apparatus the value of the intermediate stress is not known and true plane strain conditions cannot be achieved since the axial deformation in the steel rod is not equal to zero during the test. The deformation in the

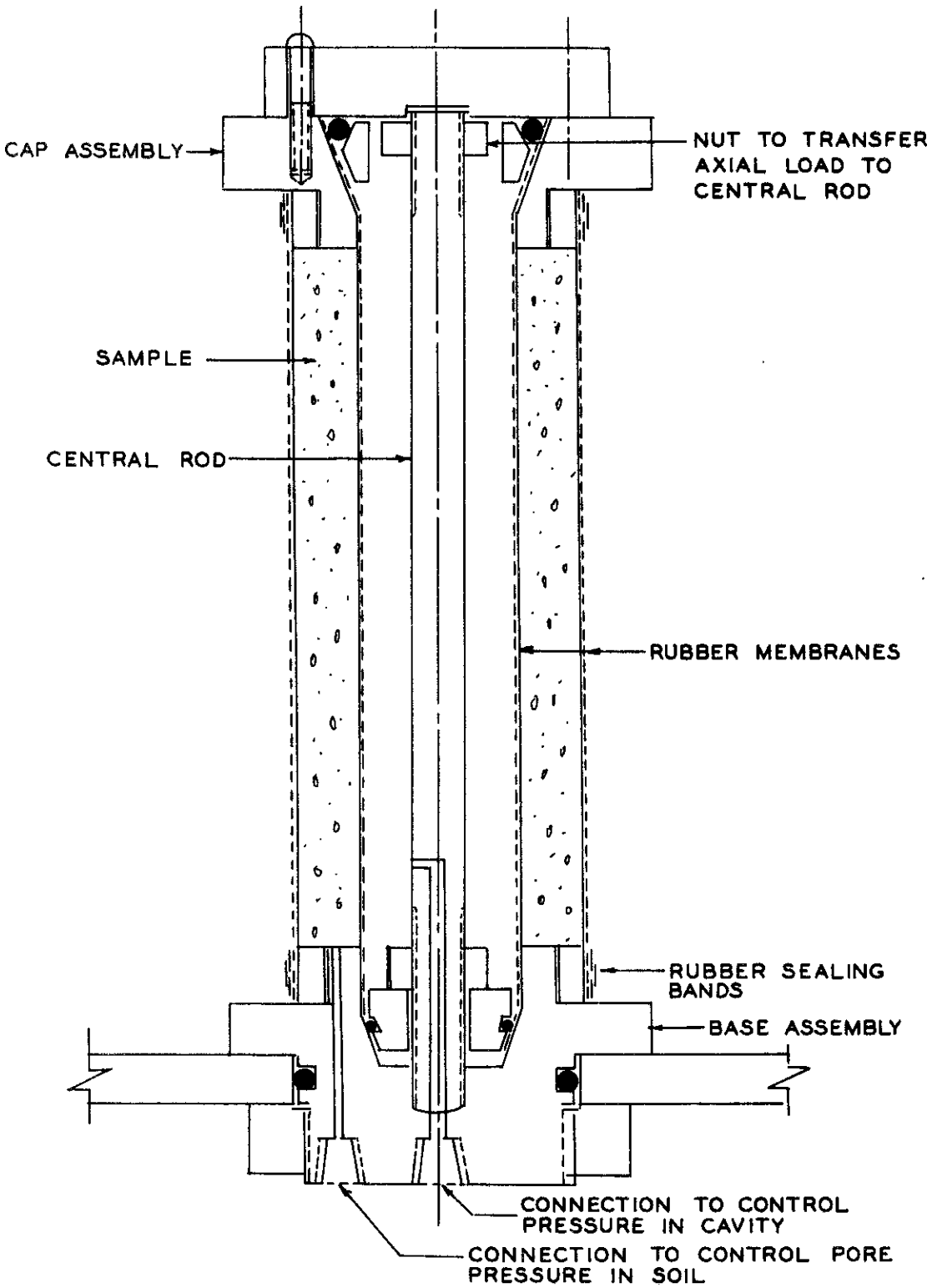

Figure 3. Hollow Cylinder Plane Strain Apparatus

specimen was calculated from the measurement of water expelled from the sand during the test and by filling the inside pore or the outside chamber, respectively, with water and assuming the space which is filled with water exhibits no strain. This procedure may be correct only if the pressure chamber and the connections exhibit no deformation under pressure. It is most probably that the strain distribution throughout the soil mass is not uniform.

A novel method of determining the strain distribution throughout a soil mass deformed under plane strain conditions was developed at the University of Cambridge by Roscoe (6). The testing apparatus consists of two glass plates each 3 feet long, 1 foot high, and 5/8-inch thick. The two plates are placed 6 inches apart and held firmly from the bottom and sides by a steel frame to form a box container. The sand is placed in layers of constant thickness to insure uniform density throughout the specimen. A row of lead shot is placed at a regular interval at the top of each layer and along its center line. The strain throughout the soil is calculated by measuring the displacement of the lead shot which was observed by transmitting x-rays through the sample during the test. The method of calculating the strains is based on change in geometry of whole grid system formed by the lead shot. Several sources of error may effect the results; among them are the relative movement between the lead shot and the surrounding sand, and errors in measuring lead shot displacement. There are also errors due to the scatter of radiation when the x-ray beam strikes the sand grains. This scatter lowers the definition of the lead shot image and consequently introduces errors in the displacement measurements. The apparatus was designed primarily to investigate the strain distribution during shear and no attempt was made to calculate the stress throughout the soil specimen. The method

of calculating strains is very tedious, thus it is limited to research.

H. Leussink (7) designed a plane strain apparatus which was essentially an improved version of the one designed by L. Bjerrum (3). The specimen used for testing was 100 cm long, 20 cm wide, and 60 cm high. The confining pressure was used by applying vacuum to the soil. A steel box filled with water was placed on each end of the specimen. The side of each box in contact with the specimen was made of water-tight vulcanized aluminum. The boxes were provided with pressure gages to measure the intermediate principal stress. Two dial gages were placed in contact with the aluminum plates to detect any deviation from the plane strain condition during the test. Leussink's apparatus is shown in Figure 4. The specimen was brought to failure by increasing the axial load and adjusting the pressure in the steel boxes to prevent any lateral movement in the end plates. The friction between the end plates and the membrane was reduced by using soft soap. The apparatus was designed primarily for testing material consisting of uniform spheres (glass, steel) placed in regular geometrical packing. The amount of confining pressure that can be applied to the testing material is limited to a very small range. No attempt was made to eliminate the end restraint due to the friction between the platens and the testing material.

A large plane strain apparatus was described by Marsal (8), which was used to test compacted rock specimens 0.75 m x 0.75 m in cross-section and 1.80 m high. The apparatus consists of a steel base and two parallel walls. Each wall is made of ten box girders and connected with the other wall by means of twenty hollow bars. The bars are provided with a linear-variable differential transformer to record the intermediate principal stress exerted by the specimen during the progress of the test. The walls

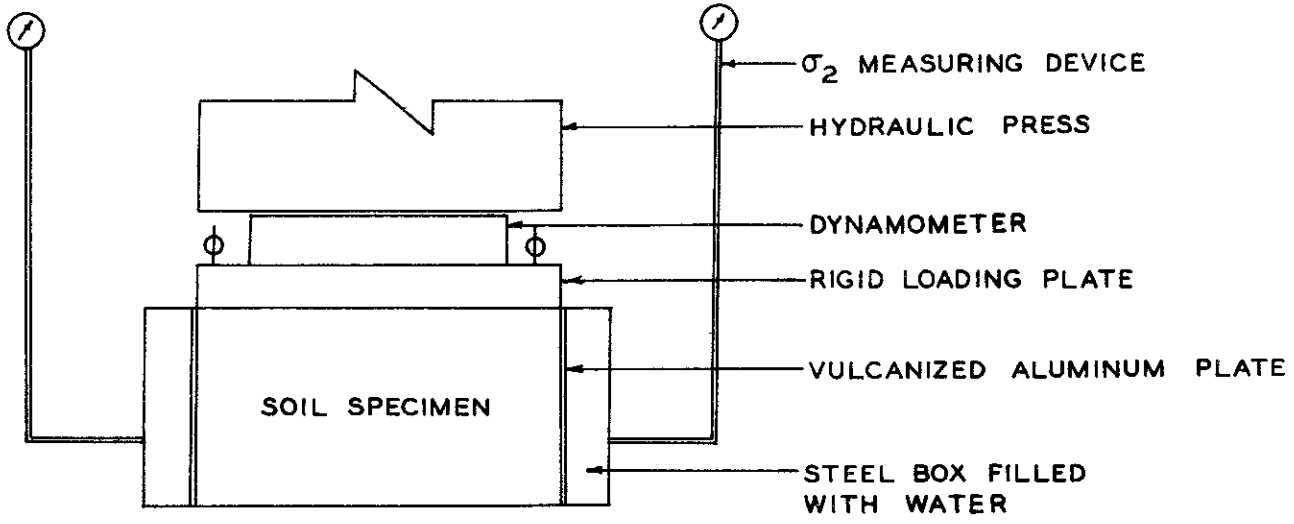

Figure 4. Plane Strain Apparatus of Leussink

are covered with several layers of lubricated polyethylene to reduce friction between the membrane and the walls. The equipment is depicted in Figure 5.

The loading procedure used consists of introducing vacuum to the specimen to provide a positive confining pressure. Then axial load is applied until the specimen fails. The intermediate principal stress is measured by a linear variable differential transformer but no positive control of the intermediate principal strain is reported in the test procedure. Since the vacuum is used to provide confining press, the testing program is limited to a low range of confining pressure. The thick layers of lubricated polyethylene, rubber membrane, and corrugated cardboard which covers the inside walls of the apparatus may deform during the test and, if so, the assumption of plane strain condition is no longer valid.

Another plane strain apparatus was developed at the University of California by Duncan and Seed (9) to test prismatic specimens of clay 1.1 inches wide by 2.78 inches long and 2.78 inches high. The apparatus consists of two lucite plates placed at the ends of the specimen and maintained at a fixed distance by diaphragm boxes, as shown in Figure 6. A water filled rubber diaphragm is placed between the specimen and the diaphragm boxes to apply the lateral pressure to the soil specimen. The specimen was enveloped by a rubber membrane before testing. The ends of the membrane were pressed between stainless steel from the inside and lucite block on the outside to prevent any leakage.

Although the soil specimens were tested under conditions approximating plane strain, the value of the intermediate principal stress was not known. The apparatus was only used to test small specimens under low confining

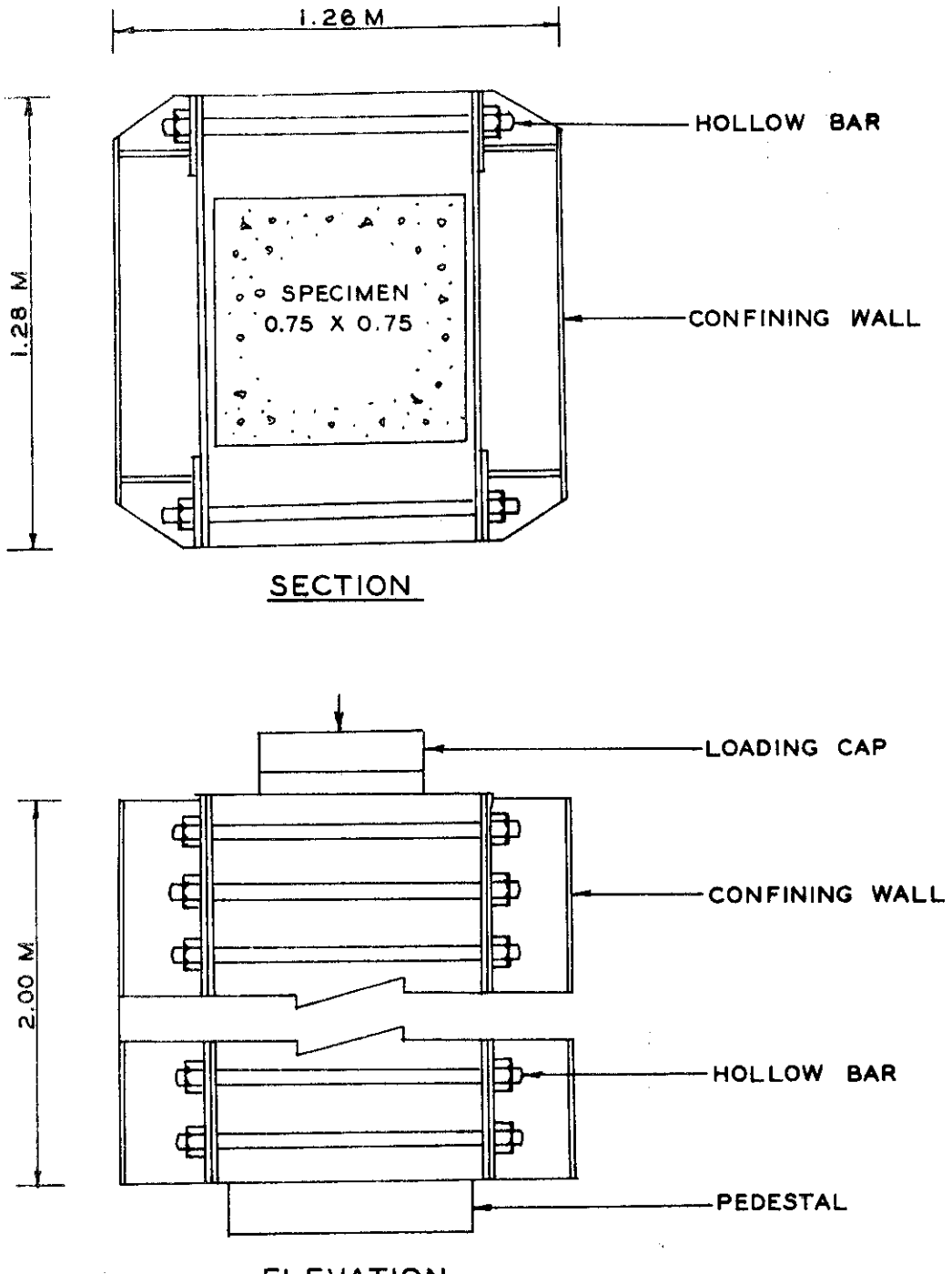

Figure 5. Plane Strain Apparatus of Marsal

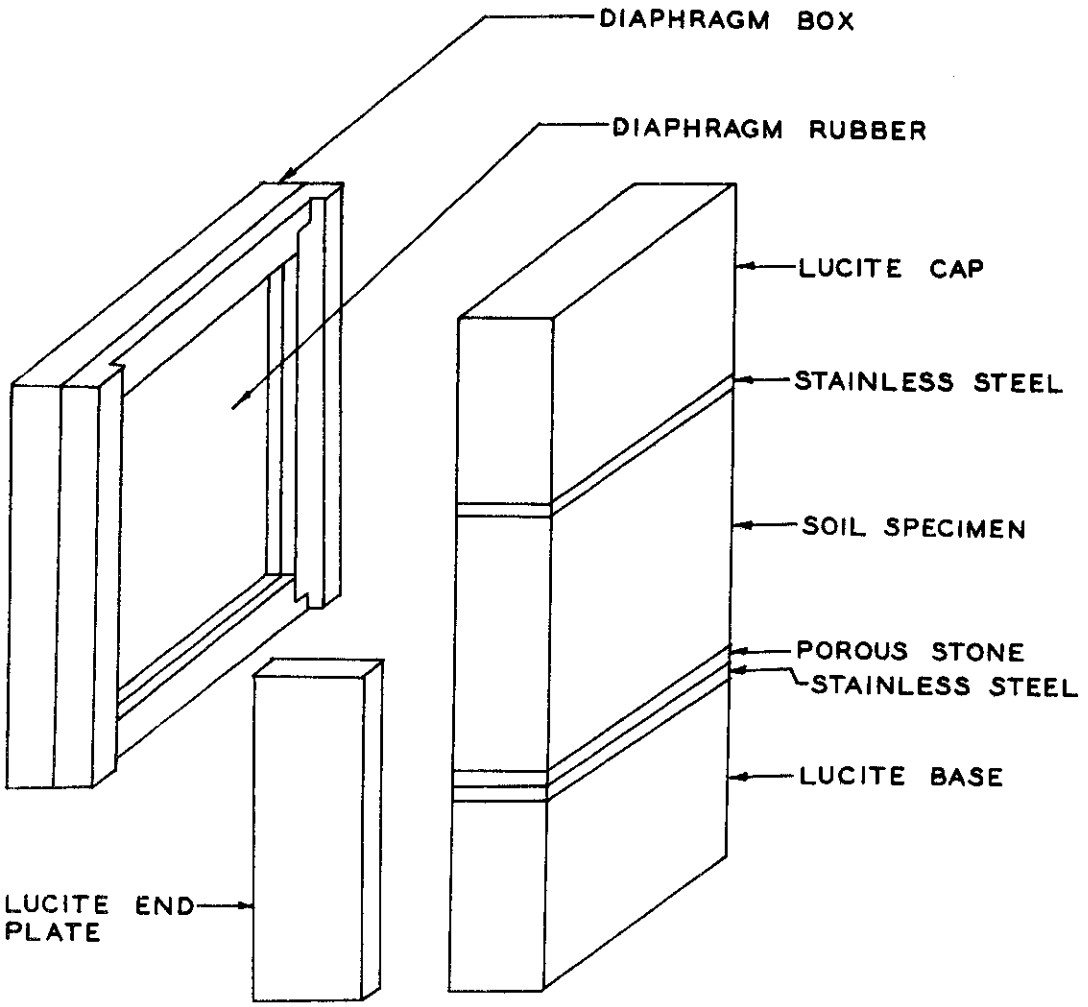

Figure 6. University of California Plane Strain Apparatus

pressure. It was designed mainly to study the effect of the orientation of principal stresses during shear on the strength of clay.

At Imperical College, London, another plane strain device was developed. The apparatus as described by Cornforth (10) consists essentially of a rectangular pressure chamber which contains a soil specimen 4 inches high, 2 inches wide, and 16 inches long. The specimen rests on a stiff brass platen and is covered with brass and a stiff steel loading cap. The specimen is placed between two aluminum plates, one is in contact with the rubber membrane which surrounds the soil, while the other forms a base of a hydraulic pressure cell with a rubber diaphragm. A thin plate is connected to the pressure cell by a locating pin and placed in contact with the end of the specimen. The pressure cell is filled with de-aired water and is connected by a lead to a null indicator similar to that explained by Bishop and Henkel (11) and placed outside the plane strain device. When the test is in progress the intermediate principal stress can be calculated by measuring the water pressure in the pressure cell. The level of mercury in the null indicator detects deviation from the plane strain condition. In order to maintain the plane strain condition, the level of mercury in the null indicator was kept at predetermined heights during the test. This was accomplished by adjusting the pressure in the hydraulic pressure cell continuously until the end of the test.

Cornforth maintained that the system has been calibrated so that appropriate corrections can be made for deformation occurring within the equipment itself. However, he failed to report the creep in the rubber membrane which might affect the results. The apparatus cannot be used to test soil under high confining pressures. No positive control on the dimensions

of the specimen during consolidation stage was used and no attempt has been reported to eliminate the end restraint caused by the friction between the soil and the platens.

A subsequent modification which consisted of a lateral strain sensor was introduced to the apparatus (12). This apparatus was used to detect any departure from the condition of non-lateral deformation. For clay testing a servo-mechanism used to control the K_o consolidation automatically was connected electrically to the lateral strain sensor. The clay specimen takes considerable time to consolidate, therefore a motor and gear train arrangement was added to the system to increase the cell pressure slowly at a constant rate. For more details of the additional equipment used in testing clay specimens, the reader is referred to Wade (12). Figure 7 illustrates the main components of the plane strain apparatus at Imperical College.

Another version of the Imperical College apparatus, but on a smaller scale, was developed at Kyoto University by Shibata and Karube (13). A modified triaxial cell was used to test clay under conditions of no longitudinal deformation. Each specimen was 6 cm long, 2 cm thick, and 3.5 cm high. The arrangement used to apply the intermediate principal stress consists of membrane cushions, aluminum plates, and a set of counterbalanced pulleys. The specimen was enveloped by a rubber membrane and placed between two membrane cushions. The membrane cushions were filled with water and connected to a pressure cell outside the pressure chamber. The membrane cushions were surrounded by two aluminum plates which rested on guide rollers, as shown in Figure 8. The guide rollers were connected to a pulley and a counterbalance. The purpose of the guides and pulleys was to reduce the friction on the sides of the specimen during the test.

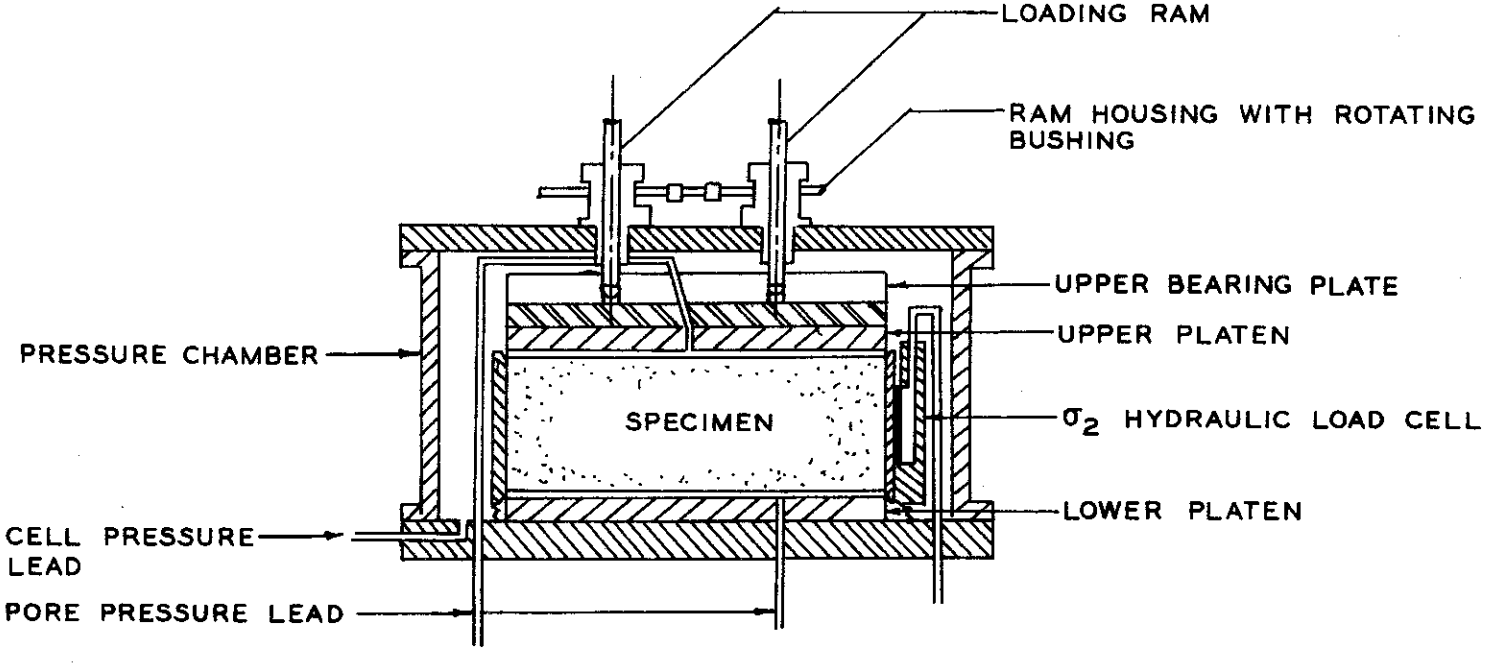

Figure 7. Imperial College Plane Strain Apparatus

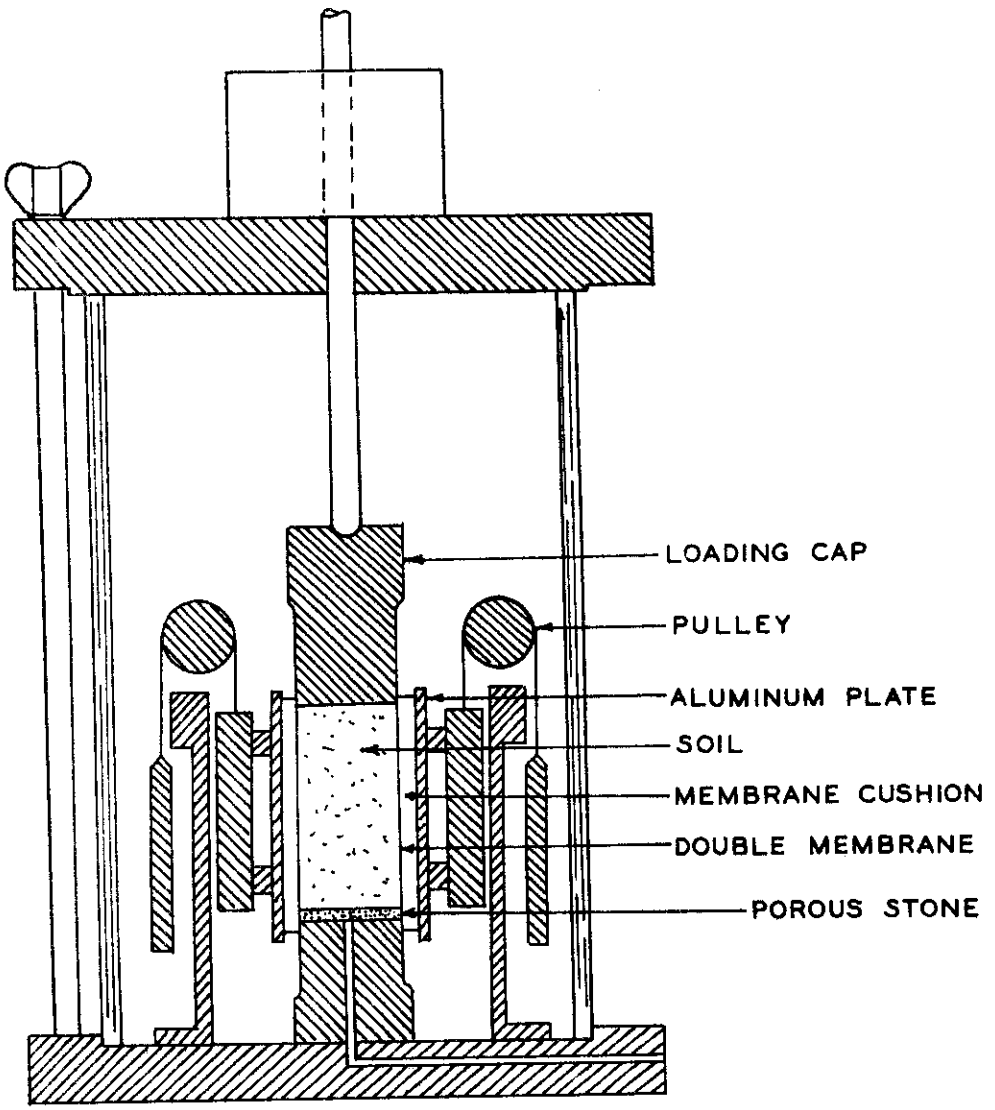

Figure 8. Kyoto University Plane Strain Apparatus

The apparatus was used to study the effect of the intermediate principal stress on the mechanical behavior of clay. No positive control of the intermediate principal strain was reported. The size of the specimen to be tested in this apparatus is relatively small. The confining pressure used in this apparatus is limited to a very small range.

The previous discussion was a brief review of some of the testing devices used to study the shear strength of soil under different systems of loading. Some of these devices were used in routine testing while others were used as research tools. None of the apparatus could be used to test soil by applying three independent principal stresses under a wide range of confining pressures with complete strain control.

CHAPTER III

THE NEW PLANE STRAIN APPARATUS

A special plane strain apparatus was designed at Georgia Institute of Technology to test prismatic soil specimens, each having the dimensions 16" x 4" x 2", under the condition of no longitudinal deformation, i.e., plane strain conditions. The apparatus was so designed to allow the specimen to consolidate first under the condition of K_o consolidation until the confining pressure reaches a certain value. The ultimate value of the confining pressure is pre-determined prior to the test. At the end of the consolidation stage the specimen is sheared.

The main parts of the testing equipment can be summarized as follows:

1. Pressure chamber

The steel chamber serves as a container for the pressure media. It consists of the following parts:

(i) Cylinder shell - The cylindrical shell is made of steel pipe 12 inches inside diameter, 2 inches wall thickness, and 30-1/4 inches long, capable of standing internal working pressures up to 5000 psi. At the top of the shell and midway between the ends a circular hole 4 inches in diameter has been cut to fit the ram housing. Next to the ram housing hole another threaded hole with a special fitting and O-ring seal is made to hold an electrical cable. The cable carries all the wires from the strain sensors and σ_2 load cell inside the shell out to a switch box. Three ports provided with quick connect fittings are located at the end of the shell;

one port for the lateral confining pressure, the second for pore pressure, and the third one for the σ_2 hydraulic jack. The cylindrical shell is also provided with a drainage outlet and filter. For pressures up to 300 psi air is used as a chamber fluid, while for higher pressures liquid is used.

(ii) End cap plates - Two circular end cap plates made of high tensile steel are placed around the ends of the cylindrical shell. Each plate is provided with a circular groove to fit a 1/4-inch diameter pressure seal O-ring. The end cap plates are also provided with twelve holes equally spaced around the center for the connecting rods.

One end cap plate is held attached to the end of the cylindrical shell by the connecting rods, while the other end cap can easily be positioned during assembly by means of a 2-ton chain hoist.

(iii) Connecting rods - The end cap plates are attached tightly to the cylindrical shell by means of high tensile steel rods, 1-1/4 inches in diameter and having a yield stress of 90,000 psi. The components of the preesure chamber are shown in Figure 9.

2. Ram housing assembly

The ram housing assembly consists of the following:

(i) Stainless steel ram - The axial load is transmitted from the loading machine to the specimen by means of a stainless steel rod 2 inches in diameter and 18 inches long. The ram is stiff enough to carry an axial load of 300,000 pounds, which is the loading capacity of the hydraulic testing machine. The upper end of the ram is seated in a special fitting which is connected to either a load cell or proving ring. For axial loads smaller than 50,000 pounds, a log cell is used, while for larger loads a strain gage instrumented proving ring is used. The lower end of the ram has a hemis-

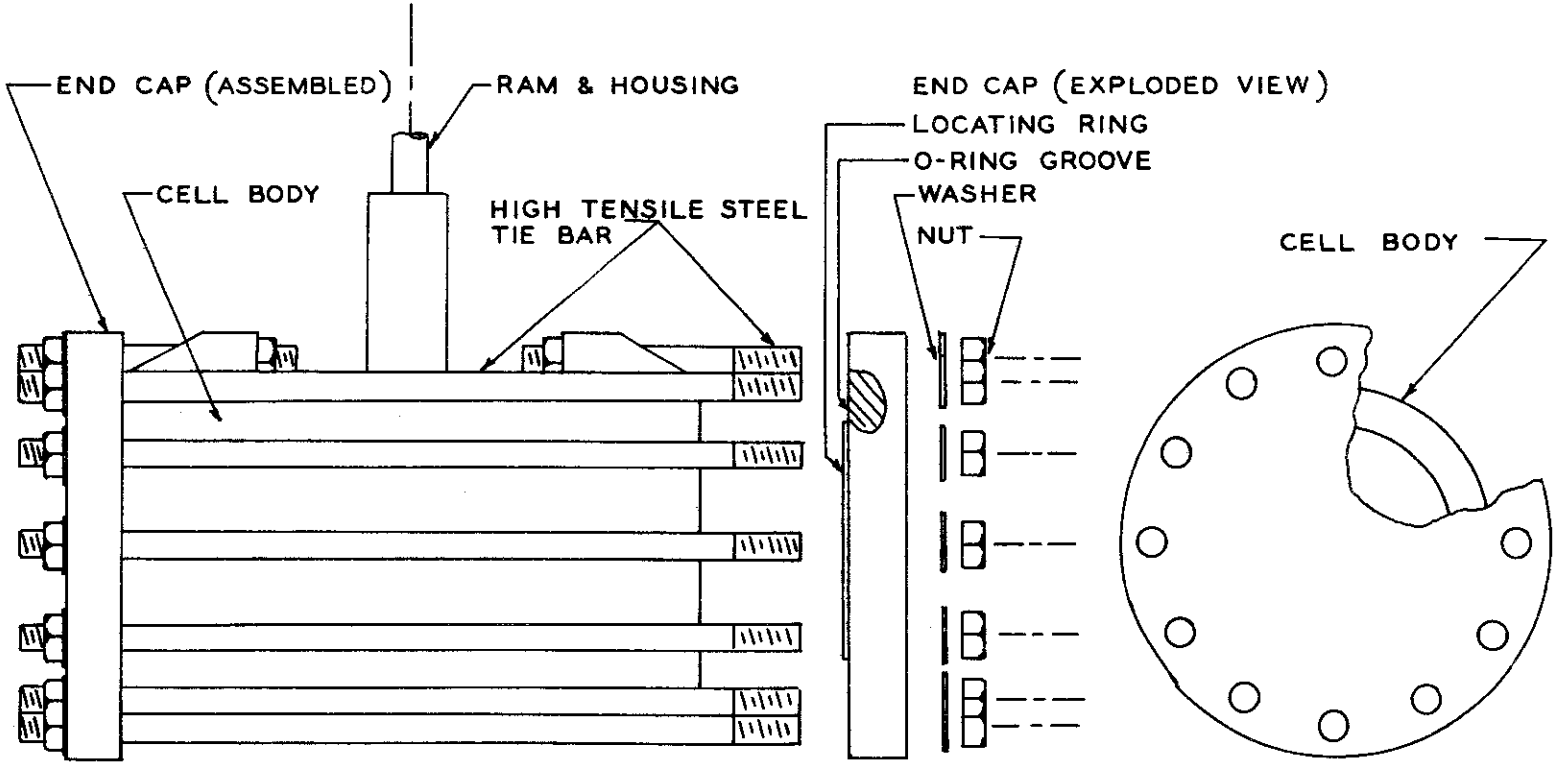

Figure 9. Plane Strain Pressure Chamber Assembly

pherical shape seated in a matching depression located at the center of the loading head, as shown in Figure 10. The spherical depression ensures that the load is applied centrally and also allows freedom of rotation of the loading cap during the test. The travel distance of the ram is sufficient to permit axial strains exceeding 25 percent in the tested specimen.

(ii) Ram housing - The ram is surrounded by a steel housing 4 inches in diameter and 14 inches long. The housing is strong enough to give the ram sufficient stability against buckling. It is provided with two sets of 4 inches long ball races to assure minimum friction force around the ram. The two sets of ball races are separated by a circular brass sleeve 1-inch thick provided with a 1/8-inch hole connected to a grease fitting. At the top and bottom of the housing two circular brass bushings are used to hold pressure O-rings and keep the ball races in position.

Leakage from the cell is prevented by five O-rings. Two are recessed in each brass bushing, the first one is on the inside and in contact with the ram, while the second is on the outside and bearing against the housing. These O-rings are tight enough to provide a complete seal with relatively small friction force. The fifth rubber O-ring is placed between the cylindrical shell and the ram housing base. Figure 11 shows the details of the ram housing assembly.

3. Loading head

The loading head serves to transmit the load from the ram to the specimen. It is made of stainless steel having yield stress of 90,000 psi and machined in a form of a prism, 16" x 2" x 3". Six holes are made in the loading cap, one to allow the passage of the volume change lead from the specimen, and four holes are symmetrically spaced around the center for

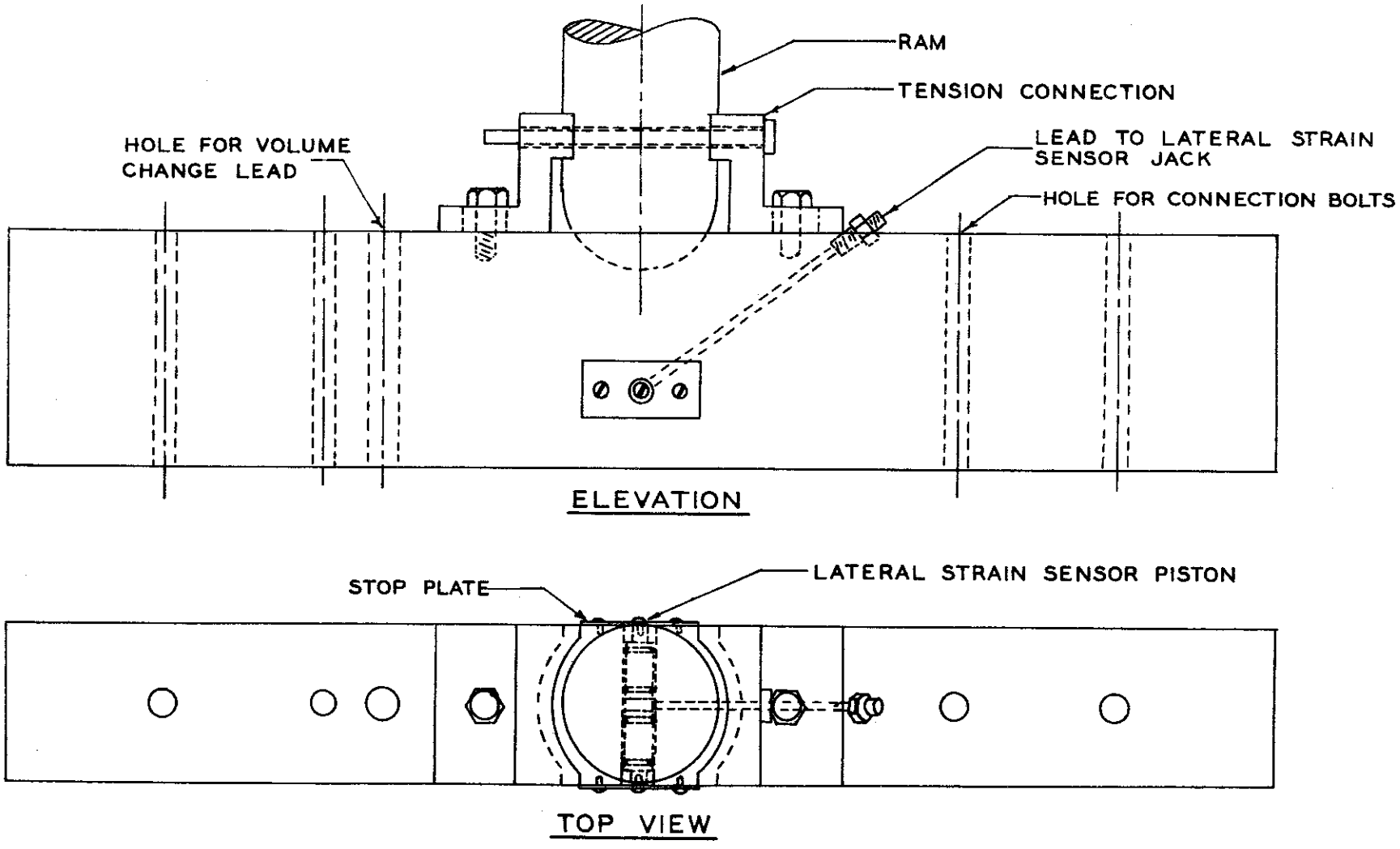

Figure 10. The Loading Head with the Tension Connection

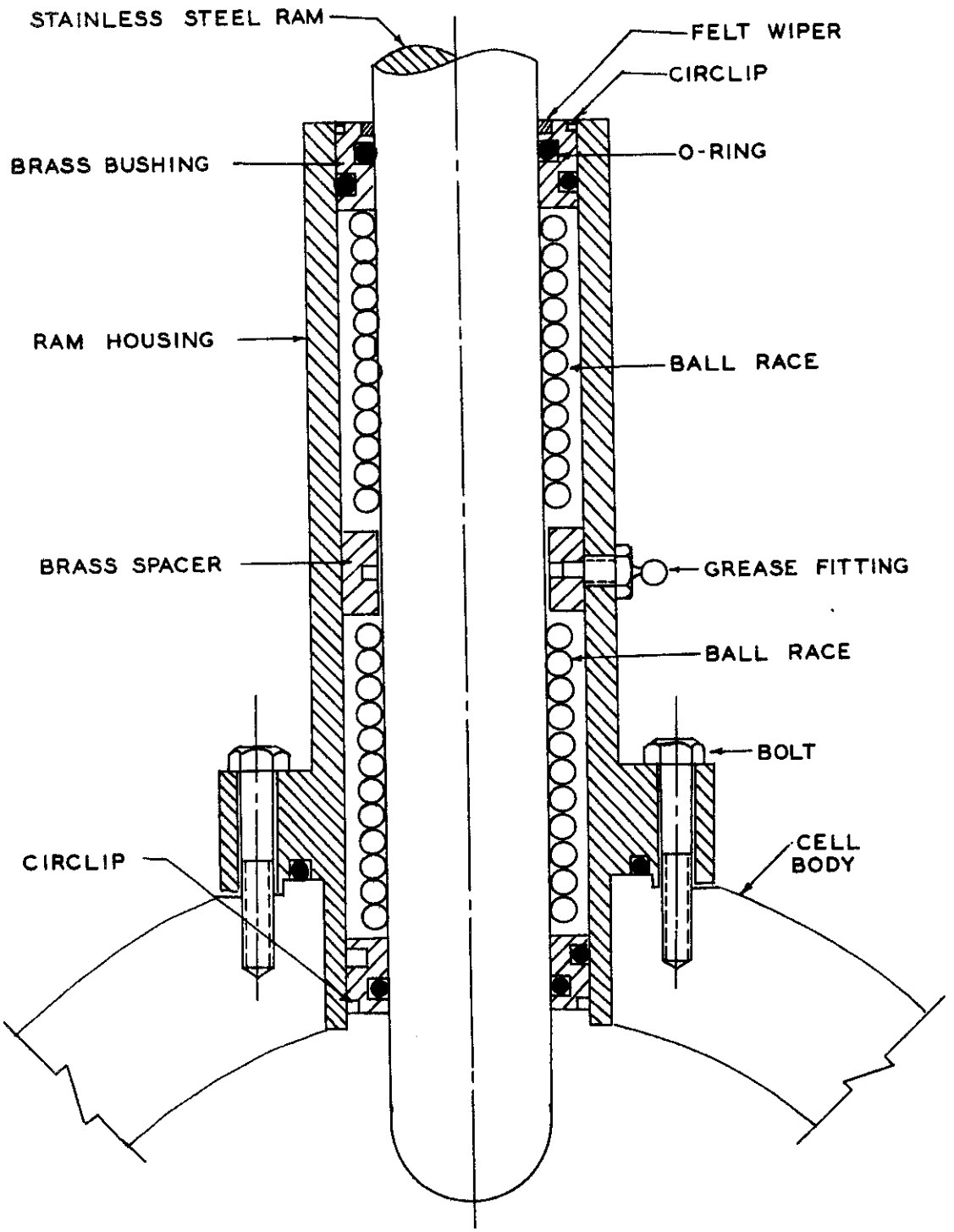

Figure 11. Ram Housing and Bushing Assembly

the connecting bolts. The sixth hole is in the shape of a T and is made oblique to the vertical line and contains the two small pistons. Each piston is provided with two pressure seal O-rings and a small screw to hold the lateral strain sensor firmly to the specimen, as shown in Figure 10.

The loading head is also used to seal the rubber membrane and provide a water-tight seal at the top of the specimen. This is accomplished by employing four connecting bolts to tie together the loading head and the upper platen with the rubber membrane between the two. The upper loading cap is provided with a tension connection which consists of two L-shaped brackets with a circular surface on the inside to fit the ram. The brackets are provided with 1/4-inch holes which are in line with the horizontal hole at the end of the ram when the ram and the loading head is brought in contact.

A lower reaction plate made of cold rolled steel, 5/8-inch thick, 2 inches wide, and 16-3/4 inches long serves as a base on which the soil specimen rests.

4. Platens

Two platens are used, one at the top of the soil specimen, termed the upper platen, and one below the specimen, termed the lower platen.

The upper platen is made of brass 16 inches long, 2 inches wide and 3/4-inch thick. On the surface facing the loading head a rectangular groove along the edges has been cut to fit a 1/4-inch diameter O-ring. Four threaded holes 5/16-inch in diameter were made to receive the bolts which connect the loading head with the upper platen. In order to provide a water-tight seal the edges of the rubber membrane are squeezed between the upper platen and the loading head. The central portion which is surrounded by the O-ring has been projected upward 1/64-inch to prevent damage to the

membrane when the specimen is loaded axially. The upper platen and the drainage screen holder are attached tightly together.

The lower platen is made similar to the upper platen except that it is made of stainless steel.

5. Drainage screen holder

The drainage screen holder is made from stainless steel plate having the dimensions 16" x 2" x 1/4" and fastened tightly to the upper platen by four screws. Along the center line a channel 3/16-inch wide, 1/32-inch deep, and 14 inches long has been cut and is filled with two layers of screen wire, No. 100 mesh. After the channel was cut the drainage screen holder and the lower platen were polished to minimize friction. A sheet of teflon, 16 inches long and 2 inches wide, and 1/32-inch thick was cut in longitudinal strips 1/4-inch wide and placed at the top and bottom of the soil specimen.

The teflon sheets were intended to minimize friction between the sample and the platens during shear.

6. Saddle plate

The saddle plate is made of mild steel plate, 2-1/2 inches wide, 27 inches long, and 5/8-inch high cut with a wide groove. The lower face is radiused to provide better contact with the inside surface of the cylindrical shell. The upper face is cut into a rectangular channel 2 inches wide and 1/4-inch deep. This channel forms a cradle for the lower reaction plate and the end plates; it also helps in preventing them from tilting or tipping. The saddle plate is positioned in the pressure chamber with two locating pins, one at each end.

7. Loading equipment

The prismatic soil specimen is subjected to three independent principal stresses; the axial stress σ_1, the longitudinal stress σ_2, and the lateral stress σ_3, as shown in Figure 12.

The lateral stress around the specimen, σ_3, is applied by air or water pressure in the pressure chamber. The axial load is applied by raising the platform of the hydraulic testing machine and forcing the soil specimen against the ram. An electronic load cell is placed between the ram and the stationary loading head and is used to measure the axial load. The axial load is registered on a strain indicator. The intermediate principal stress is applied to the soil by a hydraulic jack connected to a pump which can be operated manually or by a variable speed electronic motor. The jack base is fixed to the outer end plate which is 3/4-inch thick and bears against a second or moveable end plate in contact with the specimen.

The intermediate principal stress is determined from the reading of an electronic load cell located at the opposite end of the specimen. The load cell is positioned between the outer end plate and the sliding end plate in contact with the specimen. The sliding plate is made of a rectangular piece of steel 7/16-inch thick and provided with four ball bushings at the corners. The ball bushings enable the sliding plate to move horizontally on the tie bars connecting the two end plates. The side of the sliding plate in contact with the specimen is made of polished stainless steel to minimize end friction during the test. The intermediate principal stress, σ_2, can be applied to the soil specimen by delivering oil under pressure to the σ_2 jack, which, in turn, transmits the pressure to the specimen via the moveable end plate. The moveable plate and the sliding plate permits the

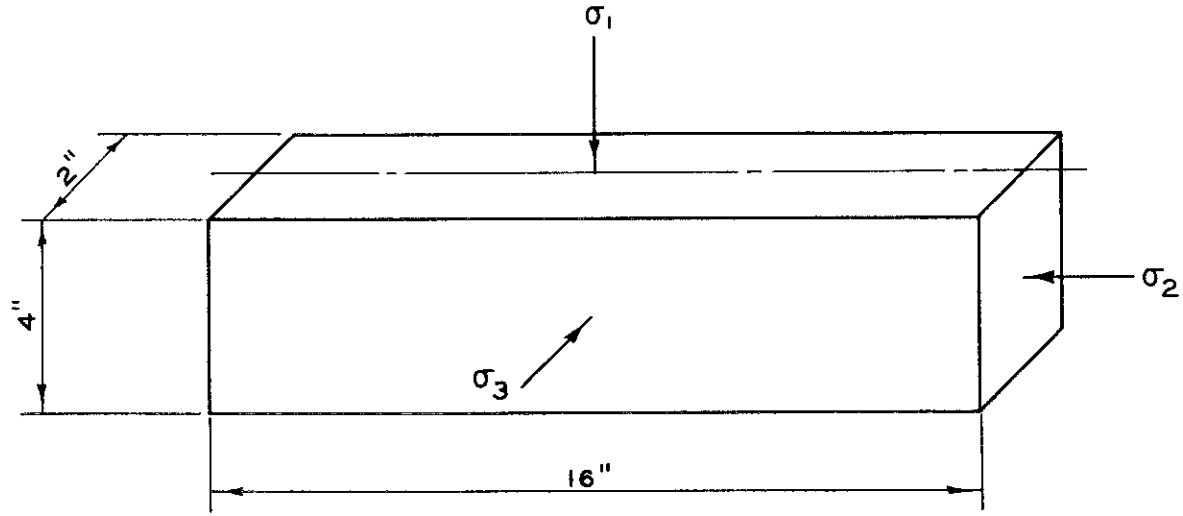

Figure 12. Representation of Principal Stresses Acting on the Soil Specimen

application of the intermediate principal stress as dictated by the longitudinal strain sensor. Figure 13 shows the principal components of the plane strain apparatus.

8. Longitudinal strain sensor

A notable feature of the plane strain device is the longitudinal strain sensor, which indicates departures from the plane strain condition. The longitudinal strain sensor consists of two stainless steel strips, 1/2-inch wide and 1/8-inch thick, and each strip bent to form a rectangular frame. Along each side of the specimen a frame is placed with one end fixed to the moveable plate and the other end fixed to the sliding plate. At the top and bottom of each frame a strain gage is placed and the four strain gages are connected together to form a temperature compensated electrical bridge. Figure 13 shows the general layout of the plane strain apparatus. When the test is in progress any deviation from the plane strain condition (i.e., any longitudinal deformation) will be indicated by the longitudinal strain sensor. It was found that a change of 0.001 inch in the length of the soil specimen will correspond to 48 microinches per inch in the strain indicator reading. Since the strain indicator can be read to the nearest 5 microinches, the minimum deviation from the plane strain condition that can be monitored is approximately 0.001 x 5/48 or 0.0001 inch, which is sufficiently small for practical purposes. The shearing stresses in the intermediate principal plane created by this condition are assumed to be insignificant. Thus, one can conclude that plane strain conditions have been maintained during both the consolidation and shear stage.

9. Lateral strain sensor

The lateral strain sensor is made of two stainless steel strips,

1 STAINLESS STEEL RAM
2 TENSION CONNECTION
3 LOADING HEAD
4 LATERAL STRAIN SENSOR
5 LONGITUDINAL STRAIN SENSOR
6 SPECIMEN
7 σ_2 JACK
8 MOVABLE END PLATE
9 TIE RODS
10 SADDLE PLATE
11 SLIDING END PLATE
12 σ_2 ELECTRONIC LOAD CELL
13 OUTER END PLATE
14 PORE PRESSURE LEAD
15 LATERAL SENSOR PISTON LEAD
16 LEAD FROM σ_2 JACK

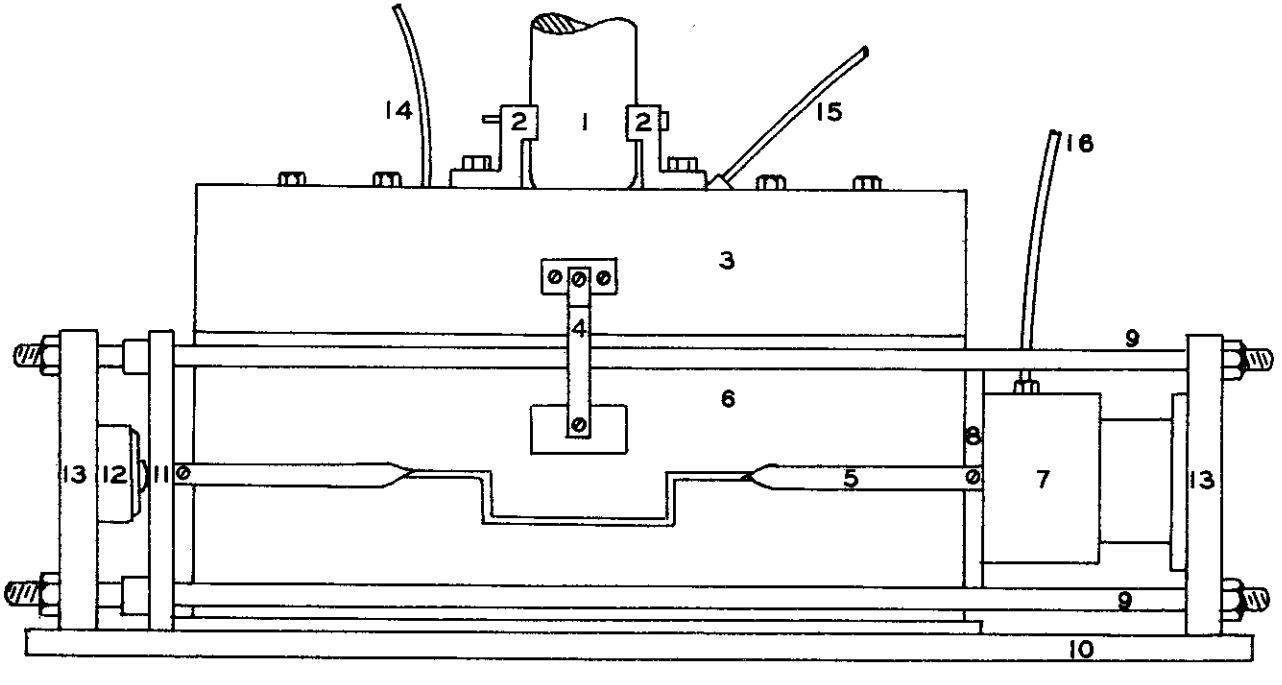

A - ELEVATION

Figure 13. General Features of the Plane Strain Apparatus

17 UPPER PLATEN
18 LOWER PLATEN
19 LOWER REACTION PLATE

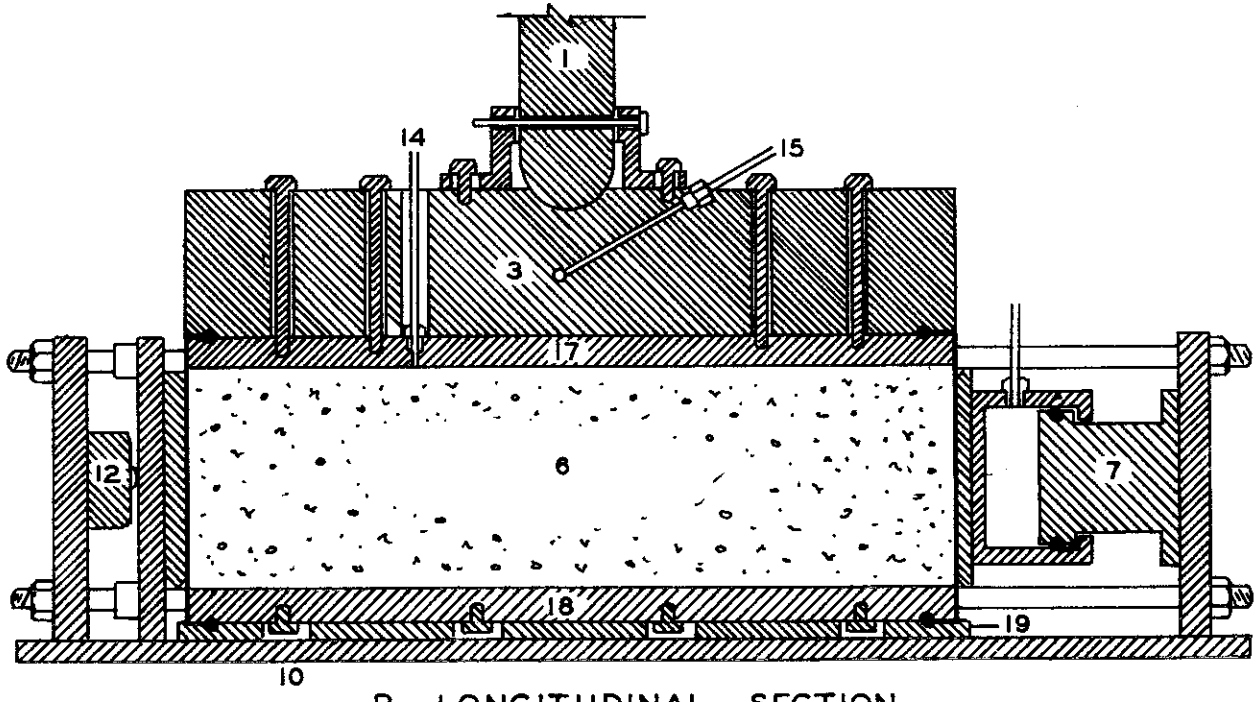

B - LONGITUDINAL SECTION

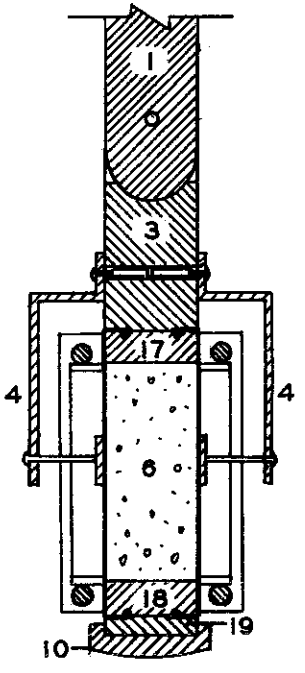

C - LATERAL SECTION

1/2-inch wide and 1/8-inch thick. Each strip is bent to a z-shape with one end fixed to the lateral sensor piston. The other end is provided with a long adjustable screw. The adjustable screw sits on a small plate which is in contact with the soil specimen. Figure 14 shows the wiring diagram used for both longitudinal strain sensor and lateral strain sensor.

Prior to the design of the apparatus several tests were performed to find the coefficient of friction between the rubber membrane loaded with sand and polished metals. The graphical results of the friction tests are presented in Appendix II. It was found that the minimum average coefficient of friction as determined in the shear box was 0.04 between the stainless steel and a rubber membrane covered with a thin film of silicone grease.

10. Stress and strain measurement

The soil specimen inside the pressure chamber is subjected to mutually perpendicular independent principal stresses. The stresses are; the major principal stress σ_1, intermediate principal stress σ_2, and minor principal stress σ_3. The major principal stress is calculated from the reading of the electronic load cell which is placed between the ram and the loading head. This load cell is accurate to the nearest 10 pounds. The intermediate principal stress is measured by a 5000-pound electronic load cell which is accurate to the nearest 5 pounds. The minor principal stress which is represented by the cell pressure is measured by Bourdon-type gage read to the nearest 1 pound per square inch.

The electronic load cells and the strain sensors are connected to a switch box which in turn are connected to the strain indicator. Load cell calibrations relating strain to applied load were made and found to be linear. The change in the height of the soil specimen is measured by a

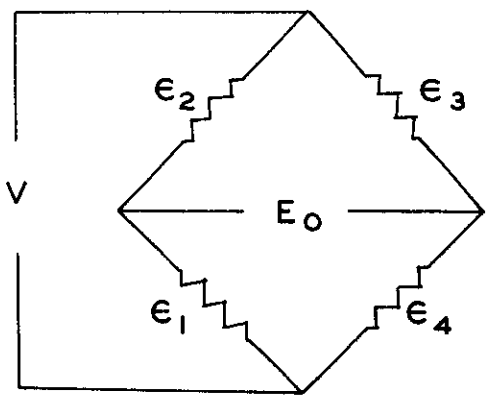

E_o OUTPUT VOLTAGE IN MICRO-V

V BRIDGE EXCITATION

K GAGE FACTOR

$E_o = K\epsilon V$

$\epsilon = (\epsilon_1 - \epsilon_2 + \epsilon_3 - \epsilon_4)/4$

$+\epsilon$ FOR TENSION

$-\epsilon$ FOR COMPRESSION

Figure 14. Wiring Diagram for Lateral Strain Sensor

micrometer dial indicator read to the nearest 0.001 inch.

11. Volume change device

The volume change measurement device used in the test program is basically similar to the one outlined by Bishop and Henkel (11). Figure 15 shows the hydraulic system used in the test program.

Triaxial Apparatus

The standard triaxial cell was used in testing all the cylindrical specimens reported in this study. Although many objections have been raised against the conventional triaxial cell, the shortcomings are minimized in the K_o consolidation test. This was accomplished by introducing two modifications to the triaxial cell. The first modification was made by passing four electrical leads for the K_o belt through the base of the cell. The second alteration was to pass a steel wire through a plug in the top cap of the triaxial apparatus. This wire was to release the pin which locked the K_o belt around the specimen during the consolidation stage. The K_o belt consists of a band of thin brass foil. The brass foil was welded to a short piece of hose clamp containing a thumb screw. The brass foil and the hose clamp form a circumferential belt around the specimen. Four BLH post-yeild strain gages were placed on the brass foil to form a temperature compensated bridge. The K_o belt was connected electrically to a strain indicator unit, as shown in Figure 16. The axial load applied to the soil specimen was measured by an electronic load cell accurate to the nearest 2 pounds. The cell pressure was measured by a Bourdon-type gage read to the nearest 1 pound per square inch. A micrometer dial indicator read to the nearest 0.001 inch was used to measure the change in the height of the specimen. It was very

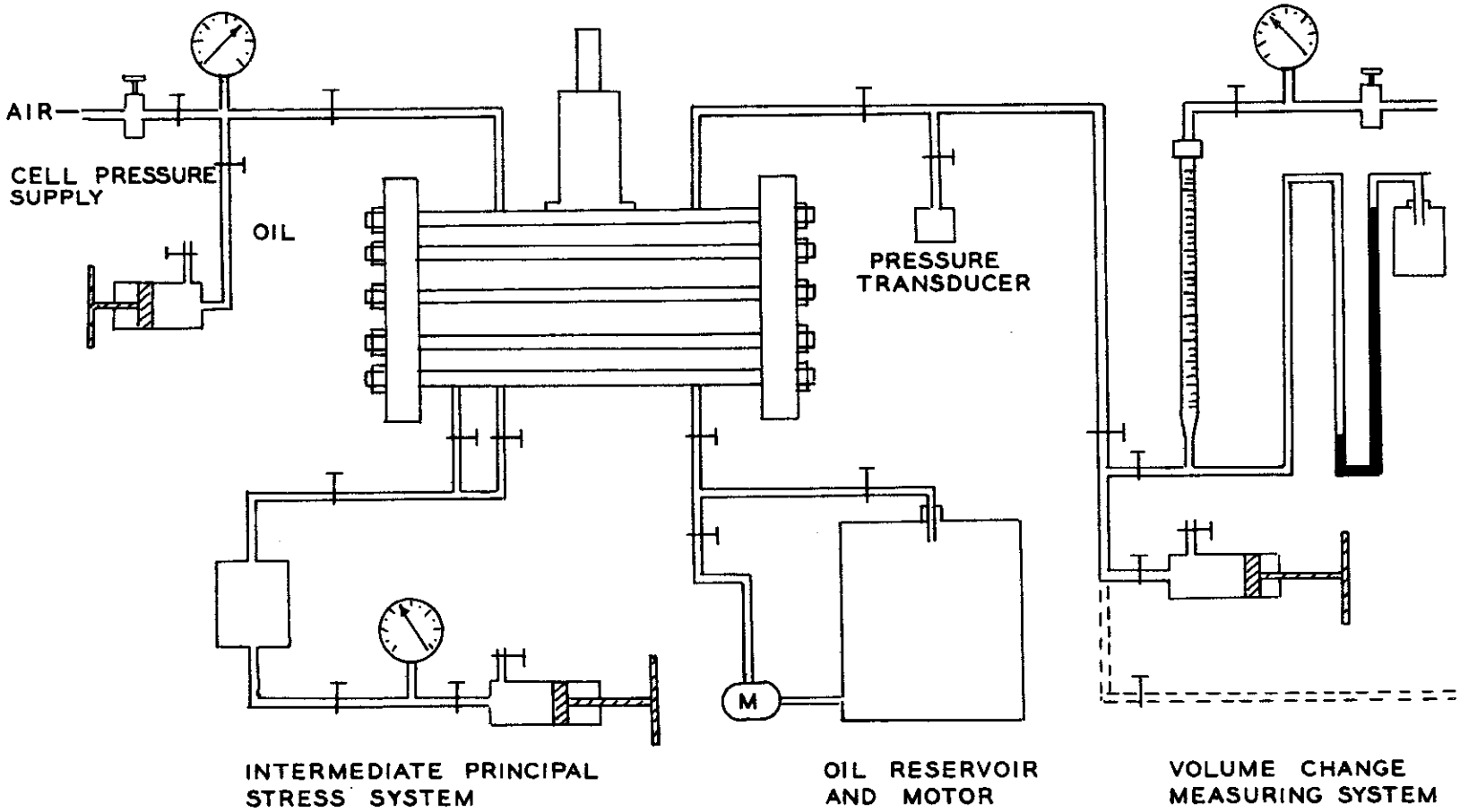

Figure 15. General Layout of the Hydraulic System

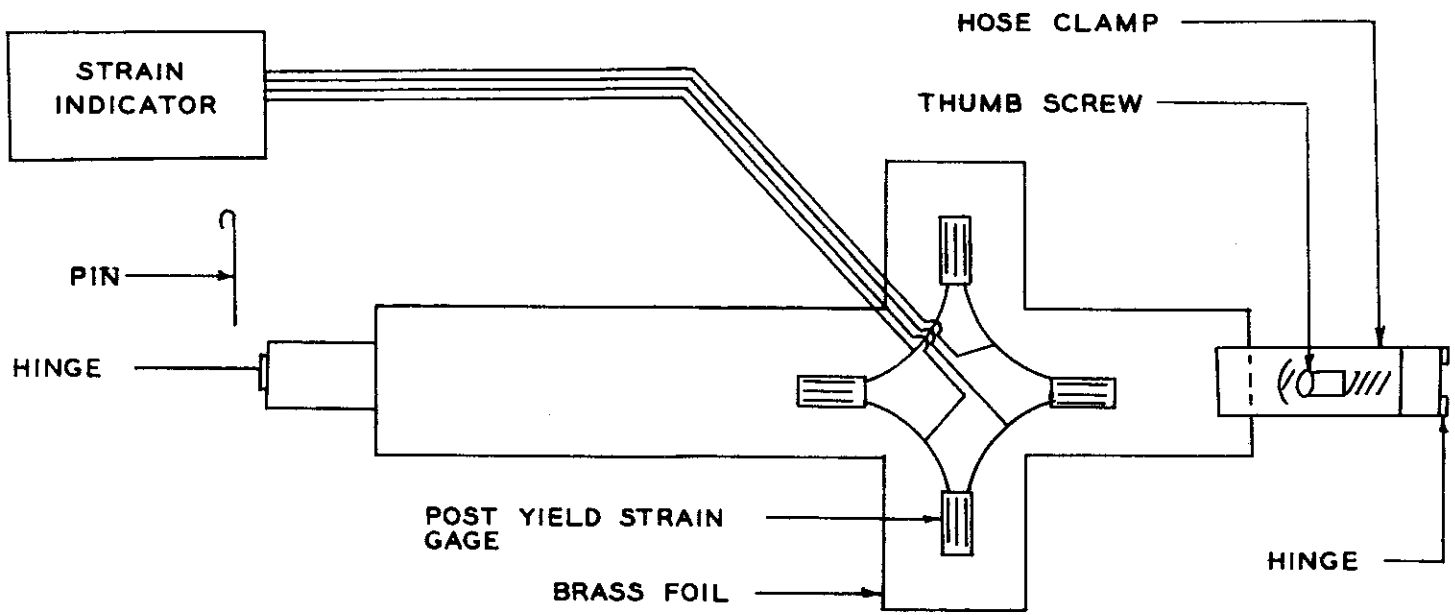

Figure 16. Wiring Diagram for the K_o Belt

difficult to measure the lateral deformation allowed in the specimen, but assuming the sensitivity of the strain gages mounted on the K_o belt is similar to that of the strain sensor of plane strain apparatus, the change in diameter of a 2.8 inch specimen was approximately equal to $\frac{5}{48}$ x 2.8 x 0.001 = 0.0003 inch.

CHAPTER IV

MATERIAL AND SPECIMEN PREPARATION

Several factors were considered in deciding the extent of the current investigation. Some of these factors were concerned with the material on which the research was conducted. Others were related to the testing equipment with which the investigation was carried out. Among the factors which decided the range of the current research are the following:

1. Rate of strain

The minimum rate of strain of the loading machine used in testing plane strain specimen was about 0.005 inch per minute. This limitation made sand a favorable material for testing.

2. Testing material

The sand used in the test program was obtained from the Chattahoochee River near Atlanta, Georgia and much data has been accumulated on it at the Soil Laboratory of Georgia Institute of Technology. It consists of a uniform subangular quartz particles with some mica, which is mostly muscovite. The physical properties of the sand as determined by A.S.T.M. standards, are given in Table 1, and the average gradiation curve before testing and after shearing the specimens under confining of 110 psi, is shown in Figure 17.

Most of the sand used for testing was saturated but a few specimens were tested dry. The placing density varied from one test to another, the range in relative density being 30 percent to 100 percent.

Table 1. Physical Properties of Chattahoochee River Sand

Specific gravity	2.66
Maximum void ratio	1.09
Minimum void ratio	0.593
Mean grain diameter	0.37 mm
Coefficient of uniformity	2.00
Mica content	0.1 %

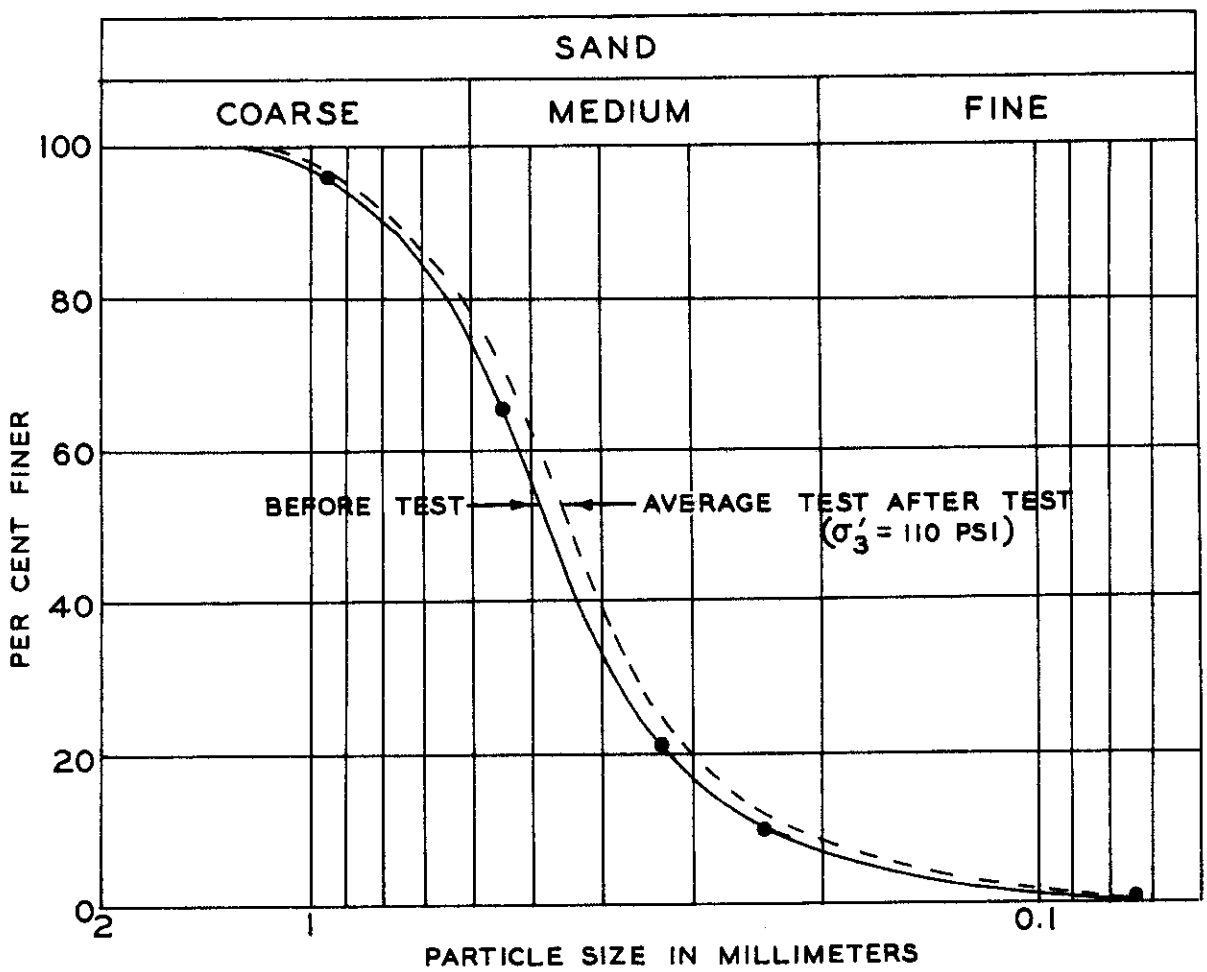

Figure 17. Gradation Curves for Chattahoochee Sand

3. Range of maximum confining pressure

Three ranges of maximum confining pressure were found to be convenient; 70 psi, 100 psi, and 285 psi.

Preparation of the Specimen

The weight of a certain amount of sand was determined. The sand was then saturated by flooding it with distilled water and allowing it to boil for about five minutes to remove entrapped air. The mixture was then allowed to cool to room temperature and the sample was prepared for testing.

Preparation of the Specimen for Plane Strain Test

First, the rubber membrane was sealed between the lower platen and the lower loading cap. An aluminum former consisting of four plates bolted together was placed around the rubber membrane to make the soil specimen maintain a prismatic shape. The whole assembly was then positioned inside the radiused saddle plate. A stripped teflon sheet was placed on the lower platen and then distilled water was poured in the membrane and entrapped air was allowed to escape.

As it was difficult to make a uniform specimen of predetermined density, emphasis was placed on obtaining a uniform specimen with either a dense, medium,or loose packing. Loose specimens were made by allowing the sand to flow through the water in the membrane in layers of approximately equal thickness to ensure uniformity. Dense specimens were prepared by spreading the sand evenly in layers and densifying each layer with a small mechanical vibrator. Specimens of medium density were made in the same manner as the dense specimens, but each layer was tapped by a 1/2-inch diameter aluminum rod. When the sand reached the required height in the former,

the surface of the sand was leveled and then covered by another stripped sheet of teflon. The platen was then gently lowered inside the rubber membrane to rest on the teflon sheet. The upper loading cap was placed on the platen and the edges of the membrane were squeezed between the top loading cap and the upper platen to ensure no leakage. A small negative pore pressure was applied to give the sand sufficient rigidity to make the specimen self supporting. The former was removed and measurements of the specimen dimensions were taken. The stainless steel plates in contact with the ends of the specimens were smeared with a thin layer of silicone grease to reduce end friction. The measuring and controlling devices for the intermediate principal stress, which included the σ_2 load cell, σ_2 jack, and the longitudinal sensor were carefully placed around the specimen. For specimens which were to be K_o consolidated, the lateral strain sensor was also used. After all the components were placed properly in position around the specimen, the complete assembly was transferred to the pressure chamber. The load cells and strain sensors were connected to the switch box, and the platform of the loading machine was raised slowly until the ram came in contact with the top loading cap. Zero readings for all the load cells and strain sensors were recorded. The end cap of the pressure chamber was placed in position and the air pressure inside the pressure chamber was increased while the negative pore pressure was reduced by equal amounts until the pore pressure was atmospheric. Finally, zero readings of both the volume change device and the axial deformation dial gage were taken and the specimen was ready for testing.

Preparation of Specimen for Triaxial Test

A rubber membrane 0.025 inch thick was attached to the base of the triaxial cell by O-rings and a former jacket was placed around it. A vacuum was introduced to the former to make the membrane take the cylindrical shape of the former. The procedure in varying the density of the sand was similar to that used in preparing the plane strain specimen. With the specimen height at approximately 6 inches, the top loading cap was placed on the sand and the membrane was placed around it. Two O-rings were stretched around the membrane and the top cap. This was sufficient to prevent leakage as water could not be discerned through the membrane. The burette of the volume change device was lowered approximately 18 inches to produce negative pore pressure inside the specimen and made the sand self-supporting. Specimen dimensions were then taken.

For the test consolidated under no lateral deformation, the K_o belt was attached in the following manner: the thumb screw was loosened and the pin was placed in the hinge, then the thumb screw was tightened snugly without causing any lateral deformation in the specimen. The four wires from the K_o belt were connected to the strain indicator.

Finally the pressure chamber and top cap were assembled around the specimen and the loading ram was brought in contact with the specimen.

Preparation of Dry Specimen

Dry specimens for both the plane strain and triaxial tests were prepared in exactly the same manner as the saturated specimens with the exception that the procedure for saturation of the sand was omitted.

CHAPTER V

TEST PROCEDURE AND PRESENTATION OF THE RESULTS

The primary objective of this research was to determine the behavior of sand under plane strain conditions at elevated confining pressures. For this purpose the new plane strain apparatus which was developed at Georgia Institute of Technology was used in the test program. Another series of tests was conducted on the same sand in the conventional triaxial cell. In each series the sand was tested under the same placement density and consolidation pressures. The results are presented in a tabulated form in Appendix 1 and typical tests are illustrated graphically.

Plane Strain Tests

Three series of tests were conducted under plane strain conditions, each series corresponds to a maximum confining pressure used in this study. In the 70 psi and 110 psi series the specimens were consolidated either under one dimensional consolidation (K_o consolidation) or isotropic conditions. The specimens in the third series were consolidated only under isotropic compression.

Consolidation Stage

At the beginning of the consolidation stage back pressure was applied to reduce the effect of air which might be trapped in the specimen or volume change device and its associated connections. Back pressure was applied by a simultaneous increase of the cell pressure and the pore pressure by the same amount while maintaining a small effective confining pressure. In most

of the tests a back pressure of 20 psi was used. A set of readings was taken after the cell pressure, the level of water in the volume change device and the back pressure equalized. The sand was consolidated as follows:

(a) K_o Consolidation

In this stage the sand was forced to consolidate under no lateral deformation. The loading procedure was to increase the cell pressure until the lateral dimensions of the specimen just started to decrease. This small decrease caused a change in the electrical resistance of the lateral sensor bridge which was energized by a Baldwin-Lima-Hamilton strain indicator. The change in lateral dimension caused the pointer of the strain indicator to move from the zero position. At that moment the increase in the cell pressure was stopped and the moveable end plates were maintained in contact with the specimen by adjusting the manual screw pump connected to the hydraulic jack. A set of readings, which included the volume change, σ_2 sensor, cell pressure, axial load, longitudinal load, and dial gage which measures the axial deformation, were recorded. The axial load was then increased which, in turn, caused the specimen to start to deform laterally and the small lateral deformation activated the lateral strain sensor. The change in the electrical resistance was translated to a movement in the pointer of the strain indicator, but, this time in the opposite direction. At that instant the axial loading was stopped and a set of readings taken. The cell pressure was increased and the process was repeated until the cell pressure reached the desired value. After consolidation was completed the lateral sensor was disconnected by applying pressure to activate the small pistons on which the sensor was mounted, which in turn allowed the plates to drop.

Under the K_o condition the length and width of the specimen should

remain unchanged. If the length stays constant then the value of the intermediate principal effective stress, σ_2', should always be equal to the value of the minor principal effective stress, σ_3'. The major principal effective stress will be designated by σ_1'. By definition, the value of K_o is equal to $\frac{\sigma_3'}{\sigma_1'}$ and ideally should be equal to $\frac{\sigma_2'}{\sigma_1'}$. A typical relationship of $\frac{\sigma_3'}{\sigma_1'}$ and $\frac{\sigma_2'}{\sigma_1'}$ during consolidation is illustrated in Figure 18. The scatter of the points are due to the incremental application of the axial load and the cell pressure. It is shown that the ratios $\frac{\sigma_2'}{\sigma_1'}$ and $\frac{\sigma_3'}{\sigma_1'}$ started from a high value of approximately unity, which represents the initial isotropic confining pressure to which the sand was subjected at the beginning of the test. The values of $\frac{\sigma_3'}{\sigma_1'}$ and $\frac{\sigma_2'}{\sigma_1'}$ initially decrease with increases of axial strain, then level off and remain essentially constant until the end of consolidation. The values of K_o for all the tests were plotted with respect to the relative density, as shown in Figure 19. The general trend shows a straight line relationship existing between K_o and the relative density within the range of the confining pressures used. The best fit line was obtained by the method of least squares. Points which were far from the best fit line are attributed to inadequate application of the axial load which was applied manually. Referring back to Figure 18, it is shown that the ratio of $\frac{\sigma_2'}{\sigma_1'}$ is always higher than the ratio of $\frac{\sigma_3'}{\sigma_1'}$ by almost a constant value. This difference may be related to the small amount of prestressing applied to the tie bars prior to loading. The difference may also be related to the different boundary conditions which are associated with σ_2' and σ_3', respectively.

Volume Change During K_o Consolidation - Since there is no change in the length or width of the specimen during K_o consolidation, any change in the volume of the specimen should be related only to the change in its

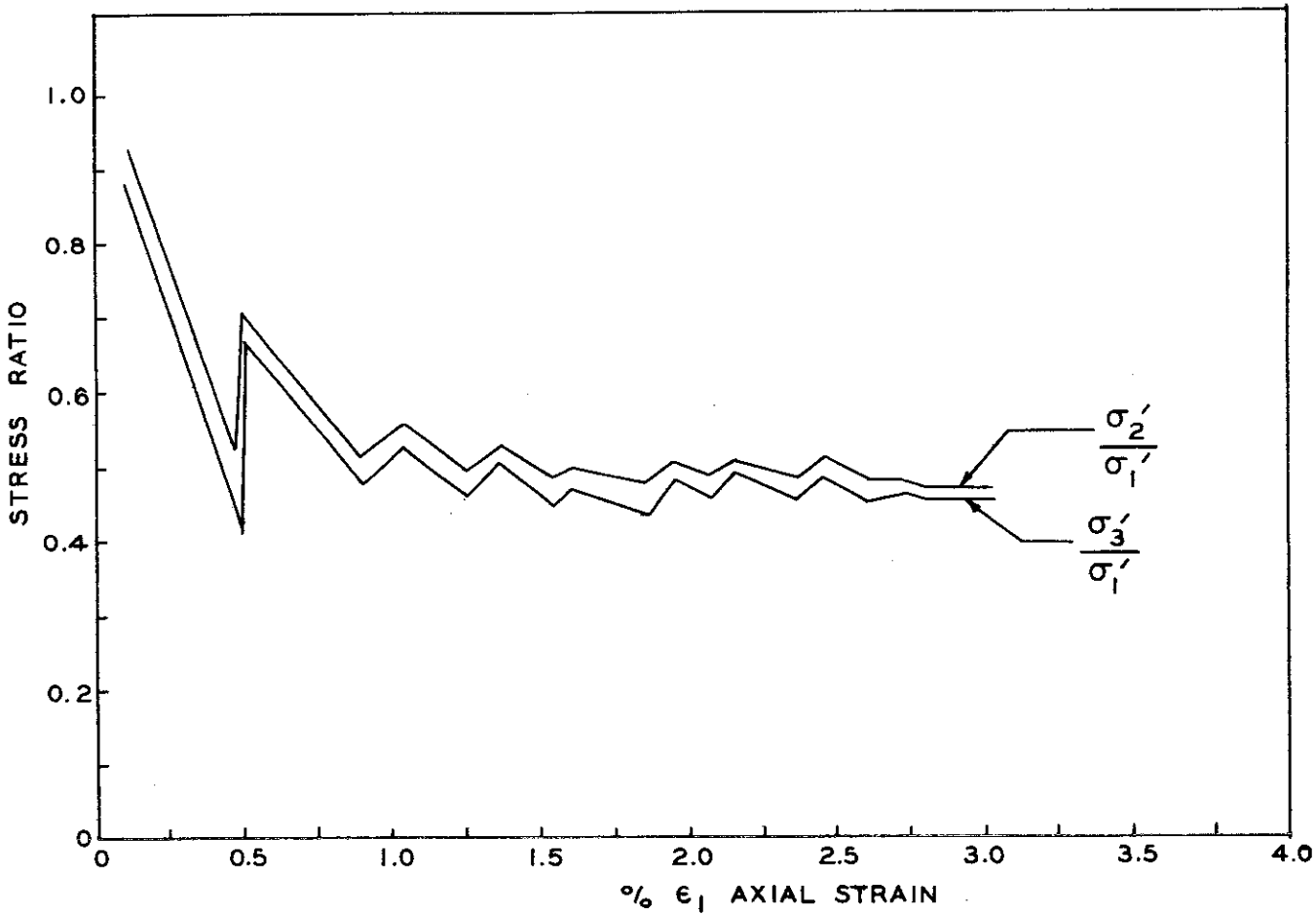

Figure 18. The Relationship Between $\frac{\sigma_2'}{\sigma_1'}$, $\frac{\sigma_3'}{\sigma_1'}$ and % ϵ_1

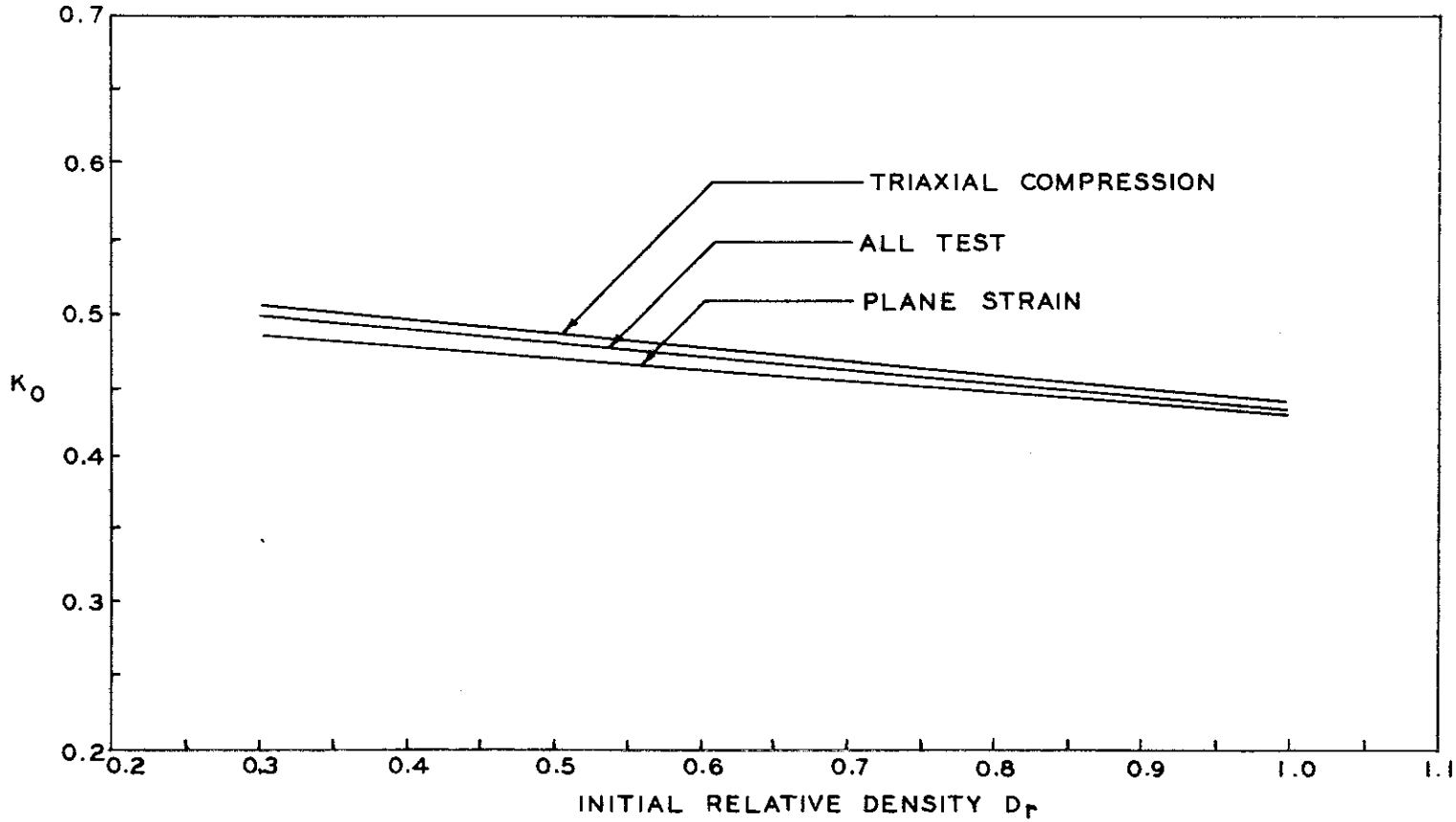

Figure 19. The Relationship Between K_o and Relative Density

height. The relationship between the change in the volume and height of the specimen is shown in Figure 20. The points should fall on a straight line passing through the origin whose slope is equal to the initial cross-sectional area of the specimen. The scatter of the points around the line indicates that the axial deformation is not uniform throughout the consolidation stage and some readings were taken before complete equilization of the volume change. The deviation from the straight line may also be attributed to the presence of air bubbles in the system.

(b) Isotropic Consolidation

In the isotropic consolidation tests the cell pressure was increased in convenient increments and measurements were taken after each increment. After the cell pressure reached the desired value the specimen was allowed to consolidate until the flow of water stopped completely in the volume change device. At that time the moveable end plates were brought into contact with the specimen and the platform of the loading machine was raised until the rim touched the loading cap. A set of readings were taken of the volume change, axial load, σ_2 load, longitudinal strain sensor, and the dial gage of axial deformation, and the specimen was ready for the shear stage.

Shear Stage Drained Test

In the shear stage the axial load was increased incrementally while the cell pressure was kept constant throughout the test. Axial loading was controlled manually by a constant flow hydraulic regulator on the testing machine. The increase in the axial load caused the specimen to deform laterally as well as longitudinally. The longitudinal deformation, however,

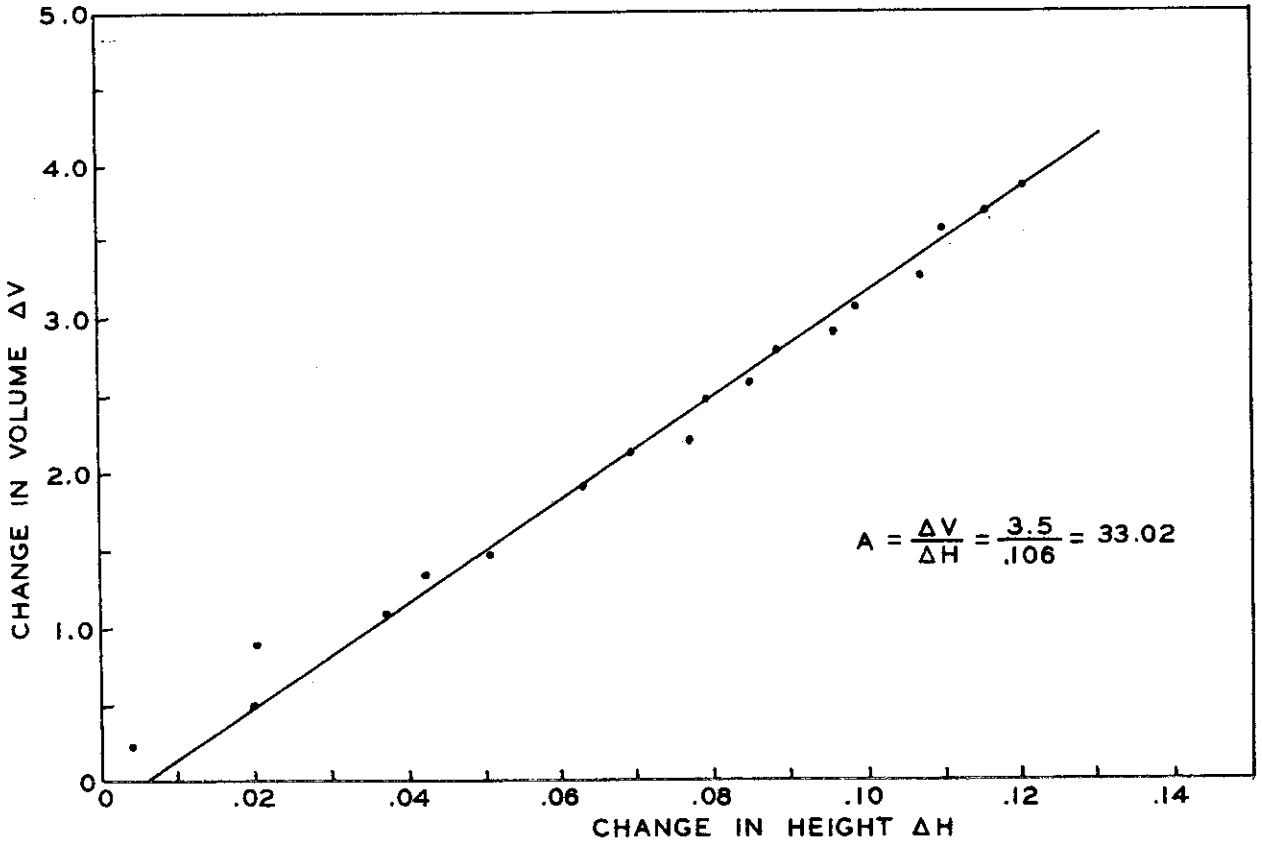

Figure 20. The Relationship Between Volume Change and Axial Deformation During K_o Consolidation of a Plane Strain Specimen

was kept to a minimum by simultaneous adjustment of the σ_2 hydraulic jack with the manual pump outside the cell as required to maintain no change in the longitudinal sensor reading. Reading of the axial load, σ_2 load, volume change, cell pressure, and axial deformation dial gage were recorded at small intervals of axial deformation. The test was not stopped at the maximum axial load, but rather was generally continued until no volume change was observed in the volume change burette.

The reduction of the data was made by the use of an electronic computer. The graphical results are presented in terms of either the effective principal stresses or in terms of some dimensionless quantities such as stress ratio, axial strain, or volumetric strain.

Stress-Strain Relationship

During the shear stage the major principal stress was increased, the minor principal stress was kept constant, and the intermediate principal stress was adjusted to create plane strain conditions. The major principal stress increased to a maximum value, then remained constant for a certain range of axial strain depending on the placement density of the sand. A typical stress-strain relationship for specimens consolidated under K_o consolidation and sheared under drained conditions is shown in Figure 21. The graphs show that the variation of σ_1' and σ_2' with ϵ_1' have the same characteristics in that both reached the maximum point at almost the same strain. In most of the cases, the value of σ_1' started to decline before σ_2'. When the specimen was isotropically consolidated the value of $\frac{\sigma_2'}{\sigma_1'}$ started with a value of approximately unity then quickly leveled off until failure, after which it increased slightly again. It was also found that the value of $\frac{\sigma_2'}{\sigma_1'}$ at failure is approximately equal to the value of K_o obtained from the

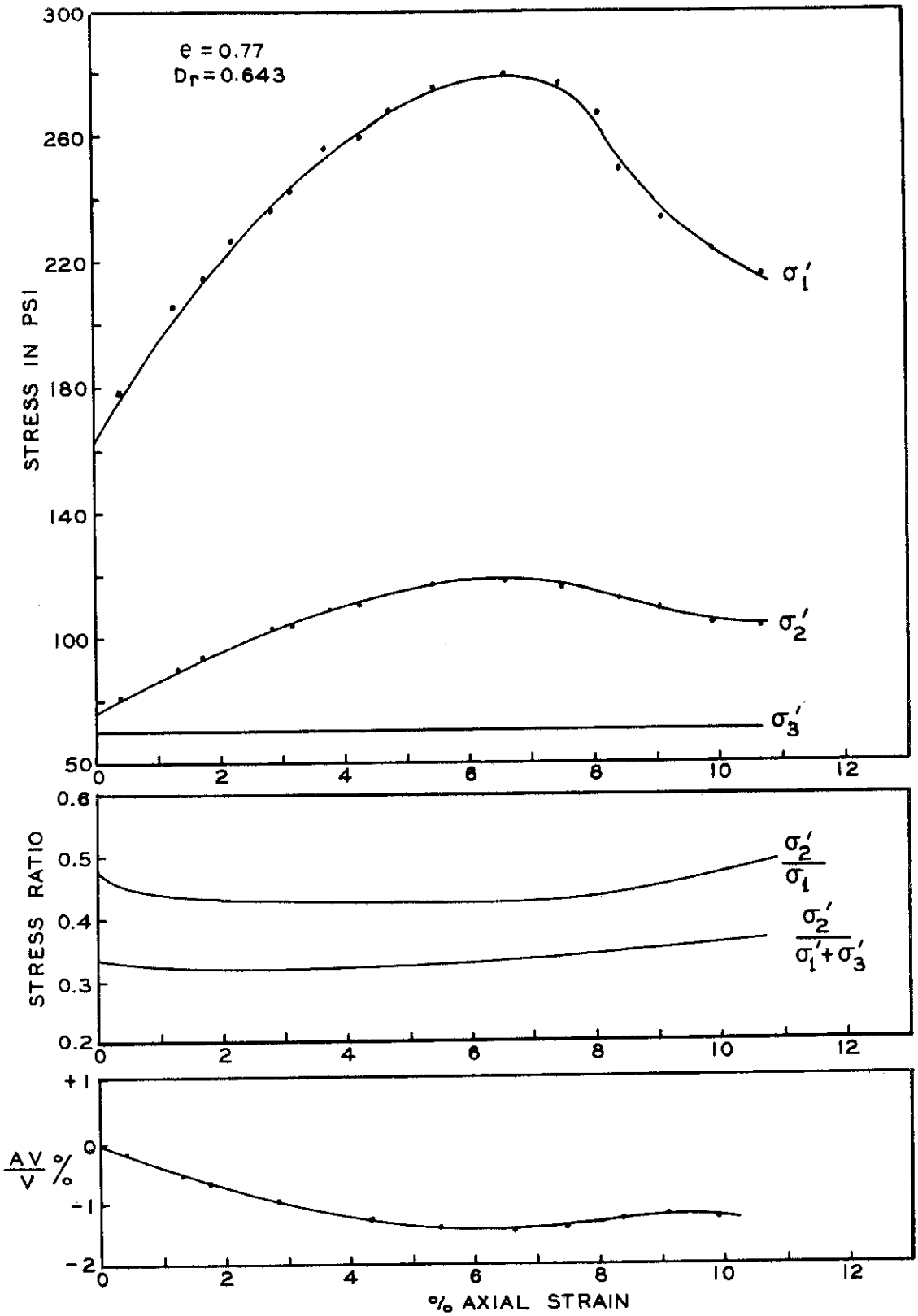

Figure 21. Typical Stress and Strain Relationship During Shear for a Plane Strain Specimen

consolidation stage. This observation has also been noticed by previous investigators (10,12) on different sands. The ratio $\frac{\sigma_2'}{\sigma_1' + \sigma_3'}$ has also started with relatively high value, then it levels off in a manner similar to $\frac{\sigma_2'}{\sigma_1'}$. The value of $\frac{\sigma_2'}{\sigma_1' + \sigma_3'}$ at failure can be related empirically to Poisson's ratio of the sand. It is interesting to know that regardless of the method of consolidation, the maximum major principal effective stress is the same for tests having the same relative density and consolidation pressure. The failure strain is higher for isotropically consolidated specimen than for K_o consolidated specimen, typical values being 2 percent to 3 percent higher. A typical stress-strain relationship for triaxial specimen consolidated under K_o consolidation and sheared under drained condition is illustrated in Figure 22.

Angle of Shearing Resistance

The conventional Mohr-Coulomb theory was used to evaluate the angle of shearing resistance, ϕ. In this theory it is assumed that the intermediate principal stress, σ_2, has no effect on failure, thus the major and minor principal stresses are sufficient to define failure provided that the stress circle touches the failure envelope (14). The value of ϕ in terms of principal effective stresses is calculated as:

$$\sin \phi' = \frac{\sigma_1' - \sigma_3'}{\sigma_1' + \sigma_3'} \quad . \tag{1}$$

In this investigation it is assumed that failure occurs when the major principal effective stress reaches a maximum value on the stress-strain plot.

The value of ϕ' was expressed, as shown in equation (1), throughout

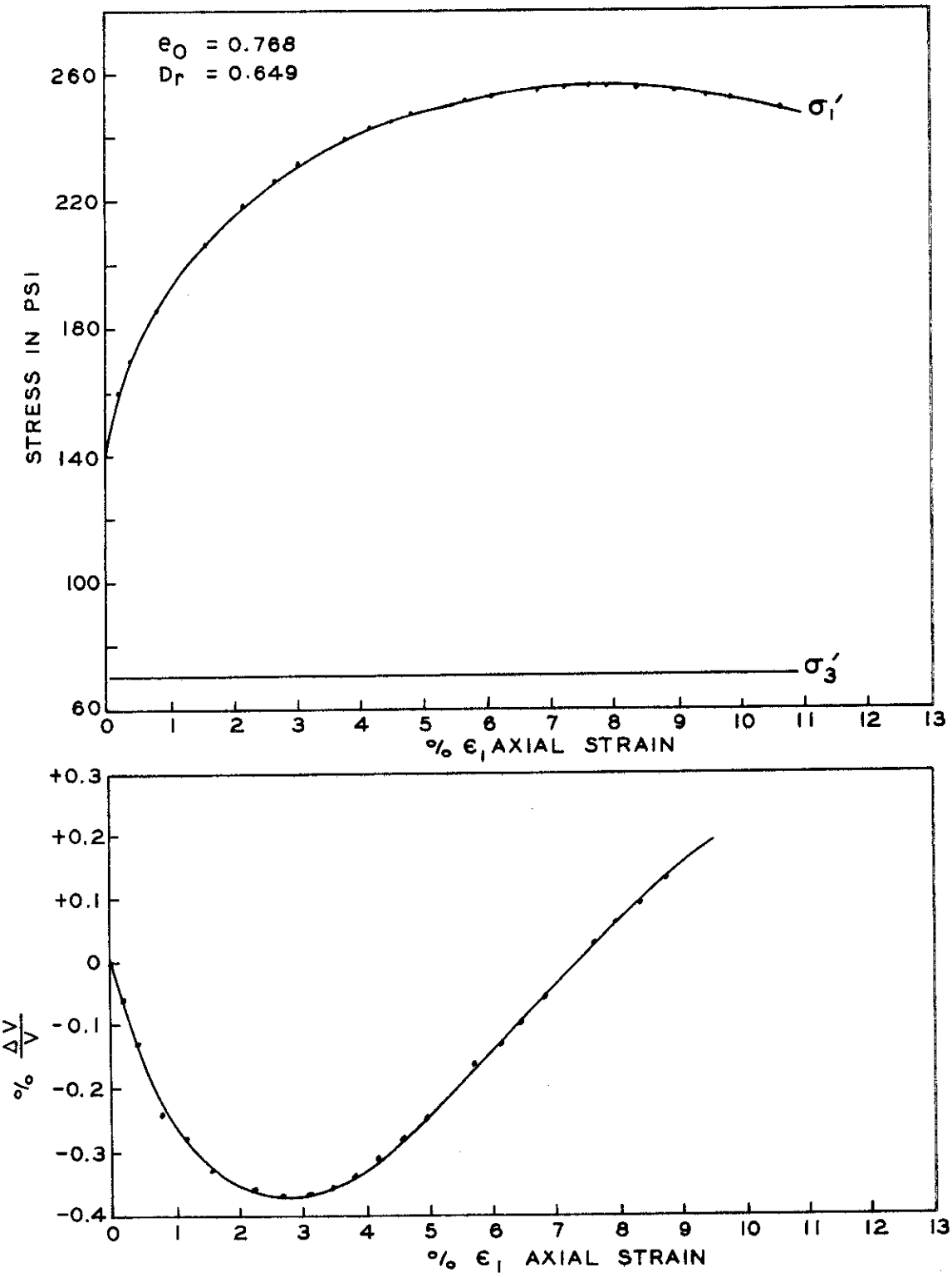

Figure 22. Typical Stress and Strain Relationship During Shear for a Triaxial Compression Specimen

this thesis for both plane strain and triaxial tests, assuming a cohesion intercept of zero. For each series of tests the value of ϕ' is plotted versus the relative density, D_r (both at the beginning of the test and at the end of consolidation). The results are shown in Figures 23 through 28.

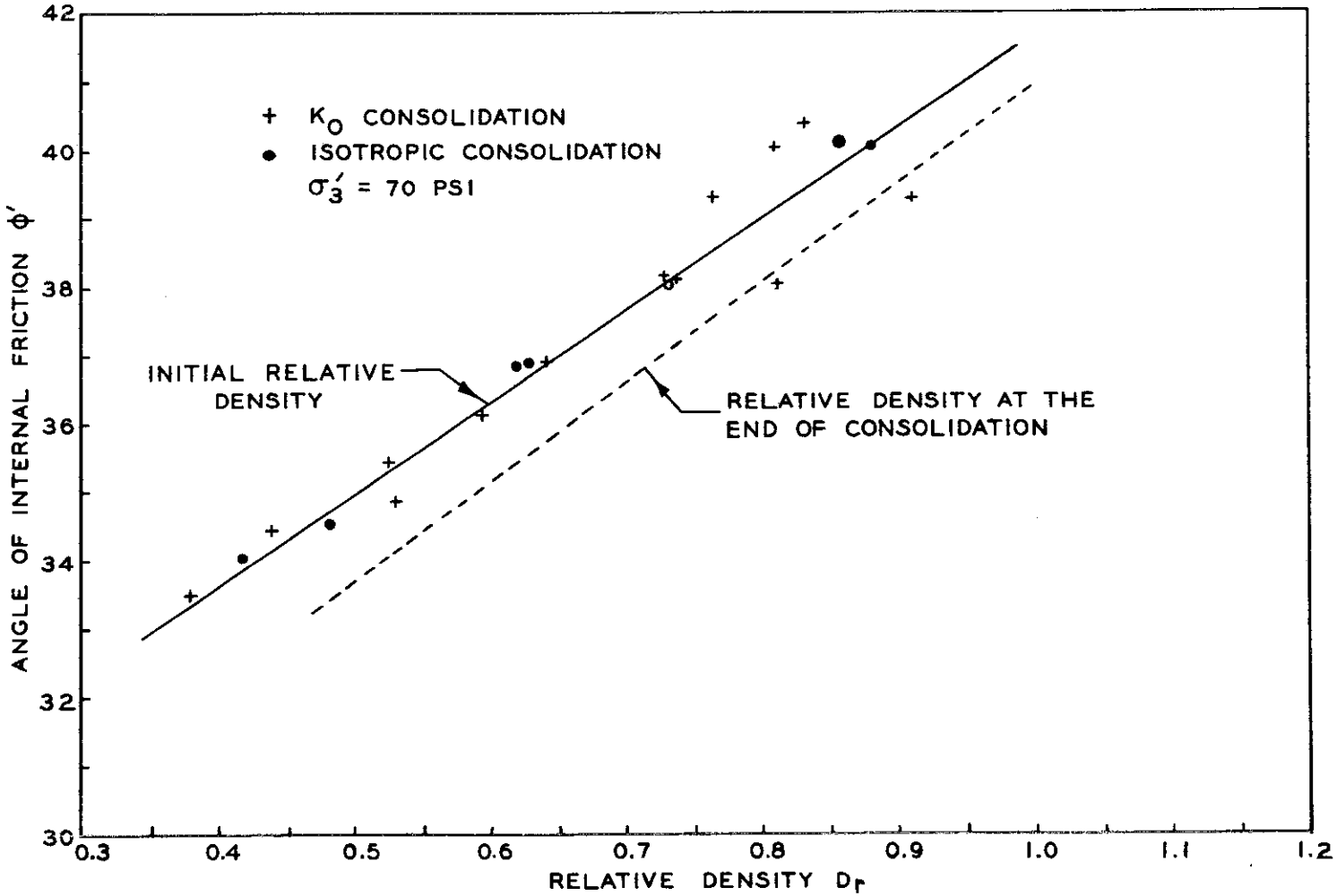

Figure 23. The Relationship Between ϕ' and D_r for Plane Strain Tests (σ_3' = 70 psi)

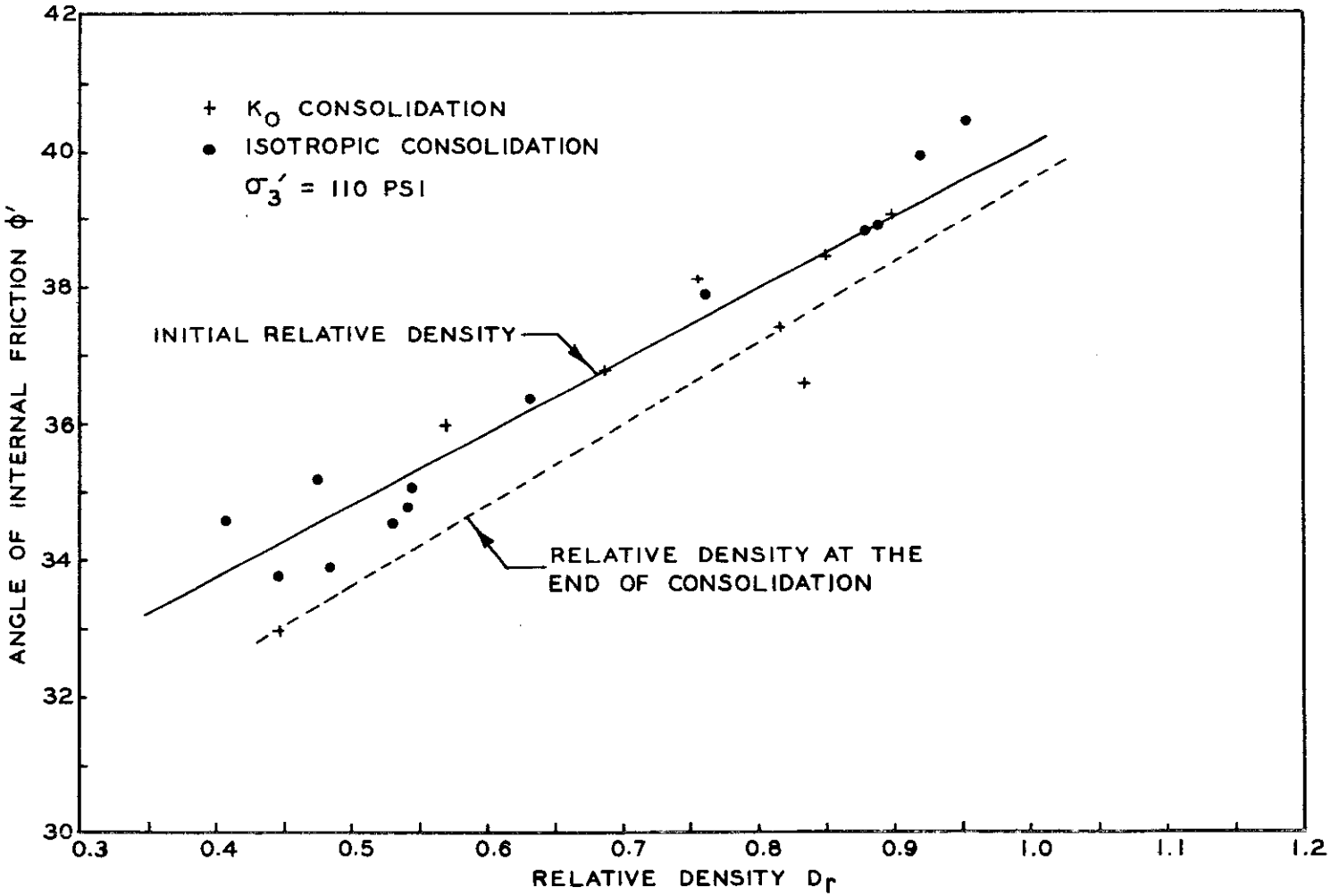

Figure 24. The Relationship Between ϕ' and D_r for Plane Strain Tests (σ_2' = 110 psi)

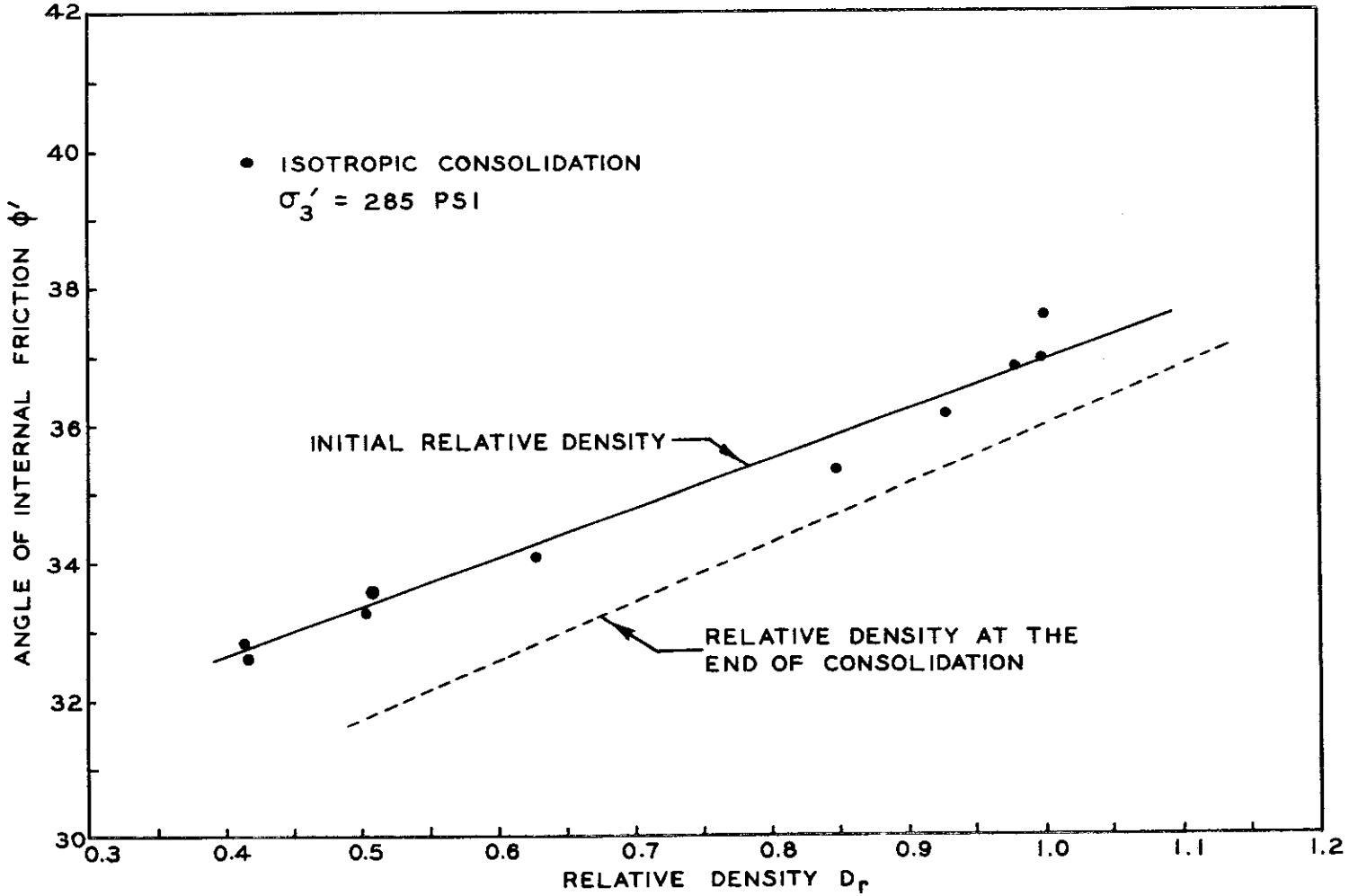

Figure 25. The Relationship Between ϕ' and D_r for Plane Strain Tests ($\sigma_3' = 285$ psi)

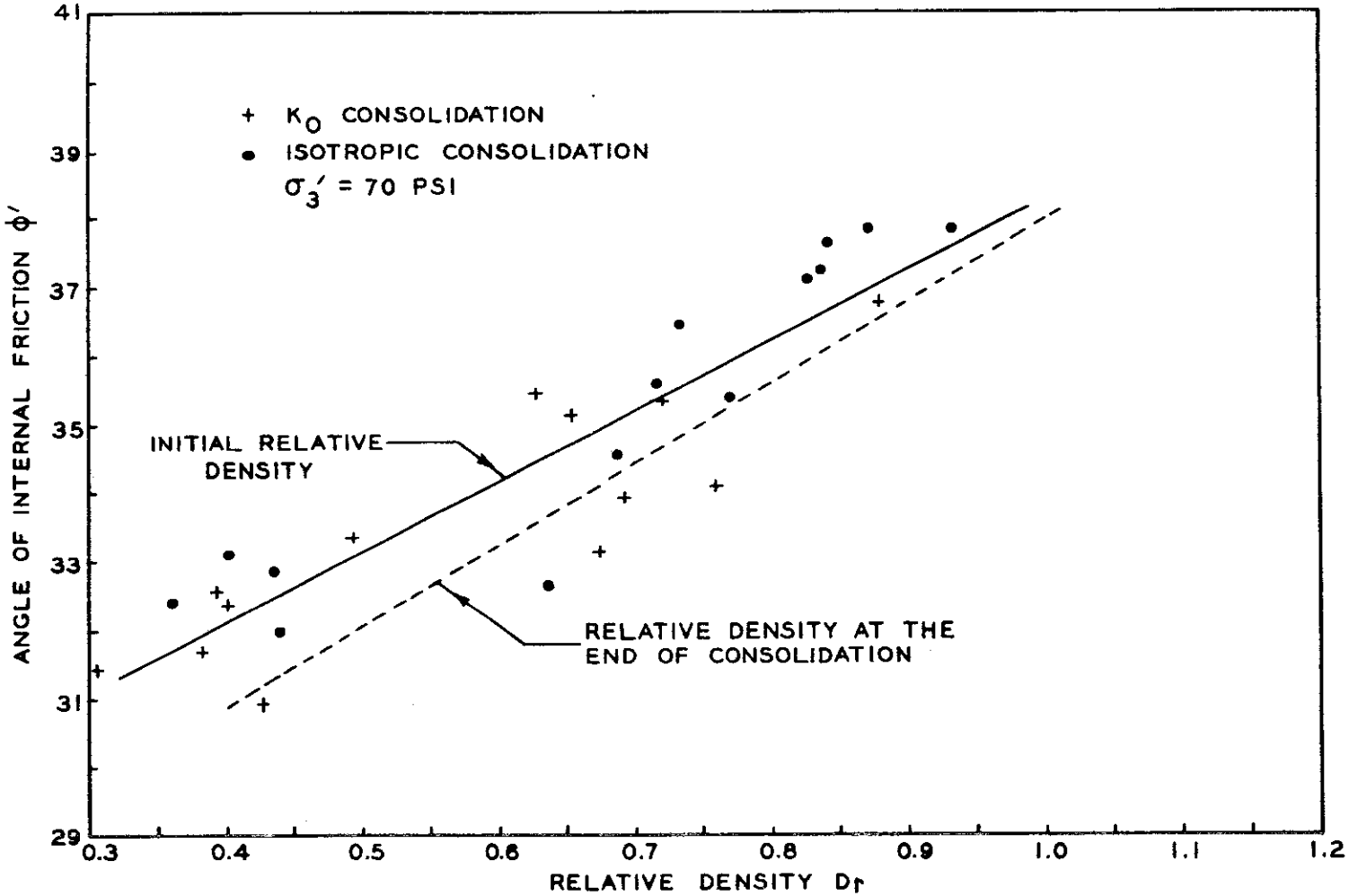

Figure 26. The Relationship Between ϕ' and D_r for Triaxial Tests ($\sigma_3' = 70$ psi)

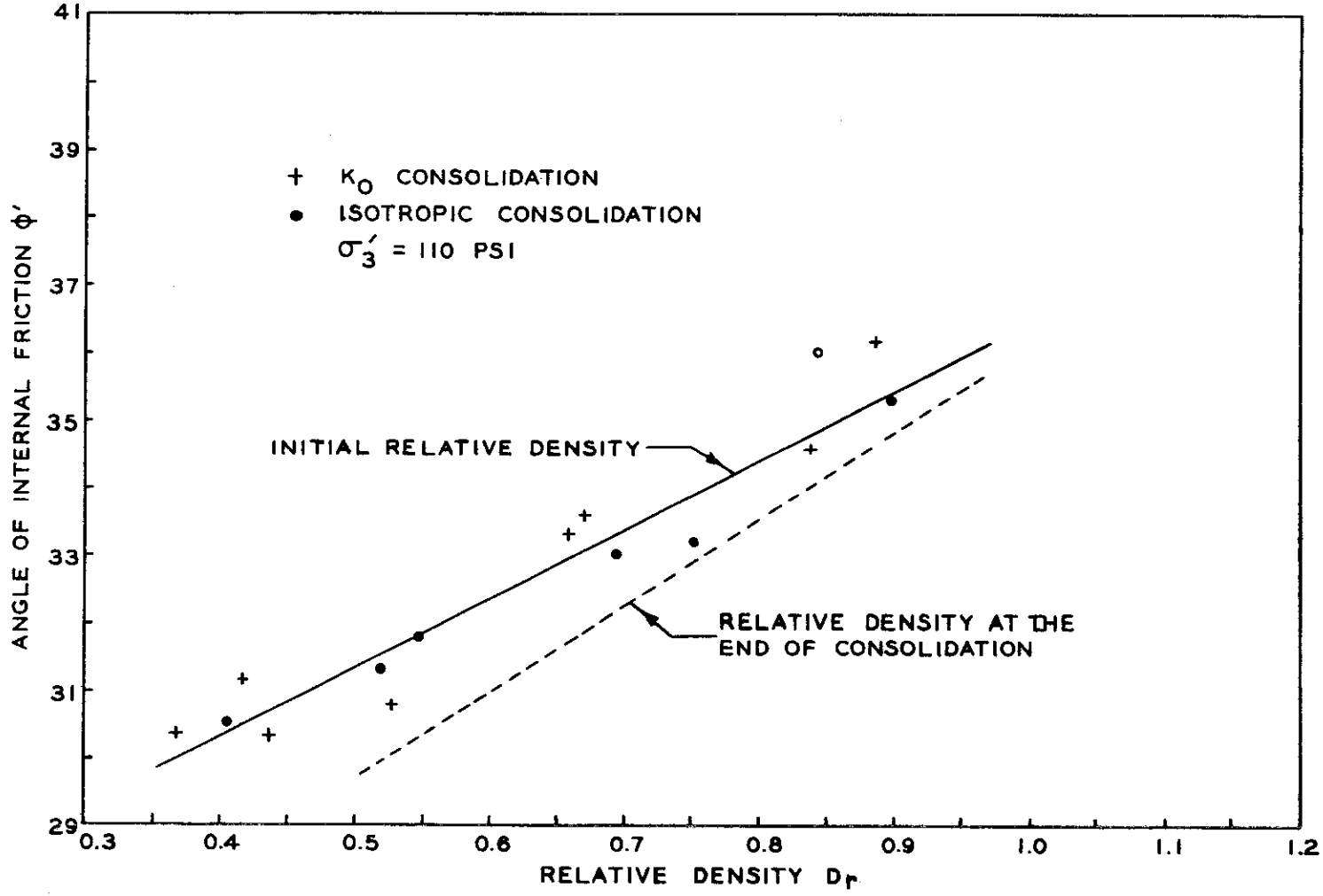

Figure 27. The Relationship Between ϕ' and D_r for Triaxial Tests (σ_3' = 110 psi)

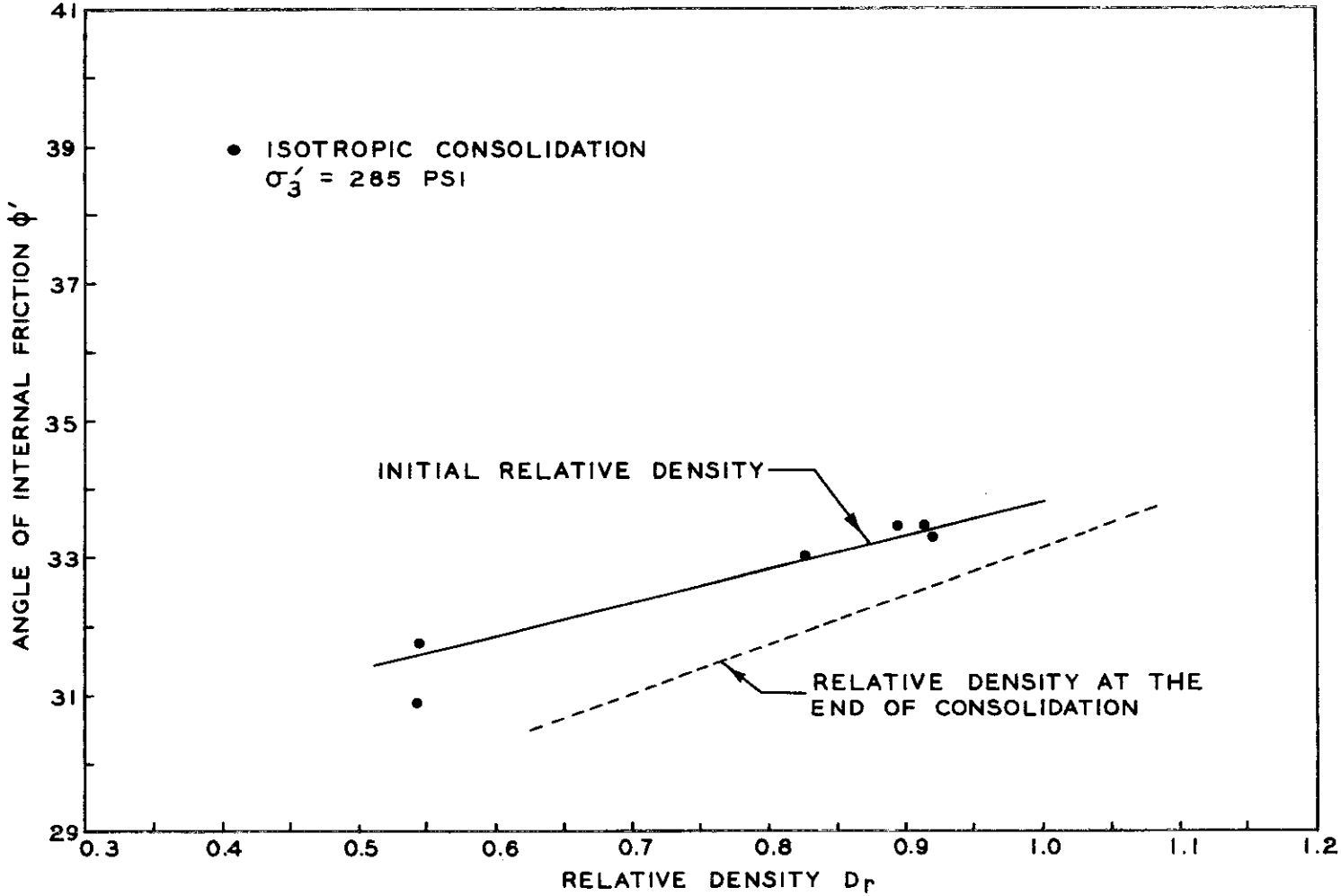

Figure 28. The Relationship Between ϕ' and D_r for Triaxial Tests (σ_3' = 285 psi)

CHAPTER VI

DISCUSSION OF TEST RESULTS

The characteristics of Chattahoochee River sand were analyzed by studying the data obtained from two types of tests. In the first type the sand was subjected to plane strain conditions. In the second type of test the sand was subjected to conditions of axial symmetry. The results from the two types of tests were compared. The results are also correlated with the work of other investigators on other types of sand and with several theories of failure.

Coefficient of Earth Pressure at Rest

The significance of K_o can best be illustrated with reference to the coefficients of earth pressure against retaining structures. Three of these are widely used in applied soil mechanics; the coefficient of earth pressure at rest which is represented by K_o (15), the coefficient of active earth pressure, K_a, and the coefficient of passive earth pressure, K_p. If we imagine a horizontal homogeneous mass of soil being placed against an immovable, long, frictionless, rigid wall then each element of soil adjacent to the wall is able to undergo deformation only in the vertical direction. Under this condition the soil behind the wall is said to be in a state of elastic equilibrium (16), and an elastic stress-strain relationship may exist. If the soil is assumed to be a homogeneous, elastic, and isotropic material then the relationship between principal stresses and principal strains can be expressed as follows:

$$\epsilon_1 = \frac{1}{E}[\sigma_1 - \nu(\sigma_2 + \sigma_3)] \tag{2}$$

$$\epsilon_2 = \frac{1}{E}[\sigma_2 - \nu(\sigma_3 + \sigma_1)] \tag{3}$$

$$\epsilon_3 = \frac{1}{E}[\sigma_3 - \nu(\sigma_1 + \sigma_2)] \tag{4}$$

where E is the modulus of elasticity, and ν is Poisson's ratio. In the case of soil under the at-rest condition, the value of $\epsilon_3 = \epsilon_2 = 0$ and $\sigma_2 = \sigma_3$, then equation (4) can be written as follows:

$$\sigma_3 = \nu(\sigma_1 + \sigma_2) \tag{5}$$

or

$$\nu = \frac{\sigma_3}{\sigma_1 + \sigma_2} = \frac{\sigma_3}{\sigma_1 + \sigma_3} \quad . \tag{6}$$

The value of Poisson's ratio, ν, also can be expressed in terms of principal effective stresses, as:

$$\nu = \frac{\sigma_3'}{\sigma_1' + \sigma_3'} \quad . \tag{7}$$

The ratio of the minor principal effective stress, σ_3', to the major principal effective stress, σ_1', is the coefficient of earth pressure at rest, K_o. Therefore, from equation (7) the value of Poisson's ratio can be expressed in terms of K_o as:

$$\nu = \frac{K_o}{1 + K_o} \quad , \tag{8}$$

or the value of K_o can be expressed in terms of Poisson's ratio as:

$$K_o = \frac{\nu}{1 - \nu} \quad . \tag{9}$$

Depending on the magnitude and direction of yielding in the earth retaining structure, there exists an infinite number of coefficients of earth pressure between the two extremes of active and passive coefficient of earth pressure.

The results of K_o tests in this study on prismatic and cylindrical sand specimens, shown in Figure 29, are expressed in terms of sin ϕ', where ϕ' is the measured angle of internal friction, as expressed by equation (1). The method of least squares was used to establish the best fit line between K_o and sin ϕ'.

Published results relating to the value of K_o on other types of sand are presented in Table 2.

Jaky (21) showed theoretically that for cohesionless soils the value of K_o can be expressed as:

$$K_o = 1 - \sin \phi' \quad . \tag{10}$$

The relationship between the value of K_o versus sin ϕ' for the results of several investigators, as well as the results of the present tests are shown in Figure 30. The results of this investigation and earlier tests generally show that the value of K_o decreases with the increase of the value of ϕ'. However, the wide variation of the value of K_o from one investigator to another may suggest that the value of K_o is greatly influenced by other soil properties or test techniques. When the data in this investigation were compared with equation (10) the results showed that the

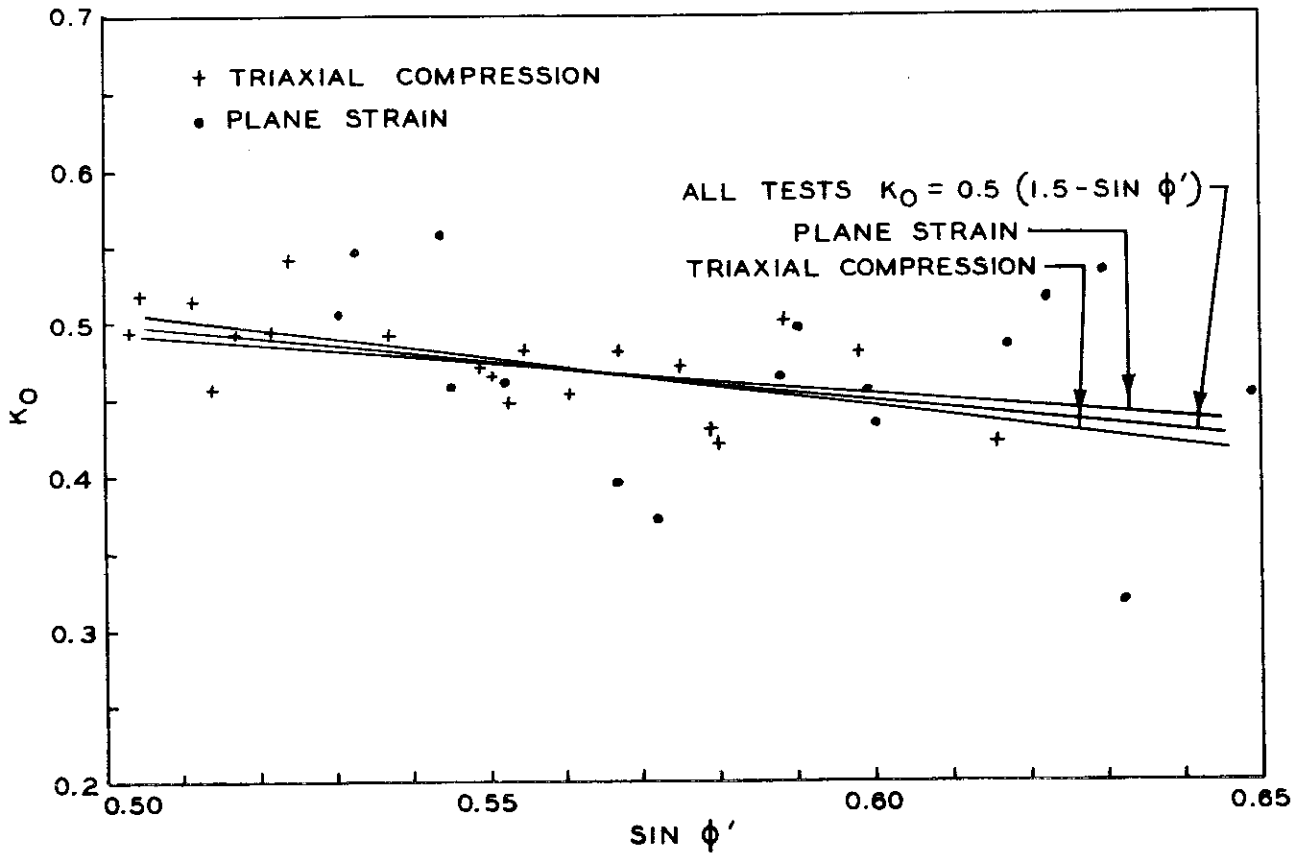

Figure 29. Experimental Relationship Between K_o and sin ϕ'

Table 2. Published Value of K_o on Different Types of Sand

Investigator	Material	K_o	ϕ'
Terzaghi (17)	Dense sand	0.40 - 0.45	
	Loose sand	0.45 - 0.50	
Kjellman (2)	German standard sand	0.5 - 1.5	
Bishop (18)	Dense Brasted sand	0.36	39°
	Loose Brasted sand	0.46	34°
Simon (19)	Dense sand	0.37	
	Loose sand	0.54	
Wade (12)	Dense Belgium sand	0.429	39°
	Loose Belgium sand	0.538	34°
Hendron (20) (as scaled from figure)	Angular sand	0.4 - 0.5	36° - 30°
	Rounded sand	0.32 - .38	34° - 30°

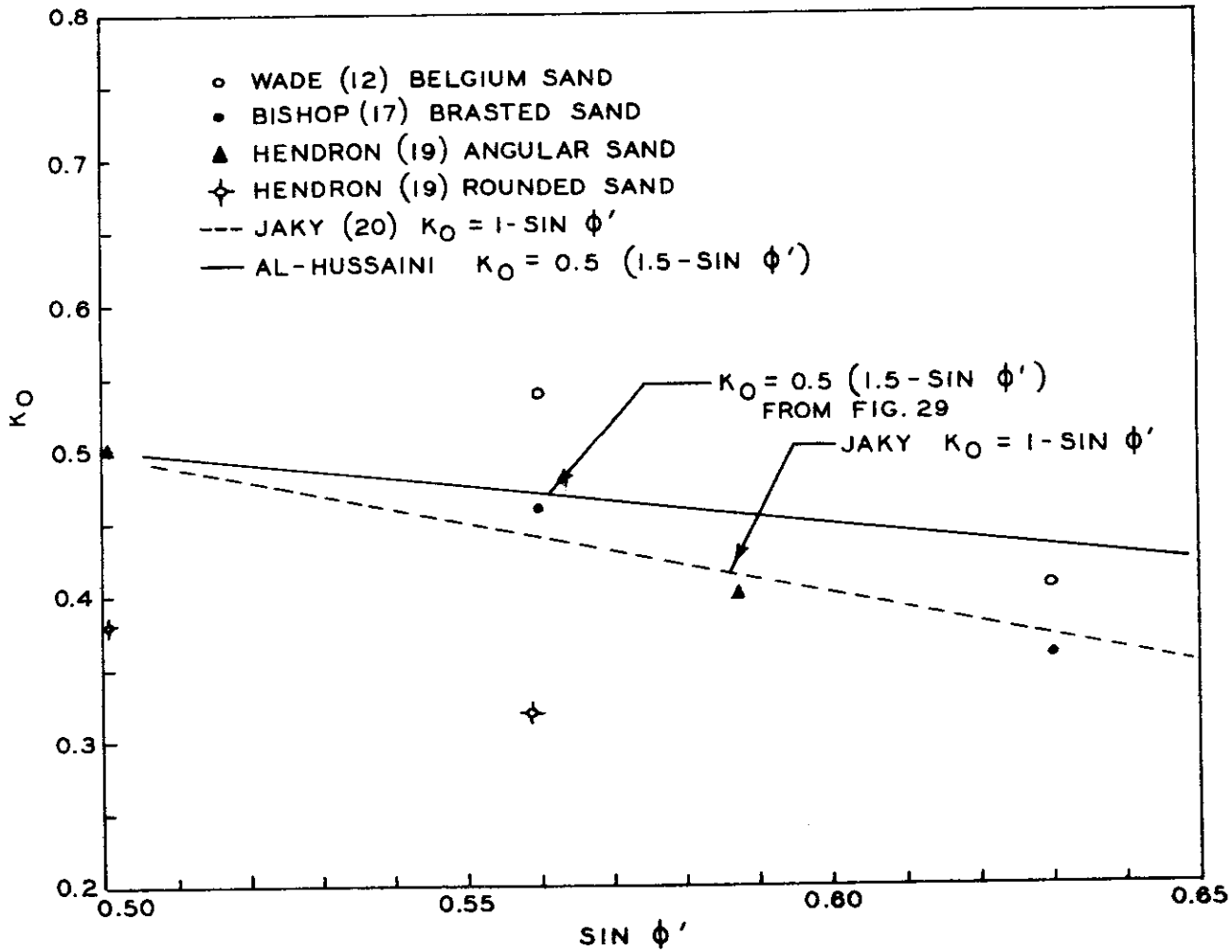

Figure 30. Relationship Between K_o and sin ϕ

Jaky expression underestimates the value of K_o. This indicates that the effective angle of shearing resistance is not a valid parameter to evaluate the value of K_o. Referring back to Figure 19, we can see that the variation of K_o with the initial relative density for plane strain and triaxial tests show two lines approximately parallel, with the value of K_o in the triaxial test slightly higher than in the plane strain test. The difference in the value of K_o may possibly be attributed to the difference in the average thickness of the rubber membrane used in the respective tests. The average thickness of the rubber membrane in triaxial test was 0.025 inch compared with a thickness of 0.050 inch in the plane strain test. This difference in thicknesses may cause different deformation characteristics in the two membranes under the same confining pressure. A possible increase in the deformation of the plane strain membrane would cause the strain indicator to call for an increase in the axial stress to compensate for the lateral deformation when there is no deformation occurring in the sample. Therefore, it may be assumed that the value of K_o is not influenced by the shape of the specimens. The value of Poisson's ratio, ν, can be found from the value of K_o, as shown in equation (8). For Chattahoochee River sand it was found that the value of ν is not particularly sensitive to variations of the relative density, and a value of $\nu = 0.31$ can be considered as an average value.

Modulus of Deformation During Consolidation

The modulus of "deformation" during consolidation may be calculated using the generalized form of Hooke's law for a homogeneous, elastic, isotropic material. From equations (2), (3), and (4), we have, respectively:

$$\epsilon_1 = \frac{\sigma_1}{E} - \frac{\nu}{E}(\sigma_2 + \sigma_3)$$

$$\epsilon_2 = \frac{\sigma_2}{E} - \frac{\nu}{E}(\sigma_3 + \sigma_1)$$

$$\epsilon_3 = \frac{\sigma_3}{E} - \frac{\nu}{E}(\sigma_1 + \sigma_2) \quad .$$

Adding the equations, we get

$$\epsilon_1 + \epsilon_2 + \epsilon_3 = \frac{\sigma_1 + \sigma_2 + \sigma_3}{E} - \frac{2\nu}{E}(\sigma_1 + \sigma_2 + \sigma_3) \quad ,$$

since $\epsilon_1 + \epsilon_2 + \epsilon_3 = \frac{\Delta V}{V}$ for saturated soil during consolidation, and $\sigma_1 + \sigma_2 + \sigma_3 = 3\,\sigma_{oct}$; by substituting and simplifying, we get

$$\frac{\Delta V}{V} = \frac{3\,\sigma_{oct}}{E}(1 - 2\nu)$$

or

$$E = \frac{3\,\sigma_{oct}}{\frac{\Delta V}{V}}(1 - 2\nu) \quad . \qquad (11)$$

The relationship between $\left(\frac{\Delta V}{V}\right)$ and the initial relative density D_r, plotted on arithmetic scale, is shown in Figure 31. The resulting best fit curve was replotted on log-log scale as depicted in Figure 32.

It is of particular interest that the results of previous investigation conducted on Chattahoochee sand by Clough (22) and Domaschuk (23) were in remarkable agreement with the result of the present investigation. The variation of $\left(\frac{\Delta V}{V}\right)$ with respect to σ_{oct} for specimens having equal relative

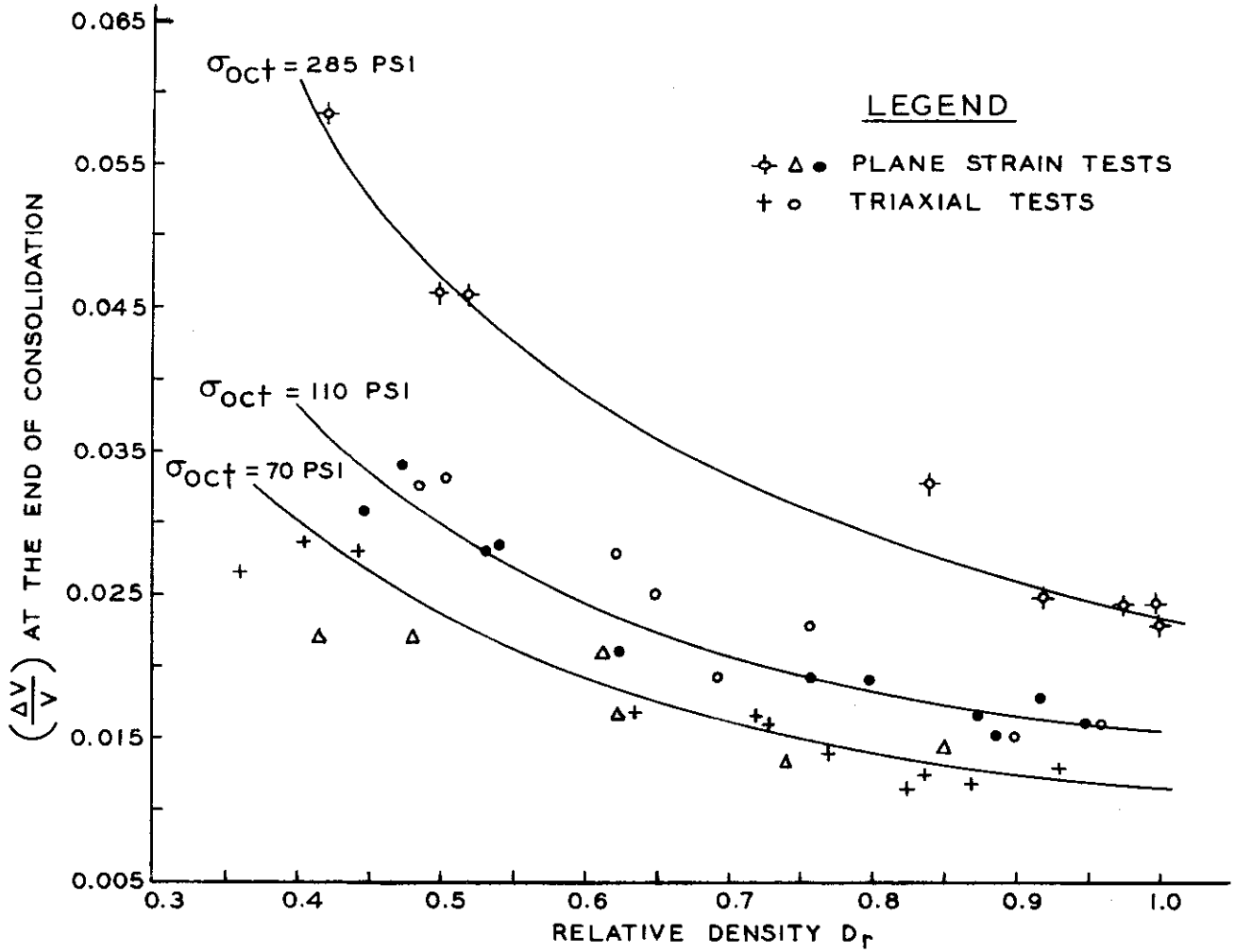

Figure 31. Relationship Between the Volumetric Strain Produced by Consolidation and the Initial Relative Density

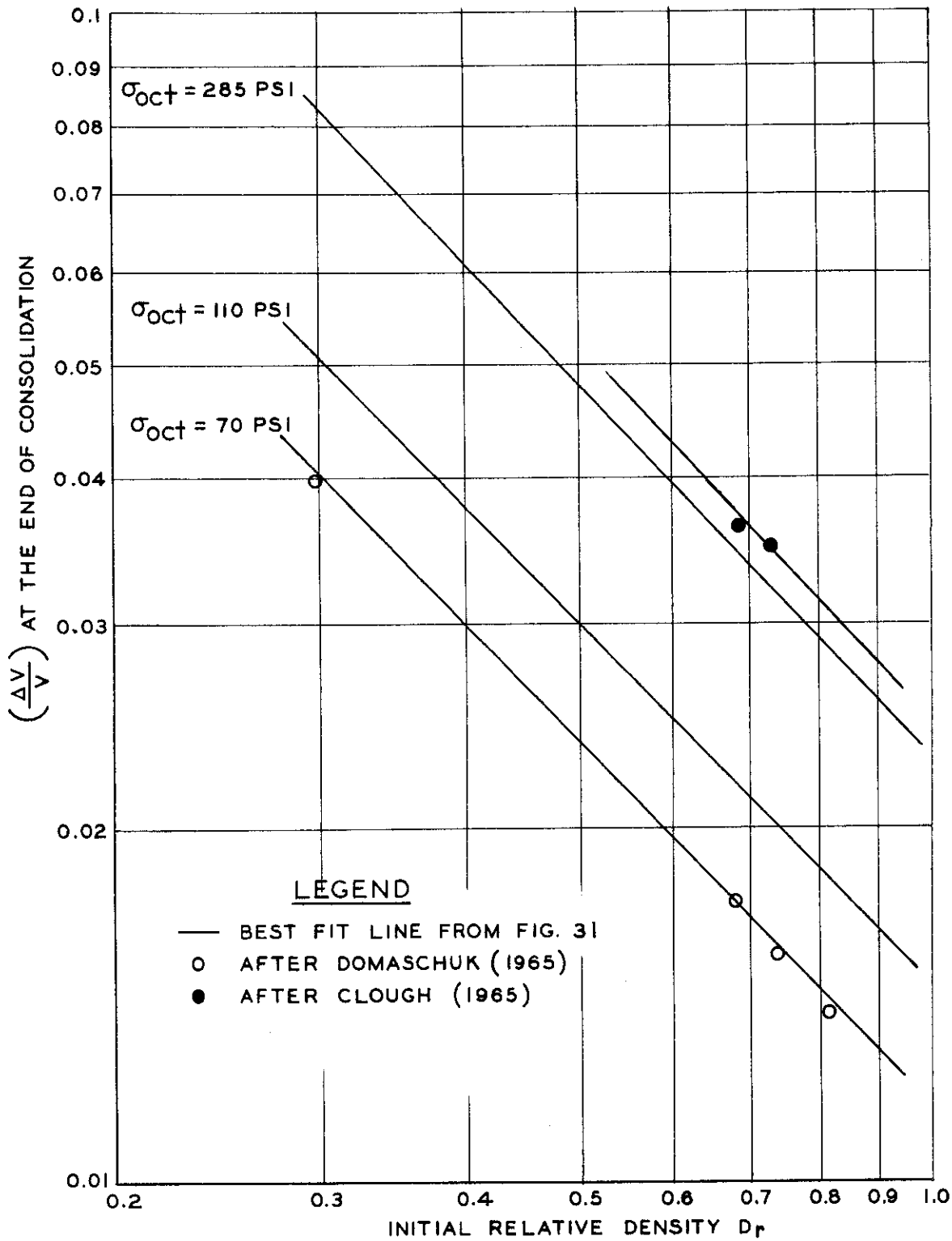

Figure 32. Relationship Between $\frac{\Delta V}{V}$ at the End of Consolidation and D_r

densities is shown in Figure 33.

By using Figures 32 and 33 an experimental equation combining $\frac{\Delta V}{V}$, σ_{oct}, and D_r was obtained. The general form of the equation is as follows:

$$\frac{\Delta V}{V} = c\ (D_r)^a\ (\sigma_{oct})^b \quad , \tag{12}$$

where a, b, and c are constants. By substituting equation (12) into equation (11), we get:

$$E_c = \frac{3}{c}\ (D_r)^{-a} \quad (\sigma_{oct})^{1-b} \quad (1 - 2\nu) \quad , \tag{13}$$

where E_c is the modulus of deformation of sand during consolidation. Average values of a, b, c, and ν for the range of consolidation pressures used were -1.025, 0.4945, 0.00141, and 0.31, respectively. By substituting the respective values of the constants in equation (13) and simplifying, we get:

$$E_c = 808\ (D_r)^{1.025} \quad (\sigma_{oct})^{0.5055} \quad . \tag{14}$$

For simplicity we may consider the final form of equation (14) as

$$E_c = 808\ D_r \sqrt{\sigma_{oct}} \quad . \tag{15}$$

Stress-Strain Relationship

In soil mechanics the stress-strain relationship is usually represented by a plot on arithmetic scale in which the ordinate represents the axial stress or the deviatoric stress and the abscissas represent the axial

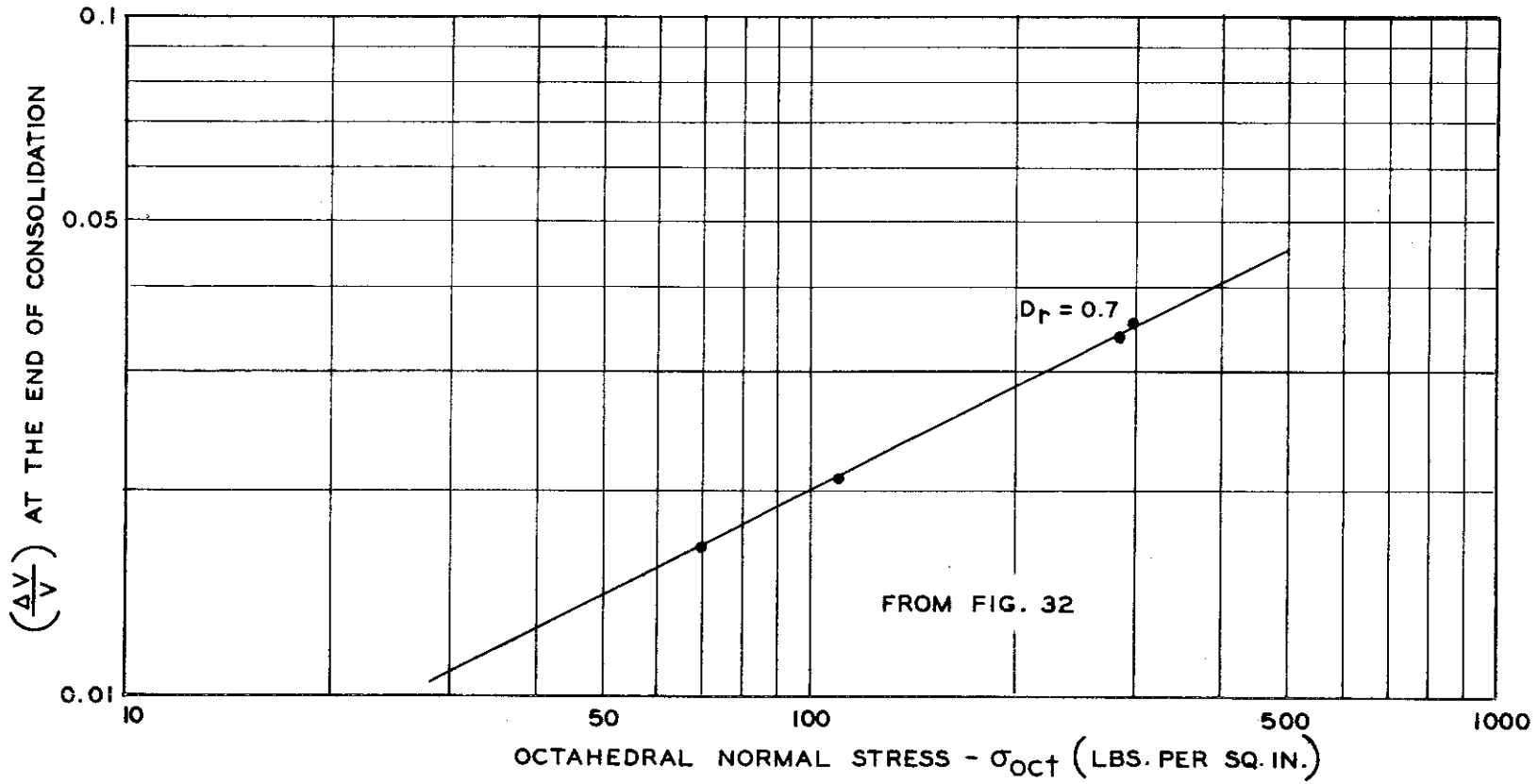

Figure 33. Relationship Between $\frac{\Delta V}{V}$ and σ_{oct} at the End of Consolidation

strain. Except for an initial linear portion, the stress-strain curve is, in general, usually curved throughout most of its length and, as a result, the stress-strain relationship cannot be expressed readily by a single numerical value (e.g., by a modulus of elasticity). Regardless of the non-linearity of the stress-strain curve, it is often used to define some significant physical properties of soil, especially the ultimate strength. However, two parameters have been widely used to study the stress-strain characteristics of soils under a static first loading, the initial tangent modulus, E_i, and the secant modulus, E_s. The initial tangent modulus, E_i, is defined as the stress per unit strain of the straight line portion of the stress-strain curve. The secant modulus is defined as the slope of a straight line joining the origin and a point on the stress-strain curve at some arbitrary value of strain. The tangent modulus represents the modulus of elasticity of the material in linear elasticity since it is obtained from the portion of the curve where stress is linearly proportional to strain.

Many investigators have tried to develop mathematical expressions to define the stress-strain characteristics of cohesionless soils. Kondner and Zelasko (24,25) have developed a hyperbolic function relating the deviatoric stress with axial strain in terms of two parameters which incorporate the tangent modulus and the deviatoric stress. The equation is stated as follows:

$$\sigma_1 - \sigma_3 = \frac{\epsilon_1}{a + b\,\epsilon_1} \quad , \tag{16}$$

where a and b are parameters which depend on the sand tested, the void ratio, and the octahedral normal stress. The equation was derived from the

stress-strain curve of sand tested under triaxial compression with constant octahedral normal stress. Wroth and Basset (26) have developed three exponential equations to describe the shear stress-strain characteristics of idealized sand. The first equation relates the normal stress and the void ratio, the second equation is an energy equation, and the third equation is a strain equation. The development of the concept was not based on real sand, but steel balls 1 mm in diameter tested in a simple shear apparatus. Another theory based on wave velocity and energy dissipation was developed by Duffy and Mindlin (27) to express the stress-strain relationship in granular media. The theory was supplemented by testing small spheres of equal diameter placed in cubical array. The results of the theoretical and experimental tests showed non-linear stress-strain relationships for the elastic spheres. The present investigation showed a linear stress-strain relationship at the beginning of shear which is followed by gradual curvature until failure for both plane strain and triaxial tests. It was found that the initial tangent modulus E_i varies linearly with the initial relative density D_r and exponentially with the maximum consolidation pressure. It was also found that for the same relative density and maximum consolidation pressure, the initial tangent modulus of elasticity of specimens tested in the triaxial apparatus is larger than those tested under plane strain conditions.

Most recently, an extensive study was made under the direction of Sowers (28) to evaluate the modulus of elasticity of sand. Two series of tests were performed. In the first series Jacksonville, Florida sand was used, while in the second series Daytona Beach sand was tested. The results of the test yield the following expression:

$$E = C_1 \sigma_3^{n} \quad , \tag{17}$$

where C_1 and n are a function of $\frac{\sigma_1}{\sigma_3}$, and their values decrease with the increase of $\frac{\sigma_1}{\sigma_3}$.

Another expression for the evaluation of the tangent modulus of sand sheared under confining pressure varies between 210 Kg per square cm. and 633 Kg per square cm. was derived by Clough (21). His experimental study produces the following relationship:

$$E = 180. \sigma_3^{0.61} \quad . \tag{18}$$

Equation (18) implies that the value of the tangent modulus is only a function of the consolidation pressure.

Based on the experimental data collected in this investigation, two expressions relating the initial tangent modulus with the relative density and maximum consolidation pressure have been formulated. The first expression is related to plane strain tests and is expressed as follows:

$$E_i = 1020\ D_r(\sigma_3')^{0.406} \quad . \tag{19}$$

The second expression is concerned with triaxial tests and is stated as follows:

$$E_i = 1100\ D_r(\sigma_3')^{0.533} \quad , \tag{20}$$

where D_r varies between 0.3 to 1.0 and σ_3' ranges between 70 psi and 285 psi.

Comparing equations (19) and (20) with equation (15), we find that the value obtained by equation (15) is between the values obtained from

equations (19) and (20).

It is particularly interesting to note that the research done by Sowers (28) on Jacksonville, Florida sand and Daytona Beach sand, and also the results of Clough (22) and the results of this investigation show that the modulus of elasticity of sand varies exponentially with σ_3'. The results of Sowers show that the constant of proportionality varies linearly with $\frac{\sigma_1}{\sigma_3}$ for a given relative density, while the results of this investigation indicate that it varies only with the initial relative density.

From the above discussion it can be concluded that the modulus of elasticity of sand cannot be expressed by a single value. It is a function of the density, maximum consolidation pressure, and the type of magnitude of deformation allowed.

Equation (15) may be used to estimate the contact settlement beneath an area carrying uniform load. To illustrate the use of equation (15), the following example can be presented:

Example 1: It is required to calculate approximately the contact settlement at the center of a circular area shown in Figure 34. The soil

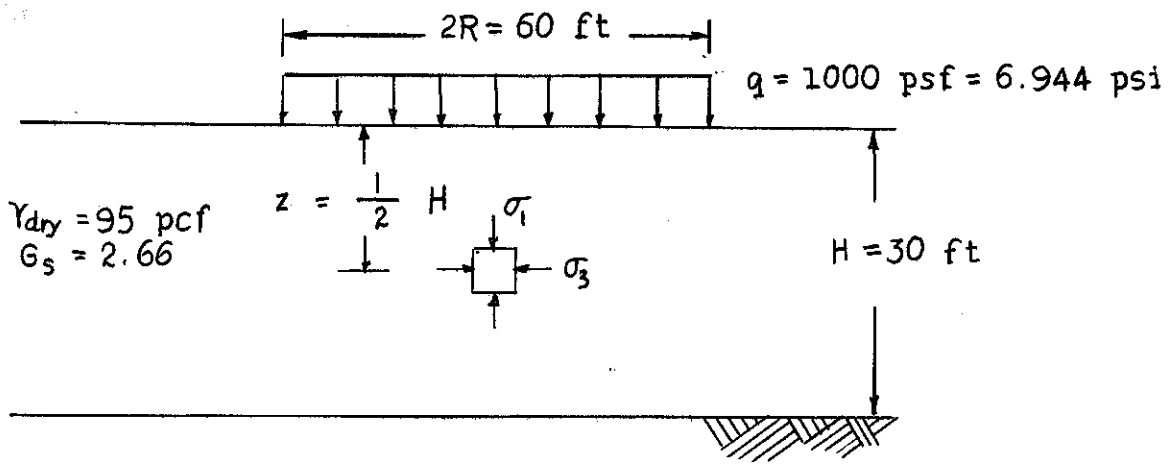

Figure 34. Illustrative Example 1

is medium sand with physical properties similar to that of Chattahoochee River sand and an average unit dry weight of 95 pcf.

Solution:

$$V_s = \frac{\gamma_{dry}}{G_s \times \gamma_w} = \frac{95}{2.66 \times 62.4} \; 0.5723 \text{ ft}^3 \text{ volume of solids}$$

$$V_v = 1 - 0.5723 = 0.4277 \text{ ft}^3 \text{ volume of voids}$$

$$e = \frac{V_v}{V_s} = \frac{0.4277}{0.5723} = 0.7473 \text{ void ratio}$$

$$D_r = \frac{e_{max} - e}{e_{max} - e_{min}} = \frac{1.09 - 0.7473}{1.09 - 0.593} = 0.6895 \text{ relative density}$$

Knowing the value of relative density, the value of K_o can be evaluated from Figure 19 as $K_o = 0.455$.

$$\sigma_1 = 95 \times 15 + 1000 = 2425 \text{ psf} = 16.84 \text{ psi}$$

$$\sigma_3 = \sigma_1 \times K_o = 16.84 \times 0.455 = 7.66 \text{ psi}$$

$$\sigma_{oct} = \frac{\sigma_1 + 2\sigma_3}{3} = \frac{16.84 + 2 \times 7.66}{3} = 10.72 \text{ psi}$$

$$E_i = 808 \, D_r \sqrt{\sigma_{oct}} \qquad (15)$$

$$E_i = 808 \times 0.6895 \times (10.72)^{\frac{1}{2}} = 1824 \text{ psi} \quad .$$

The settlement at the center of the loaded area, w, can be calculated (29) as

$$w = \frac{2(1 - \nu^2)\, q\, R}{E}$$

$$w = \frac{2[1 - (0.31)^2]}{1824} \times 6.944 \times 30 \times 12 = 2.48 \text{ inches.}$$

Answer: Contact settlement at the center is 2.48 inches.

Failure strain will be defined here as the amount of axial strain which the sand undergoes at the peak deviatoric stress. It was found that the failure strain varies with the density, the consolidation pressure and the type of test. For the same relative density and confining pressure, it was found that the failure strain for sand tested under axial symmetry is higher than that tested under plane strain. Similar phenomena have also been observed by Cornforth (10) on Brasted sand, and Wade (12) on Belgium sand. It was also observed that the ratio of failure strain in triaxial specimens to that in plane strain specimens decreases with increases in confining pressure used in this investigation.

Intermediate Principal Stress

During the K_o consolidation stage the value of the intermediate principal effective stress, σ_2', was approximately equal to the minor principal effective stress. Therefore, no difference in the behavior of sand tested under plane strain conditions or axial symmetry was observed. For K_o consolidation the stresses are related by: $\sigma_2' = \sigma_3' = K_o\, \sigma_1'$. During the shear stage the value of σ_2' deviated from that of σ_3' and the variation of σ_2' against ϵ_1 was similar to, but smaller than the variation of σ_1', with respect to the axial strain ϵ_1. The ratios $\frac{\sigma_2'}{\sigma_1'}$ and $\frac{\sigma_2'}{\sigma_1' + \sigma_3'}$ were plotted

against the initial relative density, as shown in Figure 35. It was found that a straight line relationship exists between $\frac{\sigma'_2}{\sigma'_1}$ and $\frac{\sigma'_2}{\sigma'_1 + \sigma'_3}$ at failure with respect to the relative density. The values of $\frac{\sigma'_2}{\sigma'_1}$ and $\frac{\sigma'_2}{\sigma'_1 + \sigma'_3}$ are plotted against the minor principal effective stress, σ'_3, at the end of consolidation, as shown in Figure 36. It was found that the value of σ'_3 at the end of consolidation has no significant effect on the value of $\frac{\sigma'_2}{\sigma'_1}$ and $\frac{\sigma'_2}{\sigma'_1 + \sigma_3}$ at failure. Figure 37 shows the relationship between $\frac{\sigma'_2}{\sigma'_1}$ at failure K_o, and the value of σ'_3. In this plot it can be seen that the value of $\frac{\sigma'_2}{\sigma'_1}$ at failure for dense sand may slightly underestimate the value of K_o. It is found that the value of $\frac{\sigma'_2}{\sigma'_1 + \sigma_3}$ at failure can be empirically correlated with the value of Poisson's ratio, ν. The results of this investigation are in general agreement with the test results carried out in the plane strain apparatus at Imperial College by Cornforth (10) on Brasted sand, and Wade (12) on Belgium sand at confining pressure of 40 psi.

The relationship between the value of $\frac{\sigma'_2}{\sigma'_1 + \sigma_3}$ at failure, the calculated ν, and σ_3 are plotted in Figure 38. In this figure it is shown that the value of $\frac{\sigma'_2}{\sigma'_1 + \sigma_3}$ at failure for dense sand can empirically well estimate the value of Poisson's ratio ν, while for loose sand it may overestimate it. As a result it may be said that the soil is not a perfectly elastic material.

Angle of Shearing Resistance

Sand consists of structural arrangements of small grains of differ-

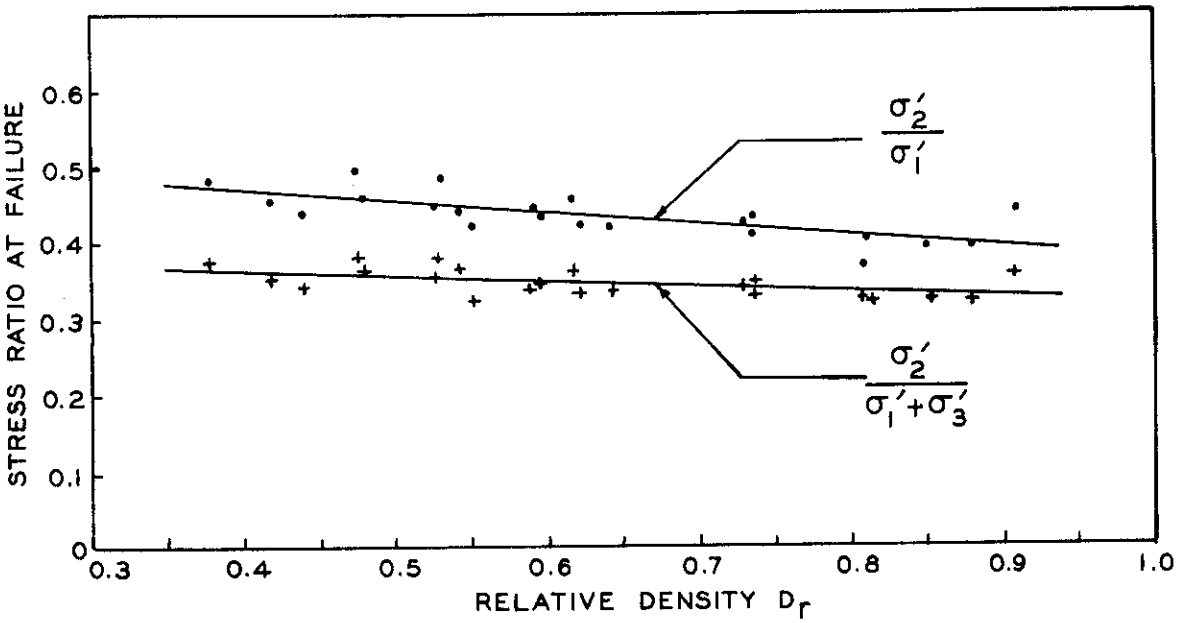

Figure 35. Stress Ratio at Failure Versus Relative Density

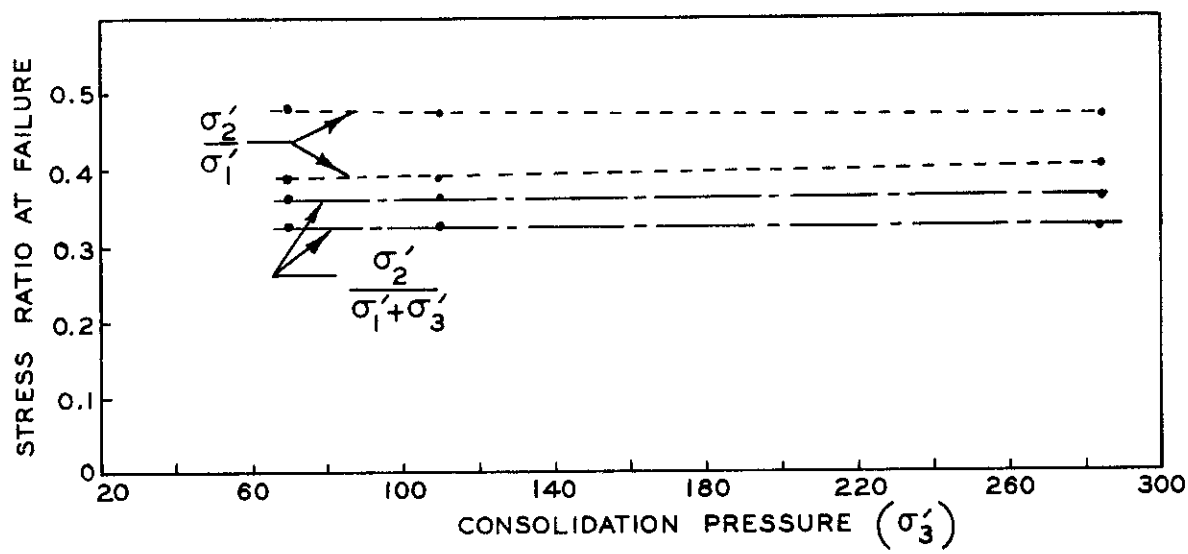

Figure 36. Stress Ratio at Failure Versus Consolidation Pressure

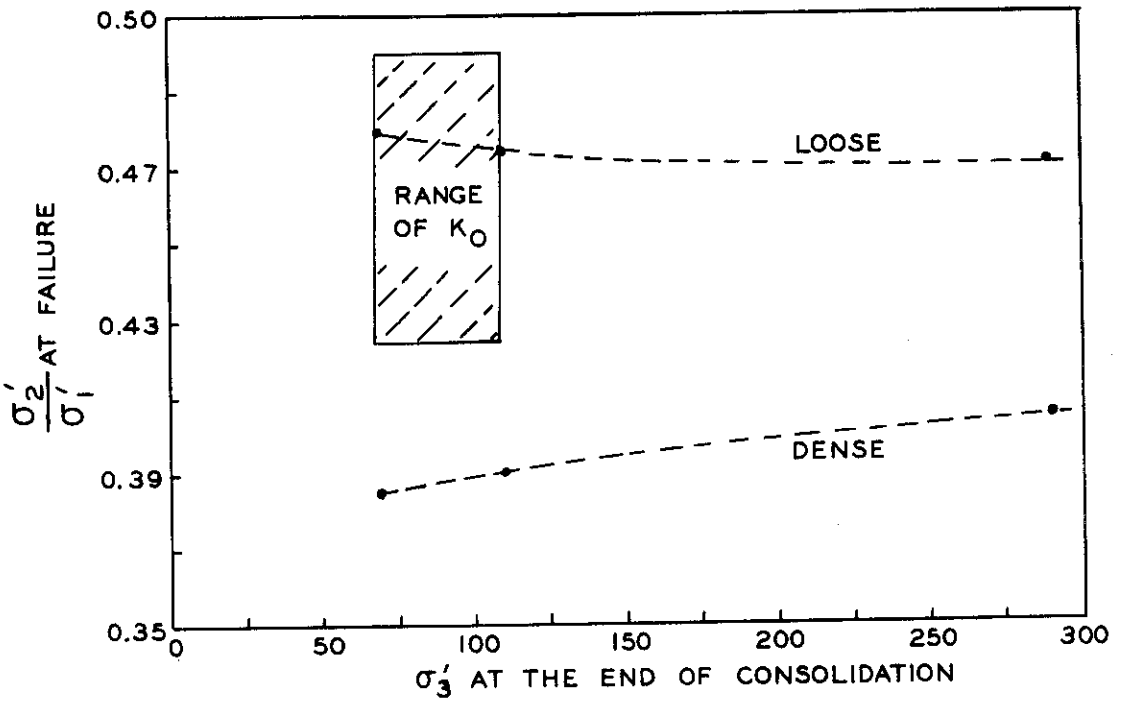

Figure 37. Relationship Between $\left(\frac{\sigma_2'}{\sigma_1'}\right)_f$, K_o, and the Consolidation Pressure

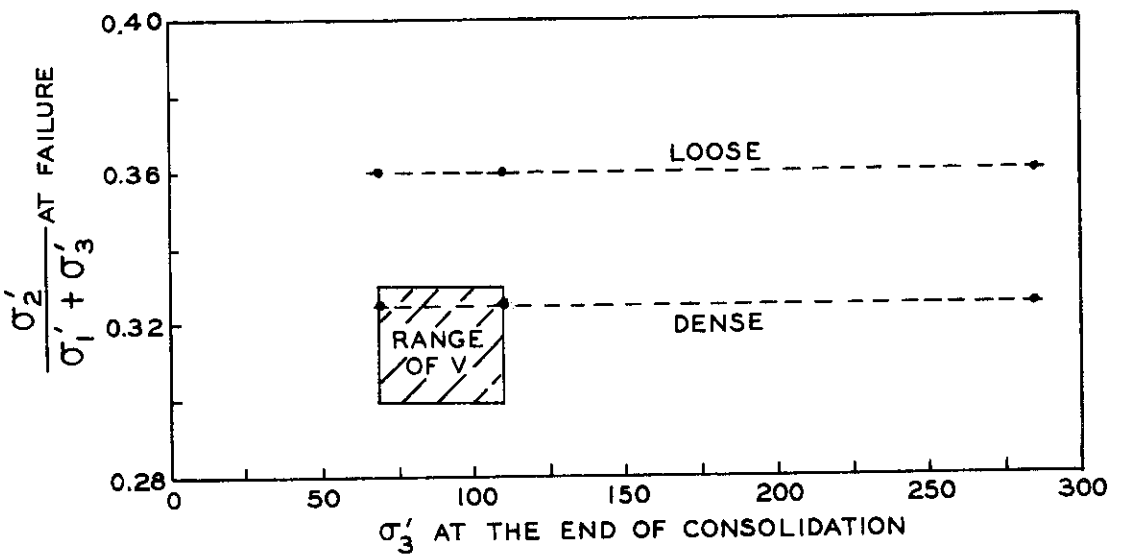

Figure 38. Relationship Between $\frac{\sigma_2'}{\sigma_1' + \sigma_3'}$ at Failure ν, and the Consolidation Pressure

ent size, shape, and mineralogical composition which in turn affect its physical behavior under load. Therefore, sand is a discrete system of particles and not a continuous medium.

When an external load is applied to sand the load will be transmitted to the mass through the points of contact of the grains. The resistance of sand to the external load is commonly associated with movements which are transmitted from one grain to another through the points of contact. The relative movements between the grains is in the direction of the lowest resistance opposing the grains. The movement between the sand grains may be in a form of rolling or sliding which is always associated with shearing stresses developed in the plane of movement. The relationship between the shearing stress, s, and the normal stress, σ_n, according to Mohr's theory for cohesionless material, is given by the relation:

$$s = \sigma_n \tan \phi \quad , \tag{21}$$

where ϕ is the angle of shearing resistance. Therefore, the shearing strength of sand is indicated by the magnitude of angle ϕ. The angle ϕ' as explained in Chapter V, can be calculated from Mohr's theory by $\sin \phi' = \frac{\sigma_1' - \sigma_3'}{\sigma_1' + \sigma_3'}$ for both plane strain and triaxial tests.

Figures 23 to 25 show the relationship between the angle of shearing resistance and the relative density under plane strain conditions. The plot shows that the relationship can be approximated by a straight line whose slope is greatly influenced by the maximum consolidation pressure. It was also found that the value of ϕ' is approximately the same whether the sand was consolidated under K_o conditions or by isotropic compression. This shows that the angle of shearing resistance ϕ' is not influenced by

the method of consolidation.

Figures 26, 27, and 28 illustrate the relationship between ϕ' and relative density for the triaxial test data. The results of the tests also showed a linear relationship between ϕ' and relative density. The variation of ϕ' at the maximum and minimum relative density, with respect to σ_3' is shown in Figure 39. This plot shows that in the range of the relative density used, the angle of shearing resistance is higher in plane strain. It also shows that the angle ϕ' at low relative density does not vary appreciably with respect to σ_3', while ϕ' at maximum relative density decreases with the increase of σ_3' for both the plane strain and the triaxial tests. Published results on the angle of shearing resistance of sand under plane strain and triaxial conditions are summarized in Table 3. The difference in the angle of shearing resistance of plane strain and triaxial tests in this study is in close agreement with the results of Cornforth, Wade, and De Merchant. The relationship between the angle of shearing resistance of different sands under plane strain and triaxial condition, respectively, is depicted in Figure 40. In this figure the results of the tests carried out on Ottawa sand by Whitman (5) and Danish sand by Christensen (4) show that the difference in the angle of shearing resistance of plane strain and triaxial tests for dense sand, as well as dense sand, is almost constant. Such findings are in disagreement with the results of the present investigation.

Comparing ϕ', as measured in terms of effective stresses, versus relative density curves for drained tests with those of consolidated undrained tests, Figure 41, it was found that in both plane strain and triaxial tests, respectively, the ϕ' angle of the consolidated undrained test

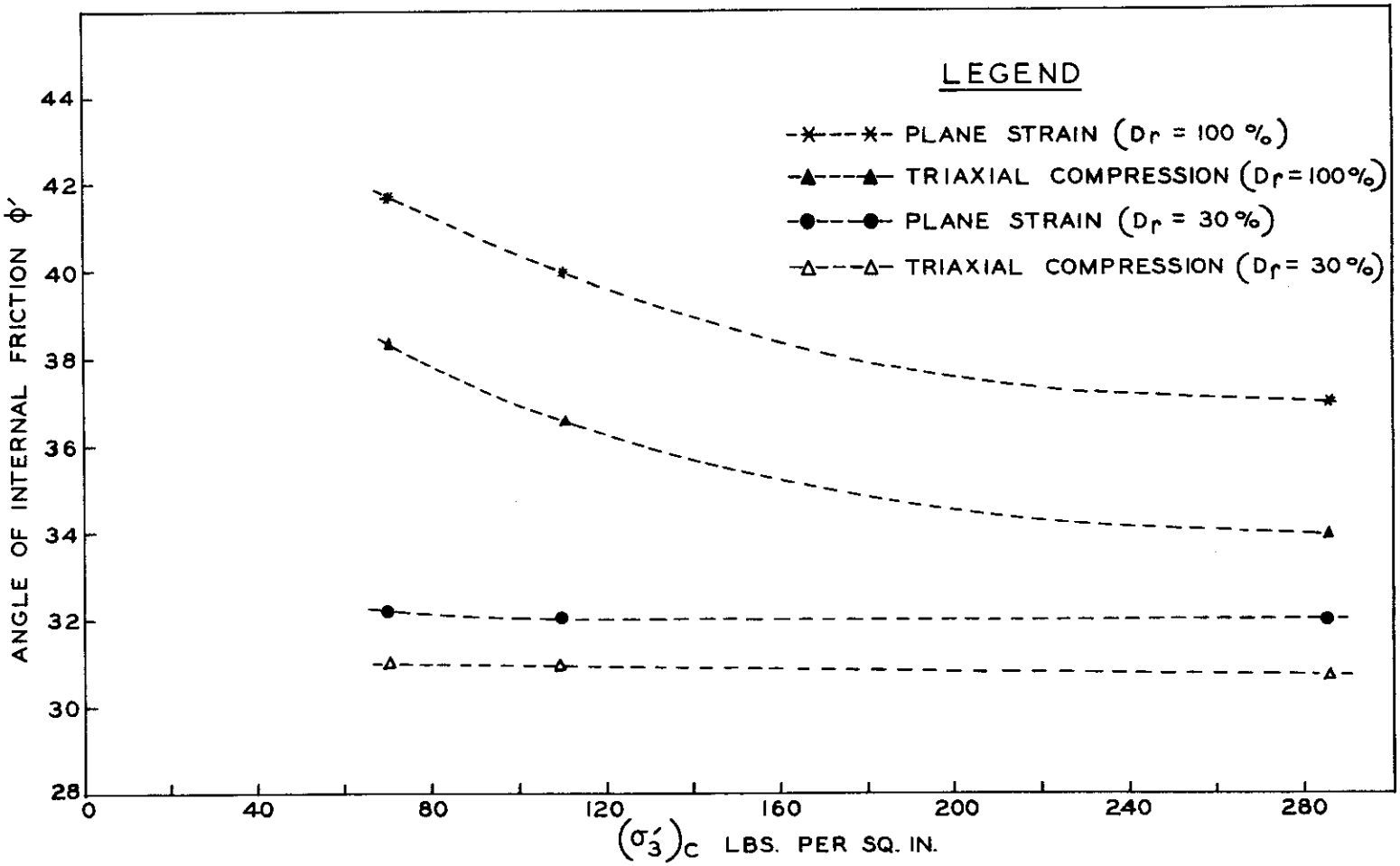

Figure 39. Relationship Between ϕ' and the Consolidation Pressure

Table 3. Summary of Published Data on Sands Tested Under Plane Strain Conditions

Investigator	Material	σ_3' (psi)	ϕ Plane Strain	ϕ Triaxial
Kjellman (2)	German standard sand	24.37	43°	35°
Christensen (4)	Danish G12 sand (dense)		44°	39°
	Danish G12 sand (loose)		33.5°	29.5°
Bjerrum (3)	Valgrinda sand (dense)	12.1	48.5°	45°
	Valgrinda sand (loose)	12.1	38.6°	34.6°
Cornforth (10)	Brasted sand (dense)	40	45°	41.5°
	Brasted sand (loose)	40	35°	33.5°
Whitman (5)	Ottawa sand (dense)	30	42.1°	35.6°
	Ottawa sand (loose)	30	39.3°	33°
Wade (12)	Belgium sand (dense)	40	39°	37°
	Belgium sand (loose)	40	34°	33°
De Merchant (30)	Chattahoochee sand (dense)	40	43°	39°
	Chattahoochee sand (loose)	40	33.7°	33°

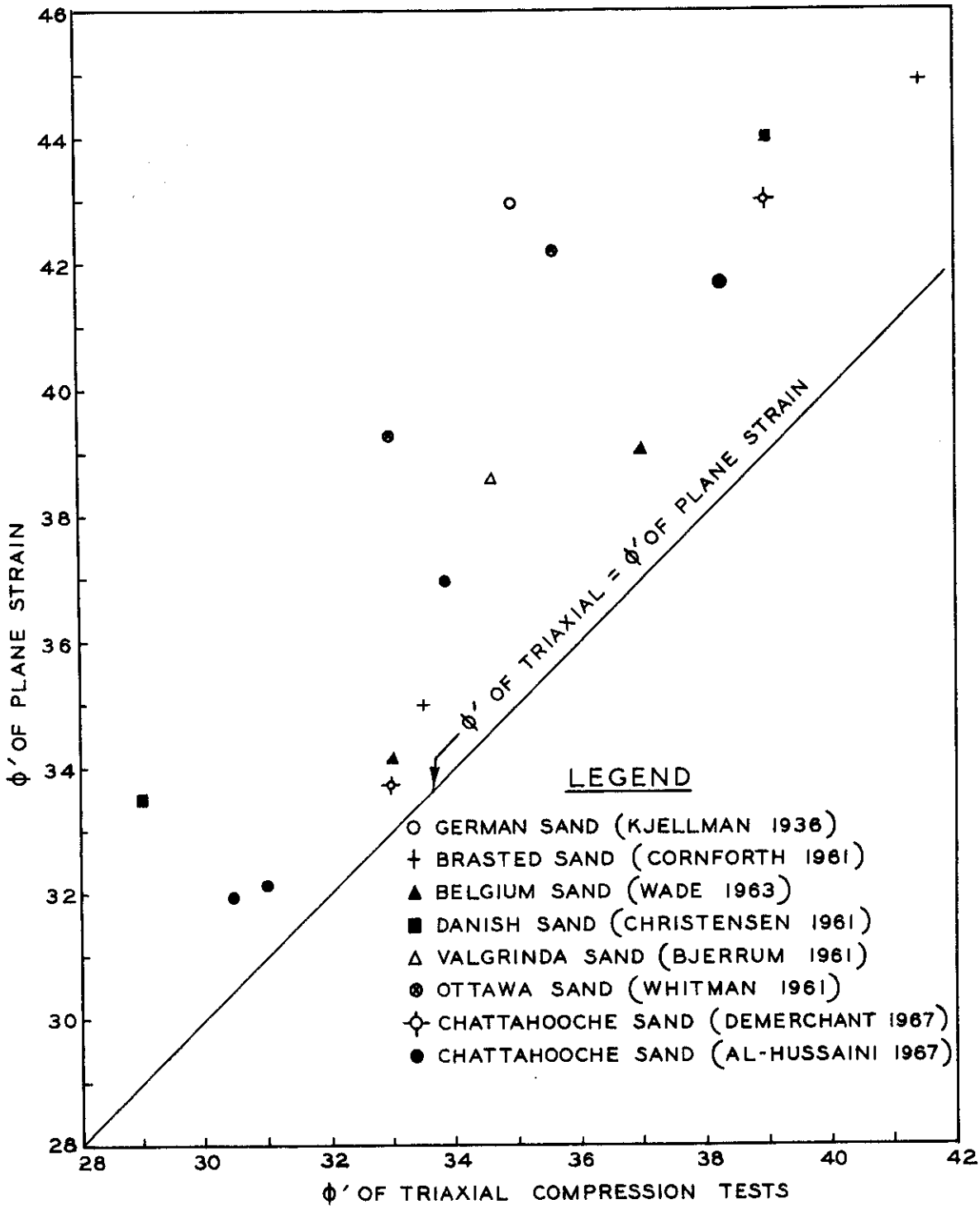

Figure 40. Comparison Between ϕ' of Triaxial Test and ϕ' of Plane Strain Test

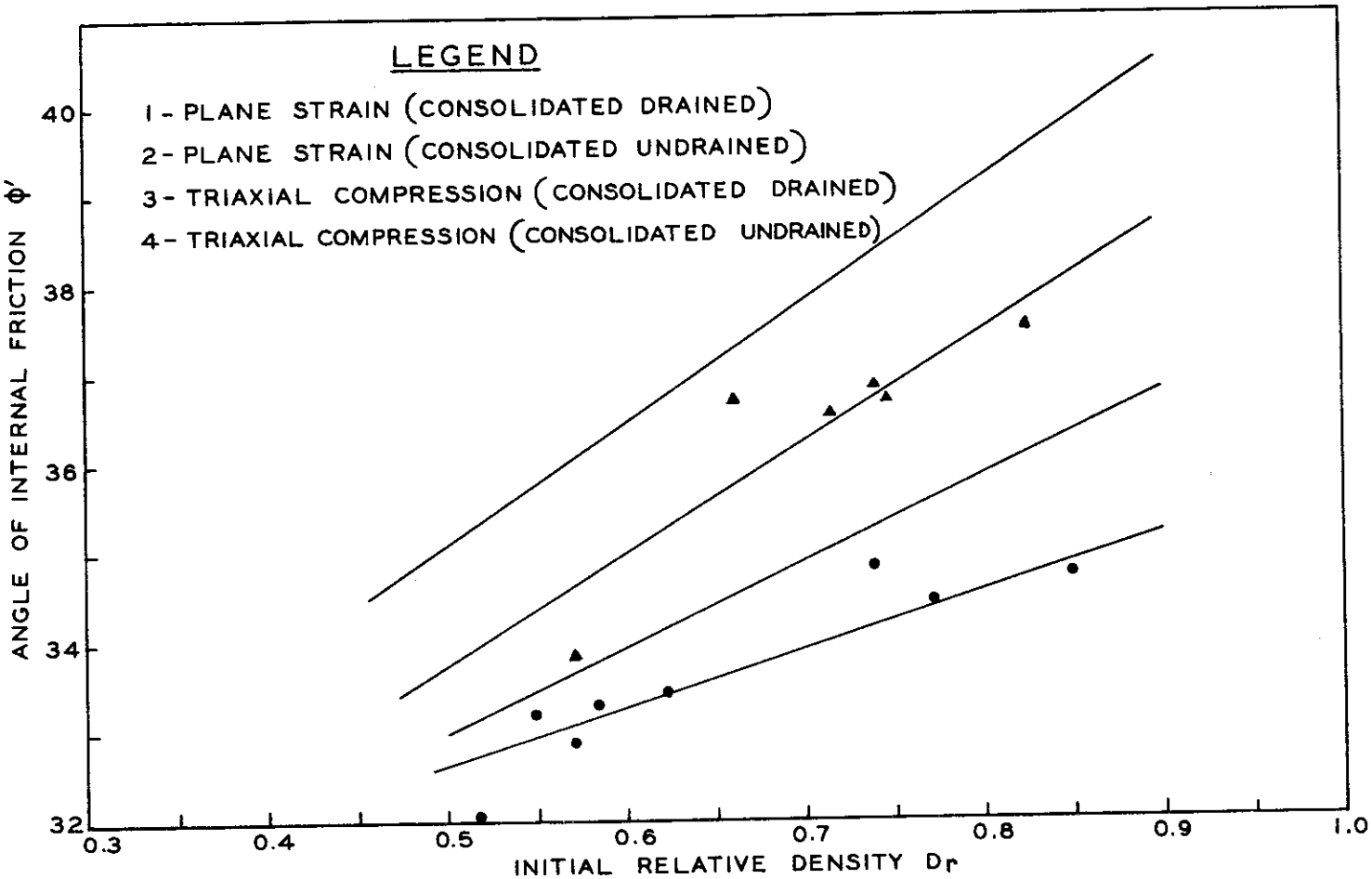

Figure 41. Relationship Between ϕ' for Drained and Consolidated Undrained Tests

is smaller than that of the drained tests at the same relative density and consolidation pressure. In 1948 Taylor (31) observed the same phenomenon in direct shear test results on sand. He assumed that the factors contributing to the difference in the value of ϕ for drained and consolidated undrained tests on sand may be attributed to the strain energy used to overcome interlocking and the strain energy resulting from the change in volume. Taylor suggested that an energy correction should be applied to the laboratory stress-strain relationship in order to obtain the true stress-strain relationship.

In 1954 Bishop (32) applied the concept of a strain energy correction to triaxial test data in which he considered only the part of the strain energy which resulted from the change in the volume to correct the peak deviator stress. Bishop's correction is derived by Poorooshasb and Roscoe (33) and is included here for clarity.

A sample of original volume V is subjected to effective compressive stresses, σ_1', σ_2', and σ_3', causing principal strains ϵ_1, ϵ_2, and ϵ_3 and total volume change ΔV. The total external energy effected by the applied force moved some distance is termed dW, and the change in the internal energy is dE. In triaxial compression $\sigma_2' = \sigma_3'$ and $\epsilon_2 = \epsilon_3$, therefore:

$$dE = \sigma_1' \, d\,\epsilon_1 + 2\,\sigma_3 \, d\,\epsilon_3 \tag{22}$$

$$d\left(\frac{\Delta V}{V}\right) = d\,\epsilon_1 + 2\,d\,\epsilon_3 \tag{23}$$

or

$$d\,\epsilon_3 = \frac{1}{2}\left[d\left(\frac{\Delta V}{V}\right) - d\,\epsilon_1\right] \quad . \tag{24}$$

By substituting equation (24) into equation (22) and simplifying, we get:

$$dE = (\sigma_1' - \sigma_3') \, d\,\epsilon_1 + d\left(\frac{\Delta V}{V}\right) \sigma_3' \tag{25}$$

$$dW = (\sigma_1' - \sigma_3') \, d\,\epsilon_1 \quad . \tag{26}$$

At failure, dW = dE, therefore:

$$(\sigma_1' - \sigma_3') \, d\,\epsilon_1 = (\sigma_1' - \sigma_3')_f \, d\,\epsilon_1 + d\left(\frac{\Delta V}{V}\right) \sigma_3' \quad , \tag{27}$$

or

$$(\sigma_1' - \sigma_3') = (\sigma_1' - \sigma_3')_f + \frac{d\left(\frac{\Delta V}{V}\right)}{d\,\epsilon_1} \sigma_3' \quad . \tag{28}$$

Equation (28) shows that the correction for the peak deviator stress at failure is $\frac{d\left(\frac{\Delta V}{V}\right)}{d\,\epsilon_1} \sigma_3'$.

Bishop suggested the correction should be applied to the observed deviatoric stress to obtain the corrected angle of internal friction. When Bishop's correction was applied to the angles of internal friction for plane strain and triaxial data, Figure 42, the results show that the corrected ϕ for plane strain is still higher than that of triaxial compression and no unique value of ϕ for a given value of relative density is achieved. However, by applying Bishop's correction to the drained tests, relatively good agreement is obtained between consolidated undrained and drained ϕ values, especially for the dense specimens, in both types of tests.

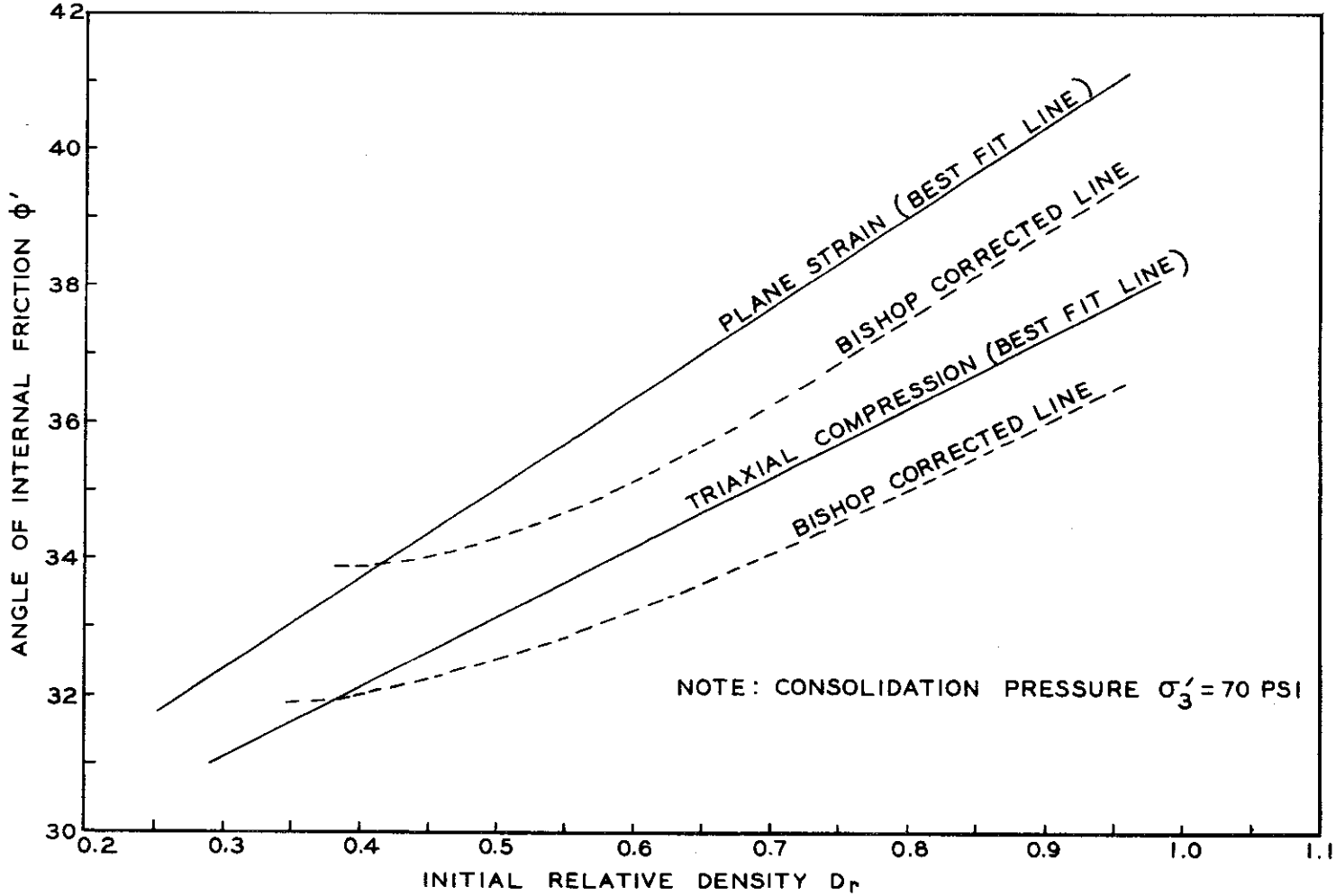

Figure 42. Relationship Between Angle of Internal Friction ϕ Using Bishop Correction and the Initial Relative Density

Poorooshasb and Roscoe showed that Bishop's energy correction is incomplete since the part of strain energy associated with the isotropic condition is omitted from equation (28). They suggested another energy correction for the peak deviatoric stress at failure, which includes the strain energy due to isotropic compression as well as distortion. Their correction for the peak deviator stress is

$$(\sigma_{oct} - r) \frac{\frac{d\,v}{d\,\epsilon_1}}{1 - \frac{1}{3}\frac{d\,v}{d\,\epsilon_1}} \qquad (29)$$

where $v = \frac{\Delta V}{Vo}$, $r = \frac{d\,U}{d\,v}$, where U is the energy absorbed during consolidation. The value of r was assumed to be equal to σ_{oct} at the end of consolidation when the material tends to decrease in volume during shear, and equal to zero for material which increases in volume during shear. It is found that the angle of internal friction of the consolidated undrained plane strain tests is higher than that of consolidated undrained triaxial tests, as shown in Figure 39. This suggests that the Poorooshasb and Roscoe hypothesis also does not give a unique ϕ', since $\frac{d\,v}{d\,\epsilon_1}$ for the undrained test is zero, a fact which makes the suggested correction equal to zero in both plane strain and triaxial tests.

Another method to evaluate the value of ϕ was suggested by De Wet (34). He also assumed that the total energy in sand consists of two components, first the energy stored due to the application of hydrostatic pressure, and secondly, the energy of distortion which acts to overcome the shearing resistance of the particles. He further assumed that failure occurred when

the energy of distortion is equal to the energy stored by the hydrostatic pressure. Finally, he concluded that ϕ could be obtained from the following expression:

$$\sin \phi = \sqrt{\frac{1 - 2\nu}{1 + \nu}} \quad , \tag{30}$$

where ν is Poisson's ratio for sand.

De Wet assumed that hydrostatic stress may cause failure. This assumption had been disproven by Bridgman (35), who showed that hydrostatic stress is responsible only for change in volume of the sample.

The current investigation on Chattahoochee River sand showed that the value of ν is the same for specimens tested under both plane strain and triaxial conditions. Therefore, according to the De Wet hypothesis the value of ϕ should be the same whether the sand is tested under axial symmetry or plane strain conditions, which is not confirmed to be true in these tests. Referring again to Figure 38, it is shown that within the range of the K_o consolidation pressures used (70 psi and 110 psi), σ_3 has no effect on ν; therefore, according to the De Wet hypothesis the value of ϕ should be the same irrespective of the consolidation pressure used. This does not agree with the experimental results.

In 1963 Rowe (36) developed a hypothesis to evaluate the angle of internal friction ϕ in a granular material. The hypothesis was based on interparticle sliding and the relationship between stresses, strains, and volume change of a two-dimensional array of regular spheres. He assumed that the equations derived for ideal spheres can also be applied to random masses of irregular particles. He also assumed that failure occurs when

the internal energy of the soil is a minimum, and the angle of internal friction at failure can be expressed as follows:

$$\frac{\sigma_1'}{\sigma_3'\left[1 + \frac{d\left(\frac{\Delta V}{V}\right)}{d\,\epsilon_1}\right]} = \tan^2\left(45 + \frac{\phi}{2}\right) \quad . \tag{31}$$

Rowe's hypothesis was applied to both the triaxial and plane strain data for specimens consolidated to 70 psi, and results are shown in Figure 43. When Rowe's expression was used to obtain the value of ϕ for the Chattahoochee sand it is found that the value of ϕ for sand tested under plane strain conditions is always higher than ϕ for sand tested under the condition of axial symmetry. Therefore, no unique value of ϕ was obtained in contrast to Rowe's hypothesis. The disagreement between the experimental results and the values determined from Rowe's may possibly be attributed to his assumption that the principal of minimum energy is valid for frictional discrete solids such as sand.

The Mohr envelopes for plane strain and triaxial tests in terms of effective stress are shown in Figures 44 and 45, respectively. The results show that the Mohr envelopes for both types of test are not straight lines. The curvature increases with the decrease of the consolidation pressure. Considering the final portion of the Mohr envelope to be a straight line, the plots show that the angle ϕ for plane strain tests is higher than that for triaxial compression tests. The difference in ϕ is about 4 deg. for dense sand and $1\frac{1}{2}$ deg. for loose sand. The shape of Mohr envelope obtained from triaxial in this test is in general agreement with those obtained by Vesic (37) and Clough (21) when Chattahoochee sand was used. However, as

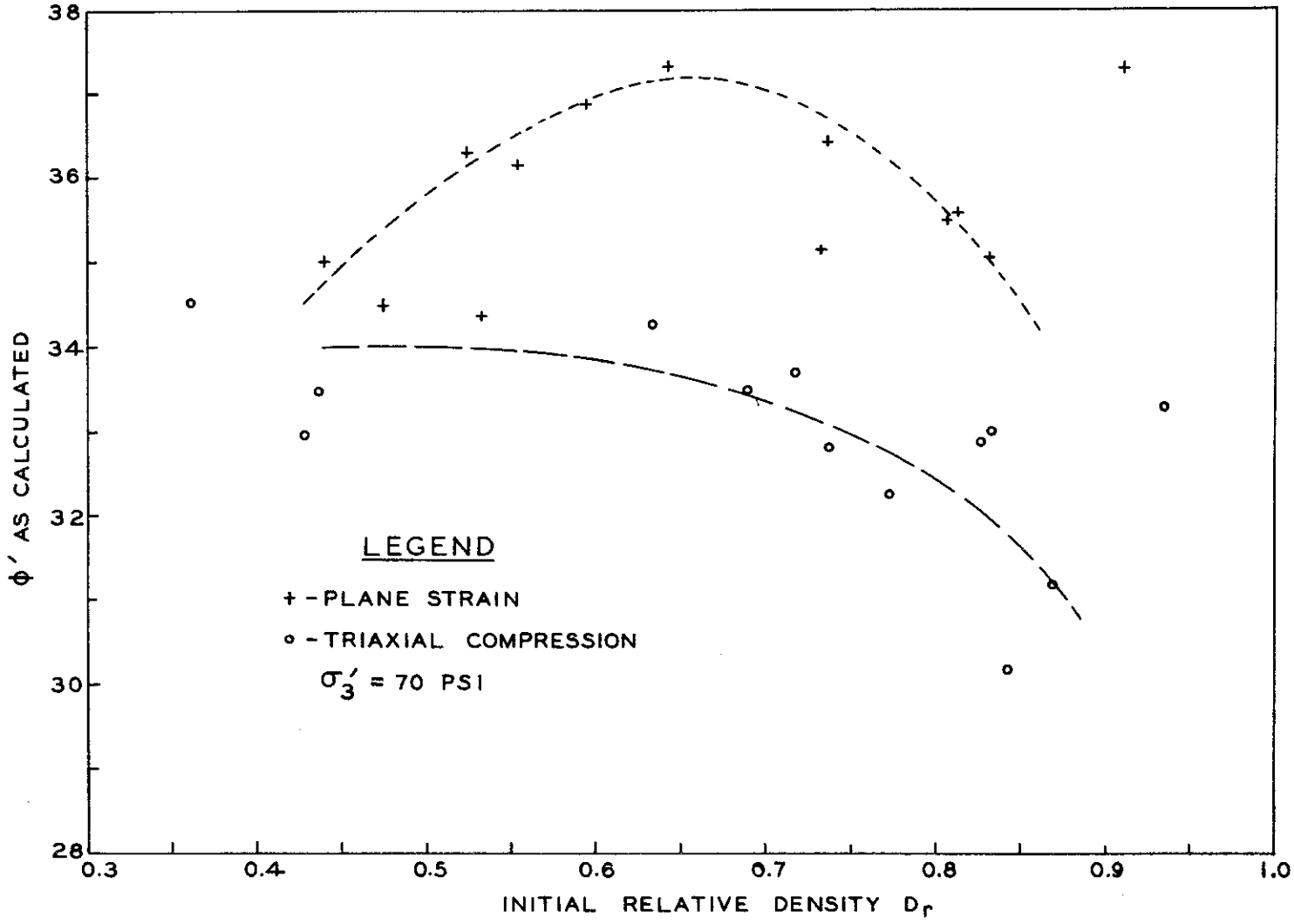

Figure 43. Angle of Internal Friction as Calculated by Rowe's Hypothesis Versus the Initial Relative Density

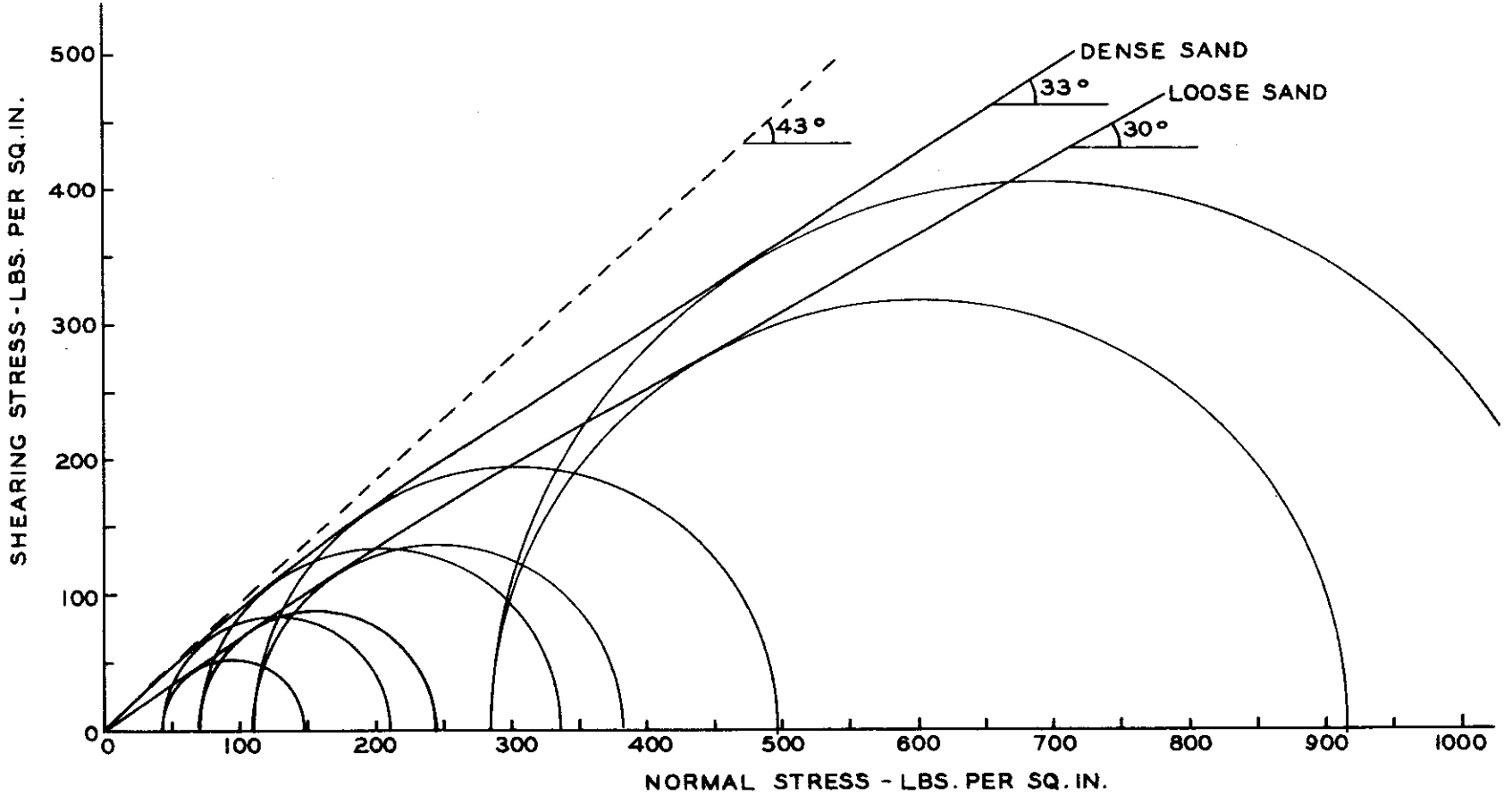

Figure 44. Mohr Envelopes for Plane Strain Drained Tests

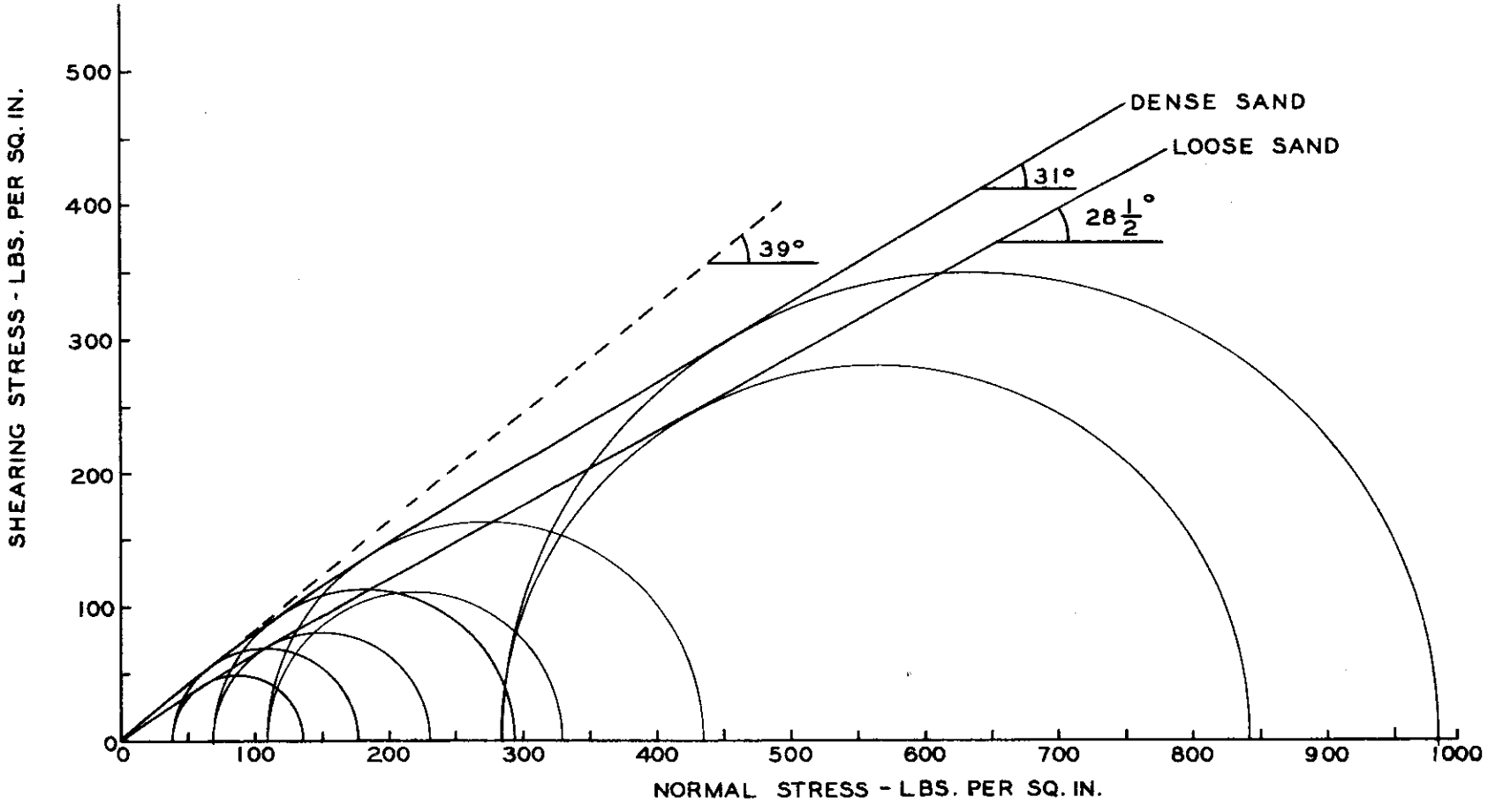

Figure 45. Mohr Envelopes for Triaxial Compression Drained Tests

far as is known there are no published data on the effect of the confining pressure on the angle of internal friction of sand when tested under plane strain conditions.

The difference in the value of ϕ may explain the discrepancies between theoretical results and actual model testing. Among these problems is that of bearing capacity in which the theoretical solution is based on the angle of friction from triaxial tests while the actual problem may be approximated by plane strain conditions. The difference in the value of bearing capacity obtained by using the angle of shearing resistance of plane strain test rather than triaxial compression test can be illustrated in the following example.

Example 2: Calculate the bearing capacity of a continuous strip footing, shown in Figure 46, resting on thick layer of dense sand. The physical properties of the sand are similar to those of Chattahoochee River sand.

Solution:

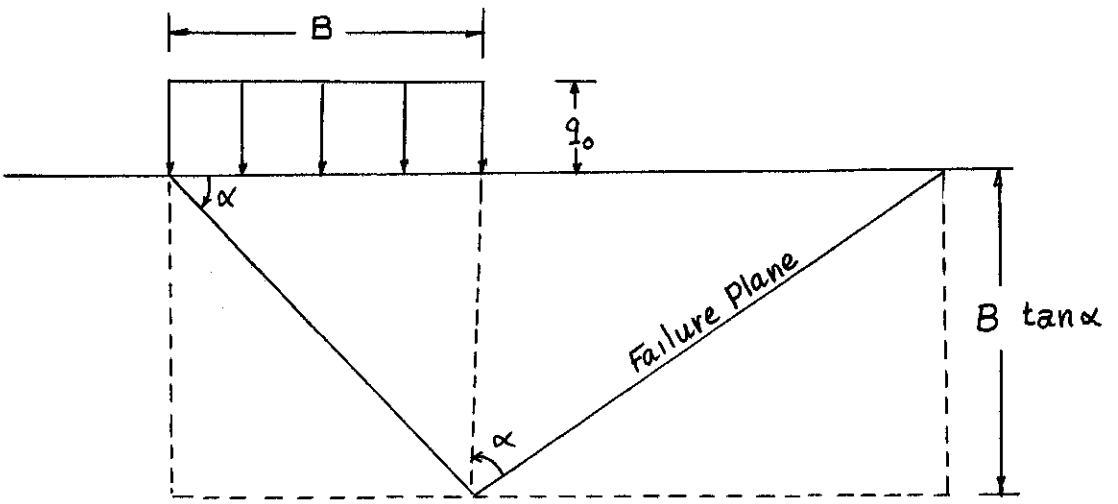

Figure 46. Illustrative Example 2

Since the value of σ_3' is not known, the slope of straight portion of Mohr envelope, shown in Figure 44 ($\phi = 33^\circ$), can be used as a first approximation. The bearing capacity, q_o, is given by:

$$q_o = \frac{1}{2} \gamma B N_\gamma$$

where γ = unit weight of soil

B = width of the footing.

Assuming a straight rupture line (the choice of the bearing capacity theory is not important in this discussion), then

$$N_\gamma = \tan^5 \alpha$$

where $\alpha = 45 + \frac{\phi}{2}$

$$\alpha = 45 + \frac{\phi}{2} = 45 + 16.5 = 61.5$$

$$N_\gamma = 21.188$$

$$q_o = \frac{\gamma}{2} N_\gamma = \frac{100}{2} \times 21.88 = 1059.4 \text{ psf}$$

$$\sigma_3 = \frac{\gamma}{2} N_\gamma = \frac{100}{2} \times 1.8417 = 92.08 \text{ psf} = 0.64 \text{ psi} \quad .$$

Since the value of σ_3 is very small, the straight portion of the envelopes close to the origin of Figures 44 and 45 can be used to obtain the value of ϕ.

ϕ for plane strain test = 43°

ϕ for triaxial test = 39°

The bearing capacity calculated in terms of plane strain ϕ is

$$q_p = \frac{\gamma B}{2} \tan^5 \left(45 + \frac{\phi}{2}\right) = \frac{100 \times 6}{2} (\tan 66.5)^5 = 300 \times 64.34 = 19302 \text{ psf} .$$

The bearing capacity calculated in terms of triaxial ϕ is

$$q_t = \frac{\gamma B}{2} \tan^5 \left(45 + \frac{\phi}{2}\right) = \frac{100 \times 6}{2} (\tan 64.5)^5 = 300 \times 40.50 = 12150 \text{ psf}$$

$$\frac{q_p}{q_t} = \frac{19302}{12150} = 1.589 .$$

In conclusion, the increase in the angle of shearing resistance by 4^o increases the bearing capacity by more than 50 percent.

Volume Change During Shear

During the shear stage the change in volume of the sand was measured by the amount of water expelled from the specimen. The percentage change in volume was presented as the ratio of the change in the volume to the volume at the beginning of the shear stage. This dimensionless ratio, $\frac{\Delta V}{V}$, is termed volumetric strain. The volumetric strain is considered here to be negative when the sand decreases in volume and positive when the sand expands. Typical volumetric strain versus axial strain relations is shown in Figure 21. The volumetric strain is composed of components, that due to reorientation of the grains, that due to distortion of the grains, that due to crushing of the grains, and that due to the shearing of the soil mass. These strain components are influenced by two stress components, the isotropic stress and the shear stress. The isotropic stress always causes a decrease in the volume of the sand. The effect of confining pressure on volumetric change in the conventional triaxial shear was studied by Clough (22)

and the results are presented in Figure 47. This figures shows that the volume change starts immediately after applying the load. Initially the rate of volume change in loose specimens is higher than in dense specimens. As the confining pressure is increased the rate of volume change for dense and loose specimens comes close together until it is approximately the same. An increase of the confining pressure is always associated with crushing of the grains. At low confining pressures the crushing of grains has negligible effect on volume change but at high pressures there can be a considerable volume change resulting from the crushing of grains.

Grain size distribution of Chattahoochee River sand before testing and after shearing at 110 psi confining pressure is shown in Figure 17. The curves show that some breakdown of particles took place during the test; however, the effect on the general physical properties of sand may be neglected because the grain size distribution before and after the test is almost the same. The change in volume associated with shear stresses can be either positive or negative, depending on whether the specimen volume increases or decreases during shear. Dense sand generally exhibits an increase in volume during shear at low confining pressures, while loose sand tends to decrease in volume. Therefore, the net volume change in sand is a combination of the volume change caused by isotropic stress, shearing stress, and reorientation of the grains. The net volume change in loose sand at failure is always negative since the components of volume change cause a decrease in the volume. In dense sand the volume change may be positive only when the increase of volume due to shear stresses is higher than the decrease of volume due to isotropic stress.

Figures 48 and 49 show the experimental results between the void

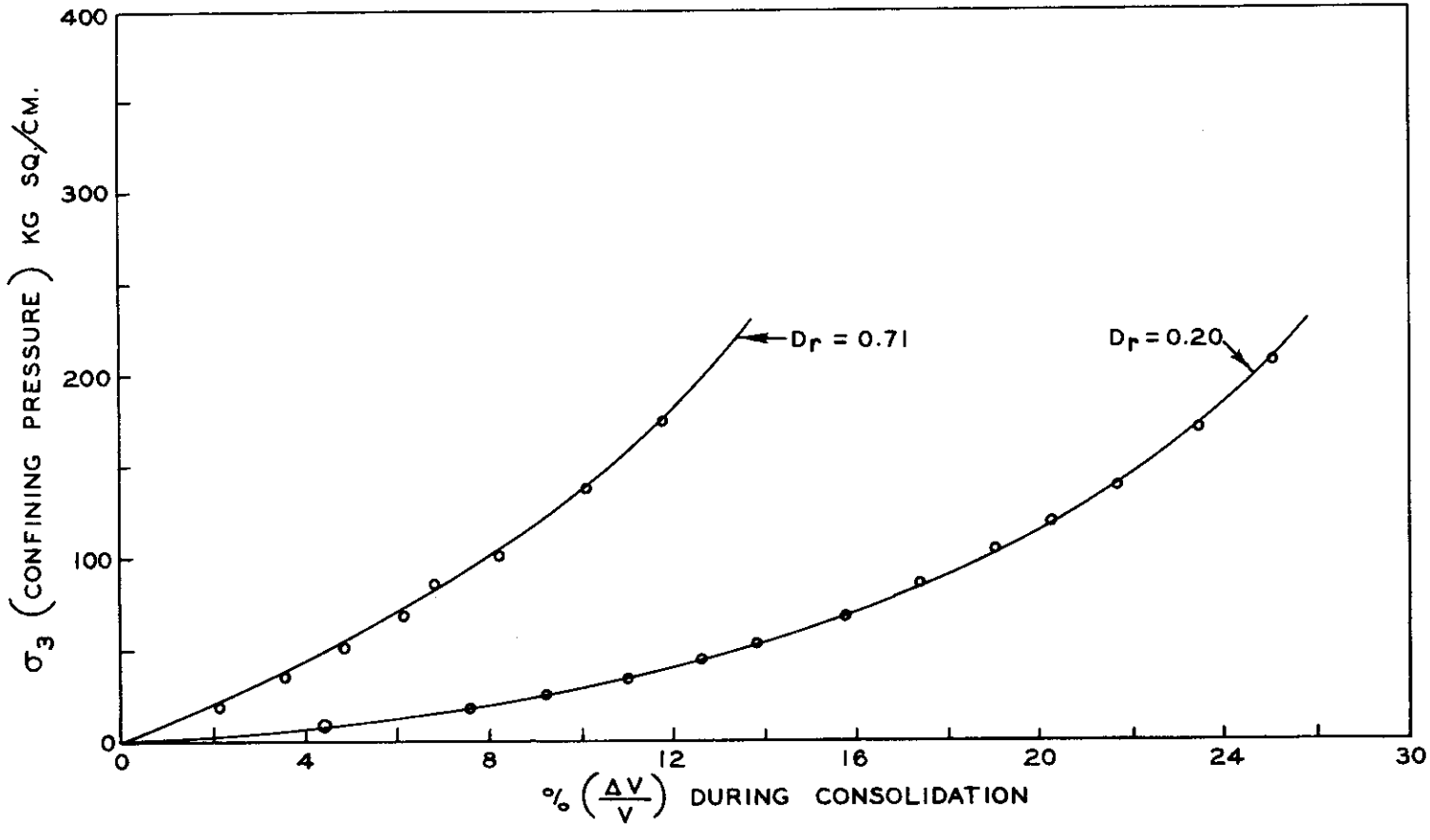

Figure 47. Relationship Between the Confining Pressure and the Volumetric Strain After Clough 1965

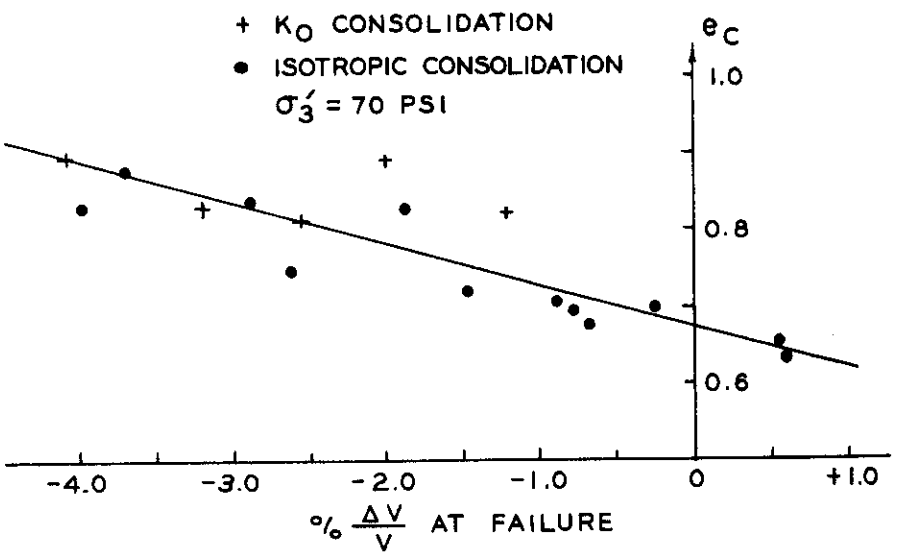

Figure 48. Relationship Between Void Ratio at the End of Consolidation and Volumetric Strain at Failure in Triaxial Test

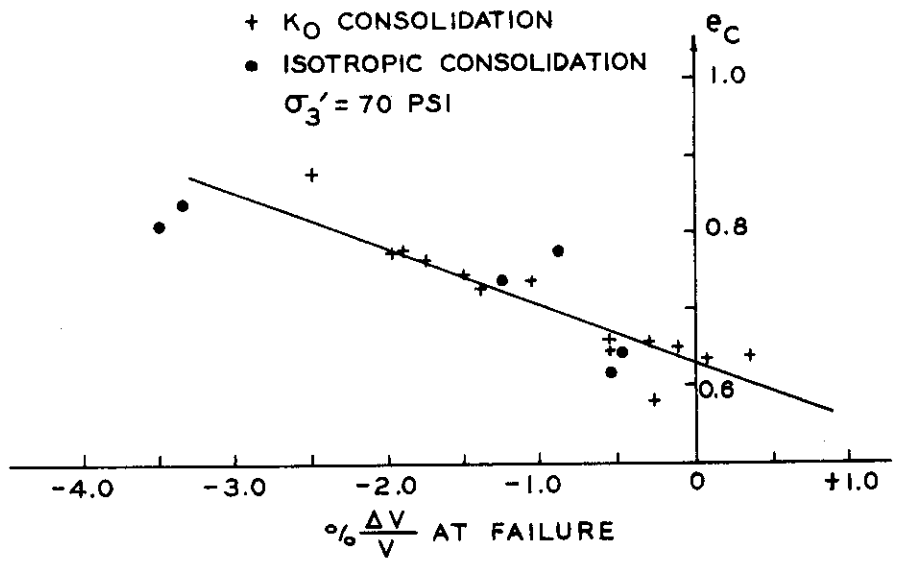

Figure 49. Relationship Between e_c and $\left(\frac{\Delta V}{V}\right)f$ in Plane Strain Test

ratio at the end of consolidation and volumetric strain at failure for a consolidation pressure of 70 psi. Although the scatter of the results makes it difficult to define the relationship between e_c and $\frac{\Delta V}{V}$, nevertheless the general trend can be approximated by a straight line. The results show that the volume change at failure is almost the same whether the sand was consolidated under isotropic conditions or K_o consolidation for both plane strain and triaxial specimens. The point at which the curve corsses the ordinate is considered to be the critical void ratio at which there is no volume change in sand at failure. Figure 50 compares the relationship between the critical void ratio and the consolidation pressure of plane strain and triaxial tests. The graphs show for the range of the pressure used that the critical voil ratios in triaxial specimens are higher than those of plane strain specimens. Figure 50 shows that there is a certain limiting consolidation pressure beyond which the volume change may always be compression at failure regardless of how high the density of sand is during shear. It is shown that this limiting pressure depends on the type of tests performed.

Figure 51 shows the relationship between the volumetric strain at failure and the consolidation pressure for all ranges of density. The plot shows that sand tested under triaxial conditions has higher positive volumetric strain than sand tested under plane strain conditions. Similar observation was noticed by Cornforth (10) at Imperial College on Brasted sand. Such phenomena predict higher positive pore pressures in plane strain compared with triaxial specimens if the sand is subjected to undrained conditions. This assumption was verified by several consolidated undrained tests in both triaxial and plane strain and the results are shown in Figure 52.

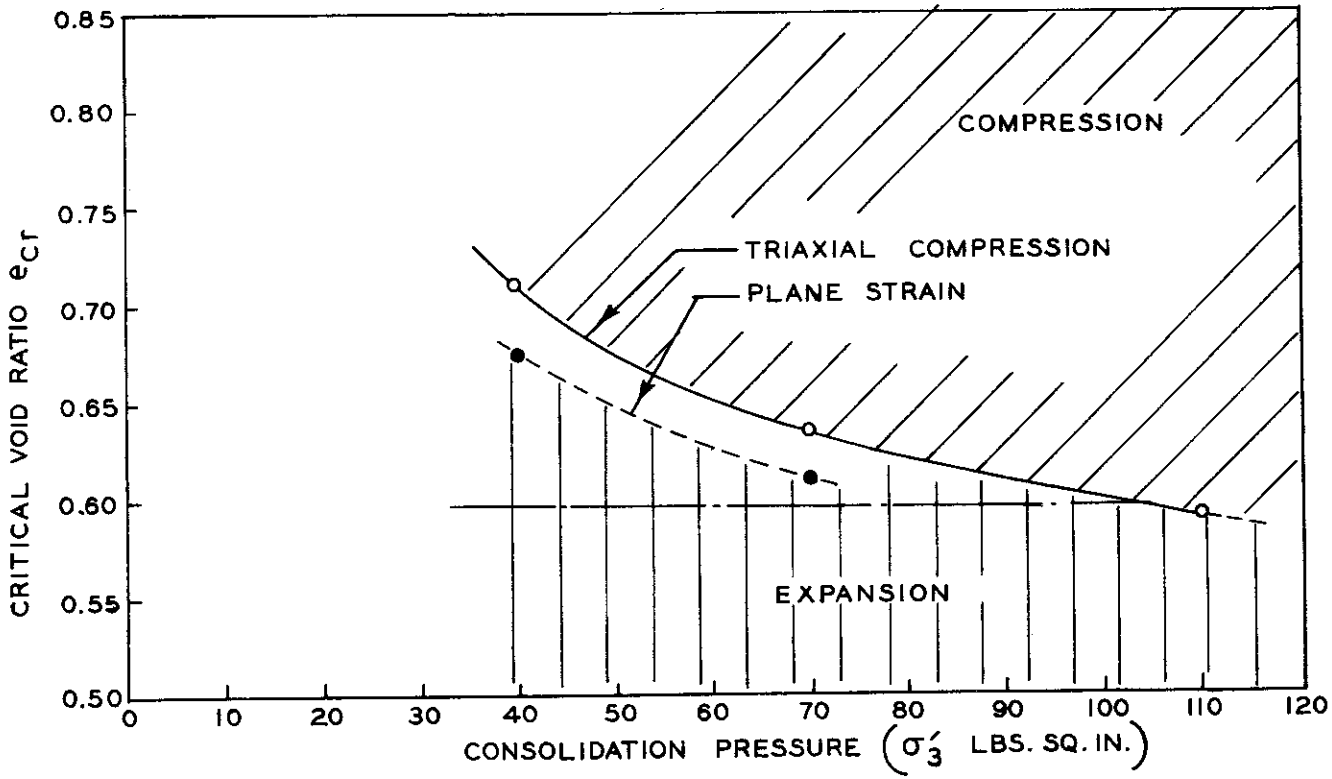

Figure 50. Relationship Between the Critical Void Ratio and Consolidation Pressure

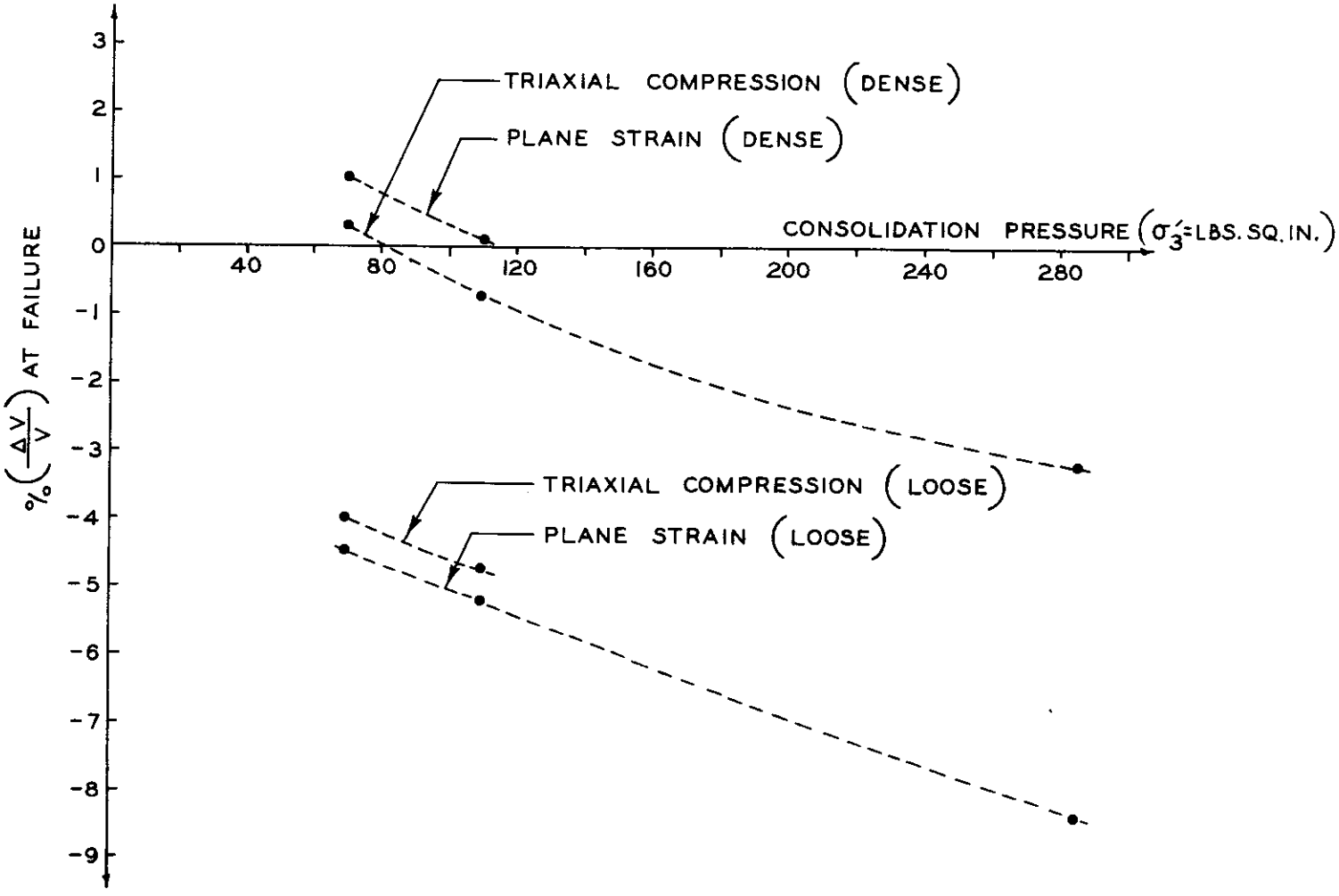

Figure 51. Relationship Between $\frac{\Delta V}{V}$ at Failure and the Consolidation Pressure

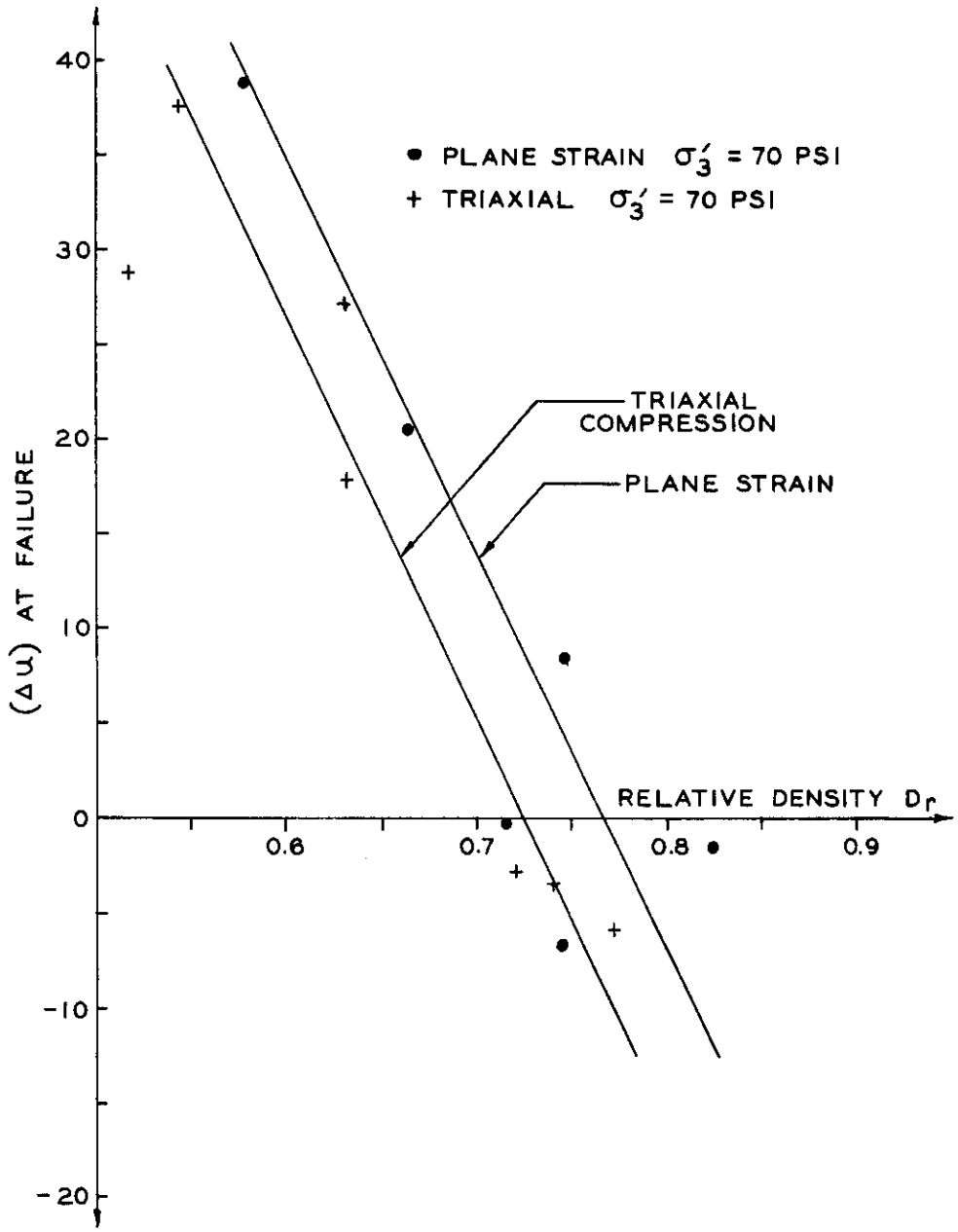

Figure 52. Relationship Between Pore Pressure at Failure and the Relative Density

However, more consolidated undrained tests are needed on different types of sand to specifically confirm this assumption.

Failure Surface

It can be assumed that the state of stress at a point of an elastic and isotropic material is symbolized by the three principal effective stresses, σ_1', σ_2', and σ_3', as shown in Figure 53. The stress vector acting on the octahedral plane can be resolved into two components. The first is normal to the octahedral plane, and the stress associated with it is the octahedral normal stress and can be expressed in terms of principal stresses as:

$$\sigma_{oct} = \frac{1}{3} (\sigma_1' + \sigma_2' + \sigma_3') \quad . \tag{32}$$

The second is associated with the shearing stress acting on the plane, is called the octahedral shearing stress, and can be expressed as:

$$\tau_{oct} = \frac{1}{3} \sqrt{(\sigma_1' - \sigma_2')^2 + (\sigma_2' - \sigma_3')^2 + (\sigma_3' - \sigma_1')^2} \quad . \tag{33}$$

Thus, state of stress can be represented in terms of σ_{oct}, τ_{oct}, and an angle.

To formulate the shape of failure surface in three-dimensional stress space, many experimental points with different combinations of σ_1', σ_2', and σ_3' at failure are needed. Since the available data are not sufficient to develop the complete failure surface, the data will only be compared with some of the existing theories of failure. In order to simplify the presentation, only the intersection of the hypothesized failure surfaces with the

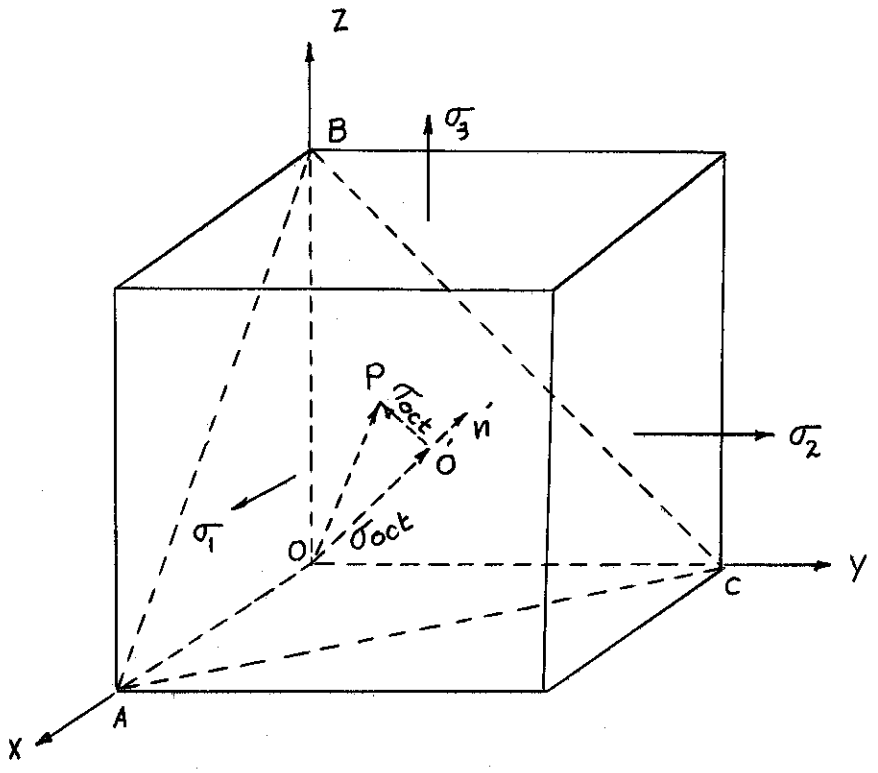

Figure 53. State of Stress Represented in Coordinate System

octahedral plane will be considered. The size of the failure surface on the octahedral plane depends on the value of the octahedral normal stress. Therefore, to make a valid comparison the experimental points should be projected on the same octahedral plane. It was found convenient to project the test results onto a plane having an octahedral normal stress equal to unity. To accomplish this objective all the stresses should be divided by σ_{oct} with the resulting values termed reduced stresses. Referring to Figure 53, we can say that any point P in the octahedral plane can be represented in a cylindrical coordinate system by radius r = OP and angle θ, where θ is the angle between the radius r and projection of the major principal axis on the octahedral plane, as shown in Figure 54.

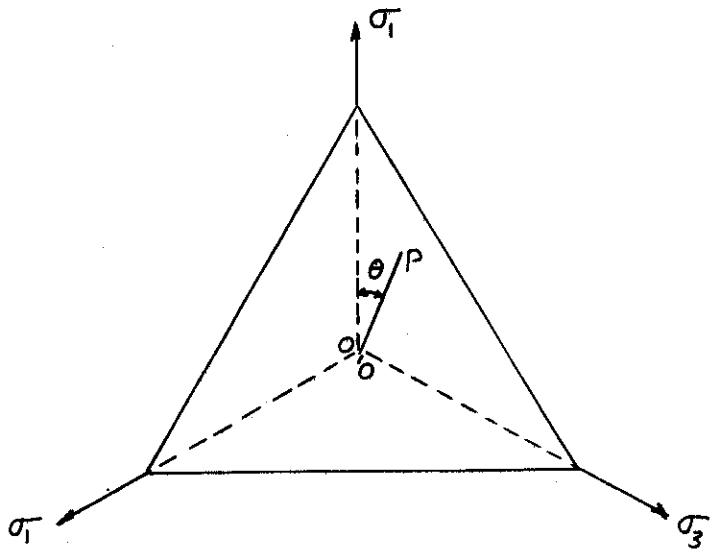

Figure 54. State of Stress in the Octahedral Plane

If we assume that the material is isotropic, then θ can be measured from any of the principal stress axes. The value of θ can be shown to be equal to:

$$\theta = \arctan \sqrt{3} \frac{(\sigma_2' - \sigma_3')}{(\sigma_1' - \sigma_2') - (\sigma_3' - \sigma_1')} \quad , \qquad (34)$$

and the numerical value of r is equal to $\frac{\tau_{oct}}{\sigma_{oct}}$. Therefore, by knowing the value of θ and $\frac{\tau_{oct}}{\sigma_{oct}}$, the experimental points can be readily plotted in the three-dimensional coordinate system. Four tests were selected for comparison, two tests under axial symmetry and two tests under plane strain conditions. It was shown earlier that stresses at failure depend on the relative density; therefore, two dense and two loose samples having approximately the same relative densities, respectively, were selected from the 70 psi series. Due to the scatter of the results, the selection of the samples

was based on Figure 55, which shows the relationship between the ratio of $\frac{\tau_{oct}}{\sigma_{oct}}$ at failure and the relative density D_r for sand tested under axial symmetry and plane strain conditions. The method of least squares was used to obtain the straight line relationship $\left(\frac{\tau_{oct}}{\sigma_{oct}}\right)_f$ and the relative density D_r. The summary of the calculations for presentation on the octahedral plane is shown in Table 4.

The graphical representation of the failure point on the octahedral plane is shown in Figure 56. It was found that the plane strain data are between the Mohr-Coulomb and Tresca theoretical surfaces, although slightly closer to the Tresca hypothesis.

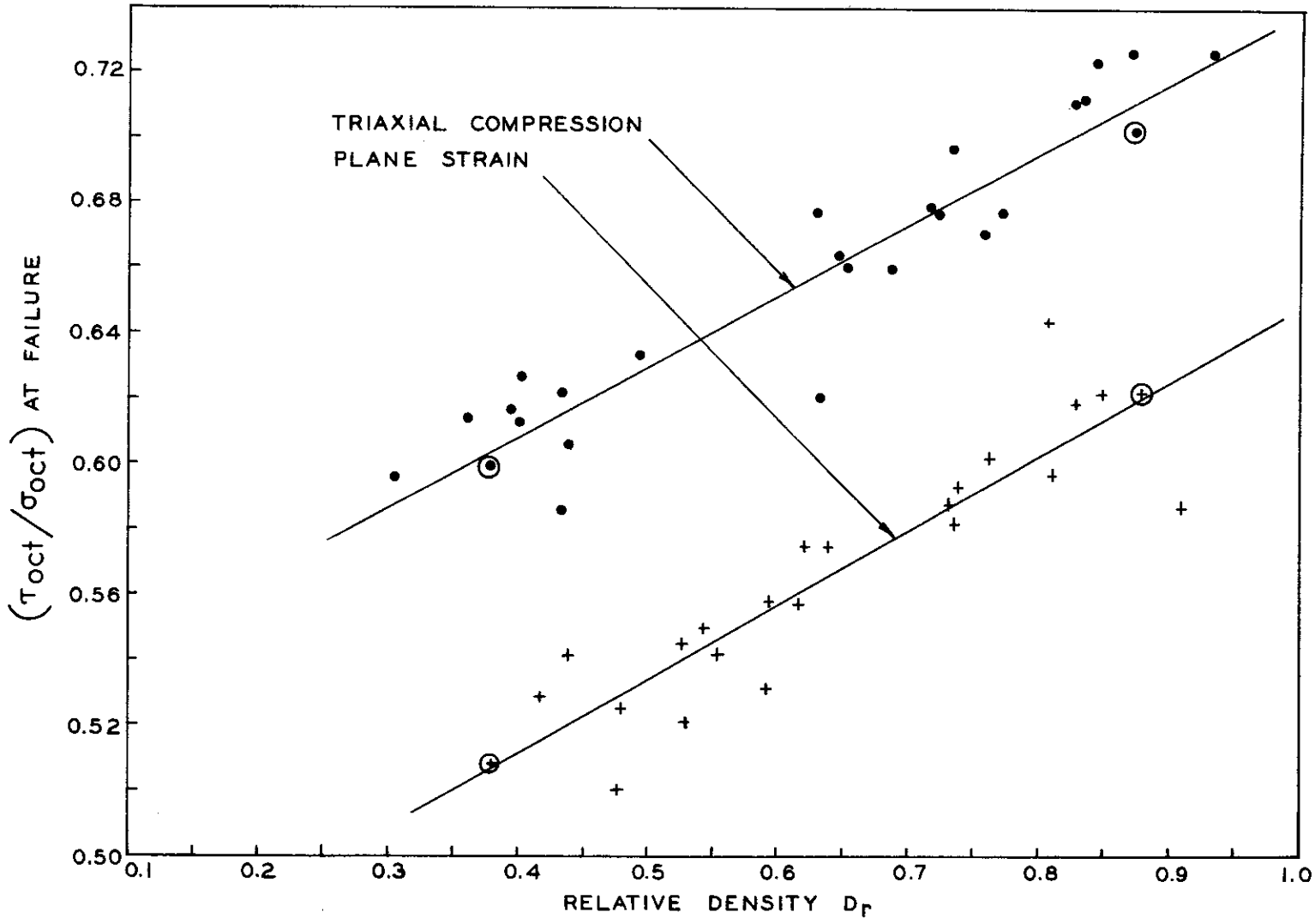

Figure 55. Relationship Between $\frac{\tau_{oct}}{\sigma_{oct}}$ and D_r

Table 4. Summary of the Data Used in Representing the Failure Points on the Octahedral Plane

Test No.	TC-7	TC-8	PS-17	PCI-4
σ_1	224.62	282.91	243.98	320.98
σ_2	70.0	71.00	117.68	127.11
σ_3	70.0	71.00	70.40	69.70
ϕ	31.65°	36.78°	33.51	40.0
D_r	0.379	0.875	0.379	0.880
$\frac{\tau_{oct}}{\sigma_{oct}}$	0.5995	0.7050	0.5090	0.62282
θ	0	0	15.85°	13.33°

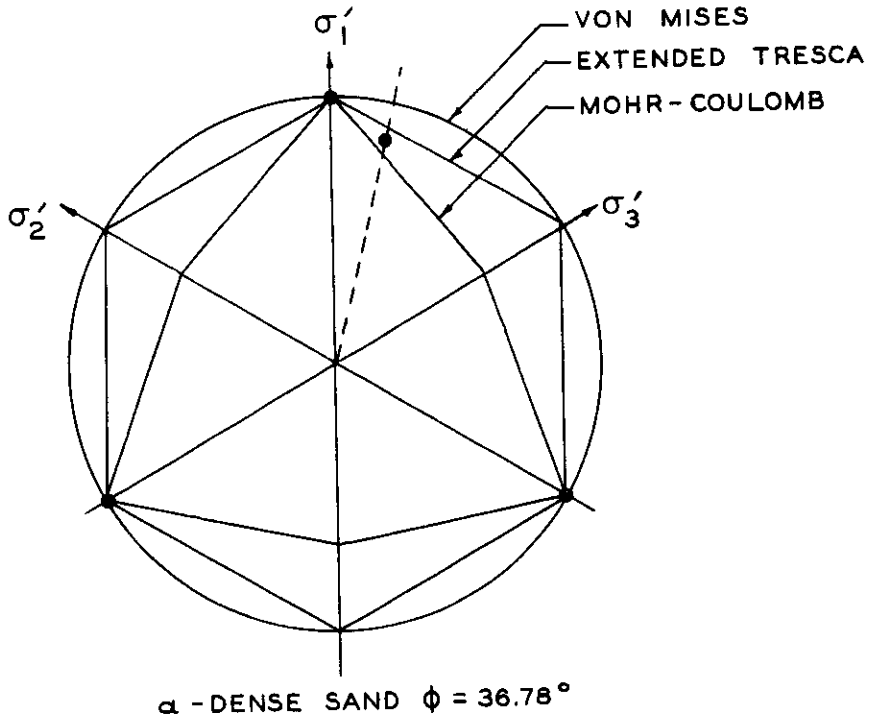

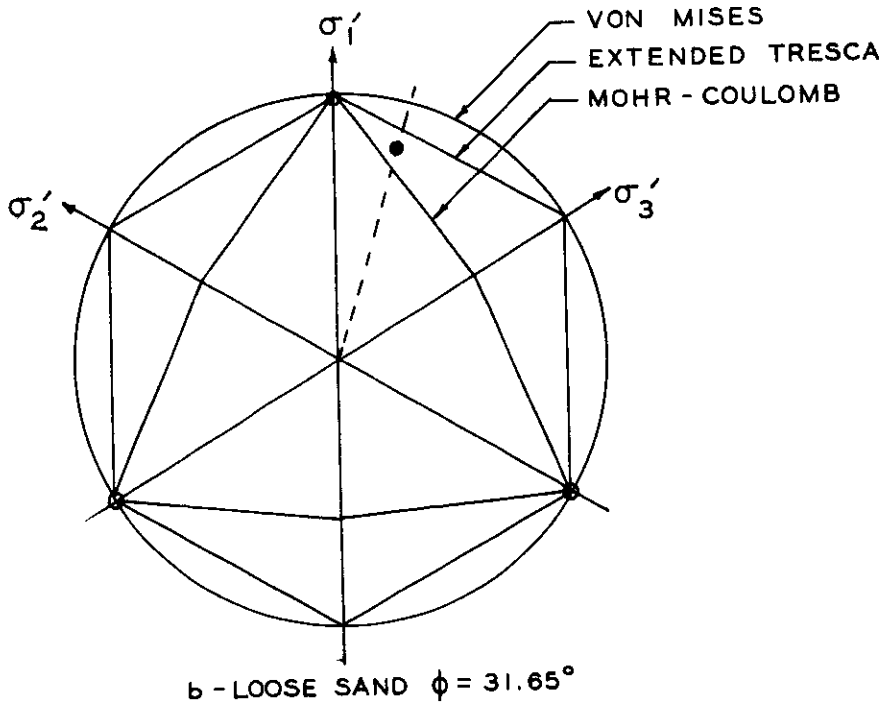

Figure 56. Representation of Failure Points on the Octahedral Plane at σ_o = 70 psi

CHAPTER VII

CONCLUSIONS

The two main objectives of this thesis were as follows:

(a) To develop an apparatus for testing soils under plane strain conditions at high pressure.

(b) To investigate the behavior of sand tested under plane strain conditions and elevated pressure and to compare it with that of sand tested in the conventional triaxial apparatus.

As a result of the investigation the following conclusions may be stated:

1. The value of K_o is inversely proportional to the relative density of sand, but it is independent of the consolidation pressure used. Typical values of K_o are 0.42 for dense sand and 0.51 for loose sand. The results are in good agreement with those of Wade (12) and Terzaghi (16), while the relationship $K_o = 1 - \sin \phi'$ as suggested by Jaky (20) underestimates the value of K_o. The values of K_o obtained herein are higher than that of Hendron (20) at the University of Illinois.

2. The value of Poisson's ratio as calculated from the value of K_o is almost the same for dense and loose, and has an average value of 0.31.

3. The initial tangent modulus of elasticity for sand tested in the triaxial apparatus is higher than that obtained for plane strain specimens with the same placement density and consolidation pressure.

4. The modulus of deformation of sand cannot be expressed by single

value but can be related empirically to the relative density and consolidation pressure. The exponential relationship between the modulus of deformation and the consolidation pressure in this investigation is similar to that found by Sowers (27) on other types of sand.

5. The ratio $\frac{\sigma_2'}{\sigma_1'}$ and $\frac{\sigma_2'}{\sigma_1' + \sigma_3'}$ at failure for the sand tested were inversely proportional to the relative density, but were not greatly affected by the consolidation pressure. The value of $\frac{\sigma_2'}{\sigma_1'}$ for dense sand is equal to 0.39 and for loose sand is 0.48. Typical values of $\frac{\sigma_2'}{\sigma_1' + \sigma_3'}$ are 0.33 for dense sand and 0.37 for loose sand.

6. The ratio of $\frac{\sigma_2'}{\sigma_1'}$ at failure approximates the value of K_o for loose sand and the ratio of $\frac{\sigma_2'}{\sigma_1' + \sigma_3'}$ at failure approximates the value of Poisson's ratio for dense sand.

7. The method of consolidation does not affect the value of the angle of internal friction for either plane strain or triaxial specimens.

8. If the cohesion intercept on the Mohr diagram is assumed to be zero, the value of the angle of internal friction is $3\frac{1}{2}$ degrees higher in plane strain than in triaxial test for dense sand, and 1 degree for loose sand. The results of this investigation are in good agreement with the test results carried out at Imperial College by Cornforth (10) on Brasted sand and Wade (12) on Belgium sand.

9. The angle of internal friction for dense sand decreases about $4\frac{1}{2}$ degrees with an increase in consolidation pressure of 70 psi to 285 psi, but it remains almost unchanged for loose sand over the same range of pressure.

10. The failure strain for sand tested in the triaxial apparatus is higher than that under plane strain conditions with the same placing

density and consolidation pressure. The results of this investigation are in general agreement with the test data of Cornforth (10) and Wade (12) conducted at lower pressure.

11. The volumetric strain at failure in plane strain specimens is lower than that of specimens tested in triaxial apparatus under the same condition of placement density and consolidation pressure. More work needs to be done on other types of sand to confirm this finding.

12. When the experimental data are plotted in principal stress space the results show that the failure points for plane strain tested fell between Mohr and Tresca failure surfaces.

13. It is concluded that Mohr theory may be used to provide a satisfactory approximation in representing the failure of sand. The ratio of the experimental value of $\frac{\tau_{oct}}{\sigma_{oct}}$ at failure to that predicted by Mohr theory for dense sand and loose sand are 1.1 and 1.15, respectively.

CHAPTER VIII

RECOMMENDATIONS FOR FURTHER STUDY

The new apparatus shows that the real behavior of sand regarding stress-strain relationship, volume change, and strength characteristics can be determined accurately. Since the apparatus used in this study is new, general conclusions regarding the behavior of cohesionless soil under plane strain condition cannot be made without additional study utilizing other sands.

The current study raises many questions still unanswered, and further testing concerning the fundamental behavior of soil under plane strain conditions is needed. The following is a summary of recommendations for further study.

(a) To further study the behavior of soil under plane strain condition with emphasis on the following:

1. An extension of the current study by using consolidation pressure higher than the one used in this investigation.

2. To test other types of cohesionless soil and compare the results with those already known.

3. To study the strength characteristics of cohesive soil under high consolidation pressure.

4. To study the behavior of cohesive and cohesionless soil under dynamic loading.

5. To make a comprehensive study of the consolidated undrained

cohesionless soil and compare the results with those obtained from the conventional triaxial test.

6. To study the effect of specimen size and length to width ratio on the strength parameter of soil.

(b) To study the effect of rotating the principal axis on the shear strength characteristics of cohesionless soil.

(c) To study the influence of the intermediate principal stress on shear strength of sand under high confining pressure.

APPENDIX I

TEST DATA

Table 5. Summary of Plane Strain Tests on Chattahoochee Sand Consolidated Under K_o Condition

Test No.	Initial Property		End of Consolidation					Peak Deviatoric Stress					
	D_r	e	D_r	σ'_1	σ'_2	σ'_3	K_o	σ'_1	σ'_2	σ'_3	ϕ	ϵ_1 %	$\frac{\Delta V}{V}$ %
PS-5	0.813	0.686	0.887	177.86	80.71	74.90	0.421	313.05	126.71	74.30	38.05000	5.98	-0.56
PS-6	0.554	0.815	0.678	153.13	74.62	73.50	0.480	252.18	106.93	72.20	33.70000	7.79	-2.23
PS-7	0.593	0.795	0.694	161.08	76.87	74.30	0.461	257.49	113.19	74.20	33.54517	7.97	-1.07
PS-8	0.477	0.853	0.626	159.95	81.92	73.10	0.457	248.09	122.05	73.00	33.04517	7.03	-1.50
PS-9	0.738	0.723	0.915	235.72	95.88	75.00	0.318	317.12	136.97	75.00	38.13117	4.85	+0.08
PS-10	0.764	0.710	0.919	241.22	97.43	69.00	0.286	308.45	128.65	69.10	39.34200	4.61	+0.37
PS-11	0.732	0.726	0.869	219.47	88.99	69.50	0.317	289.51	122.53	68.50	38.12167	3.98	-0.28
PS-12	0.440	0.871	0.661	176.03	72.97	69.30	0.394	246.89	108.59	68.40	34.47917	9.38	-1.75
PS-13	0.531	0.826	0.710	187.56	89.63	69.50	0.371	252.23	122.79	68.60	34.91517	6.91	-1.04
PS-14	0.910	0.638	1.020	223.31	91.83	70.50	0.316	312.53	138.46	70.10	39.31517	2.70	-0.25
PS-15	0.810	0.688	0.869	132.96	72.24	71.00	0.534	322.47	119.36	69.70	40.13100	5.82	-0.56
PS-16	0.831	0.677	0.887	153.10	73.64	69.20	0.452	327.86	133.89	69.80	40.44567	5.46	-0.11
PS-17	0.379	0.902	0.431	96.74	71.37	71.60	0.740	243.98	117.68	70.40	33.51317	10.49	-2.47
PS-18	0.544	0.819	0.634	126.04	70.40	69.20	0.549	260.24	115.66	68.60	35.64567	8.10	-1.82
PS-19	0.526	0.829	0.632	140.90	84.16	71.10	0.505	267.04	120.15	70.90	35.47850	8.35	-1.95
PS-20	0.596	0.794	0.692	140.40	75.42	70.10	0.499	272.18	119.58	70.10	36.18467	6.63	-1.49
PS-21	0.643	0.770	0.742	163.92	77.67	70.40	0.429	281.22	118.76	70.20	36.90417	6.64	-1.39
PS 2-1	0.51900	0.83200	0.684	236.18	119.81	109.80	0.465	422.26	183.85	109.70	35.98333	7.90	-1.74
PS 2-2	0.68600	0.74900	0.829	244.79	126.19	110.30	0.451	437.84	186.57	109.50	35.77783	8.77	-1.70
PS 2-3	0.89700	0.64400	0.969	203.87	112.74	108.50	0.532	381.78	202.06	109.50	39.02133	7.66	-1.05
PS 2-4	0.81500	0.68500	0.909	215.26	122.70	110.50	0.513	450.29	186.20	109.60	37.48033	8.91	-1.78
PS 2-5	0.83300	0.67600	0.952	269.20	125.13	110.00	0.409	436.64	182.67	110.50	36.58983	5.93	-0.95
PS 2-6	0.84900	0.66800	0.925	213.67	108.47	109.80	0.514	462.40	171.20	108.20	38.46666	7.19	-1.05
PS 2-7	0.75400	0.71500	0.891	232.98	108.88	112.20	0.482	459.51	178.09	108.80	38.10583	8.62	-1.80
PS 2-8	0.44500	0.86900	0.610	197.62	114.18	110.00	0.557	373.29	175.32	110.20	32.96666	10.95	-3.68

Note: Stresses expressed in pound per square inch

Table 6. Summary of Plane Strain Tests on Chattahoochee Sand Consolidated Under Isotropic Condition

Test No.	Initial Property		End of Consolidation					Peak Deviatoric Stress					
	D_r	e	D_r	σ'_1	σ'_2	σ'_3	K_o	σ'_1	σ'_2	σ'_3	ϕ	ϵ_1 %	$\frac{\Delta V}{V}$ %
PSI-1	0.6197	0.772	0.713	71.35	69.73	70.0		279.19	127.00	69.70	36.8667	9.64	-1.26
PSI-2	0.7384	0.723	0.794	70.58	69.51	69.90		295.50	121.75	70.00	38.1000	8.26	-0.90
PSI-3	0.8511	0.667	0.899	71.97	69.55	69.80		323.73	128.95	70.0	40.0917	7.63	-0.47
PSI-4	0.8807	0.653	0.946	70.84	70.78	69.70		320.98	127.11	69.70	40.0033	7.46	-0.56
PSI-5	0.6239	0.778	0.684	71.55	72.13	70.50		280.63	118.85	69.80	36.9834	9.63	-2.20
PSI-6	0.4815	0.853	0.564	74.04	68.8	69.50		253.48	118.95	70.00	34.5550	11.72	-3.49
PSI-7	0.4175	0.877	0.502	72.17	69.34	70.00		247.21	111.63	70.00	34.0167	10.48	-3.35
PSI-11	0.40841	0.88702	0.500	111.75	111.36	110.00		409.34	195.67	113.00	34.56333	10.87	-2.61
PSI-12	0.53096	0.85611	0.570	111.21	111.59	110.00		397.96	183.12	110.00	34.53333	12.23	-3.95
PSI-13	0.63122	0.77628	0.705	109.60	114.64	110.00		438.03	186.88	110.50	36.31666	9.64	-1.94
PSI-14	0.76130	0.71163	0.828	111.99	111.98	110.00		458.90	187.77	109.70	37.88933	9.66	-2.03
PSI-15	0.54189	0.82068	0.623	110.41	112.39	110.00		400.41	204.35	109.50	34.78600	13.87	-4.37
PSI-16	0.54018	0.82153	0.644	110.78	113.71	109.50		404.26	181.03	109.10	35.09666	13.61	-4.72
PSI-17	0.87726	0.65400	0.933	112.32	112.01	110.00		479.12	192.45	110.0	38.79750	9.01	-1.42
PSI-18	0.88982	0.64776	0.956	113.55	110.29	109.60		479.96	198.11	109.80	38.87666	8.82	-1.35
PSI-19	0.91990	0.63281	0.980	110.22	110.23	109.50		504.66	190.64	110.00	39.94683	9.15	-1.10
PSI-20	0.95094	0.61738	1.000	111.30	111.15	109.80		516.14	194.36	110.20	40.40000	9.13	-1.08
PSI-21	0.47446	0.85419	0.564	111.53	110.54	109.50		409.83	171.85	110.20	35.18333	14.12	-4.12
PSI-23	0.48550	0.84870	0.608	113.42	109.96	110.10		388.42	178.04	110.40	33.87283	12.87	-4.97
PSI-24	0.44770	0.86750	0.564	112.51	109.61	109.70		391.49	183.85	111.80	33.76033	12.91	-4.99
PSI-29	0.7982	0.60382	1.049	319.05	283.0	283.0		1131.49	494.81	283.0	36.8583	12.52	
PSI-30	1.000	0.55468	1.129	315.01	284.0	284.0		1171.20	495.88	284.0	37.5667	12.44	
PSI-31	1.000	0.54443	1.167	317.10	286.00	286.0		1149.36	465.62	286.0	36.99167	12.55	
PSI-32	0.92984	0.62787	1.046	313.97	293.61	286.0		1108.42	470.98	286.0	36.13334	14.89	
PSI-34	0.84998	0.67103	0.926	310.98	283.50	283.50		1060.31	419.32	283.50	35.3166	13.17	
PSI-35	0.50465	0.83919	0.680	313.31	293.51	285.0		978.68	462.83	285.0	33.2917	18.93	

Table 6. (Continued)

Test No.	Initial Property		End of Consolidation					Peak Deviatoric Stress					
	D_r	e	D_r	σ'_1	σ'_2	σ'_3	K_o	σ'_1	σ'_2	σ'_3	ϕ	ϵ_1 %	$\frac{\Delta V}{V}$ %
PSI-36	0.50833	0.83736	0.669	313.93	298.66	286.0		977.03	439.45	281.0	33.55	16.30	
PSI-37	0.6299	0.7769	0.794	317.04	298.10	286.0		1014.69	454.81	286.0	34.0667	20.06	
PSI-38	0.41980	0.88136	0.614	328.00	297.66	285.00		952.54	412.09	285.0	32.64167	18.83	
PSI-39	0.41529	0.8836	0.614	317.29	284.50	284.50		956.11	451.91	284.50	32.7750	18.94	

Note: Stresses expressed in pound per square inch

Table 7. Summary of Triaxial Compression Tests on Chattahoochee Sand Consolidated Under K_o Condition

Test No.	Initial Property		End of Consolidation					Peak Deviatoric Stress					
	D_r	e	D_r	σ'_1	σ'_2	σ'_3	K_o	σ'_1	σ'_2	σ'_3	ϕ	ϵ_1 %	$\frac{\Delta V}{V}$ %
TC 1-1	.495	0.844	0.565	148.26	70.0	70.0	0.472	240.72	70.0	70.0	33.32750	11.75	-2.53
TC 1-2	.396	0.893	0.523	142.84	70.0	70.0	0.490	234.18	70.5	70.5	32.53722	13.6	-3.16
TC 1-3	0.629	0.778	0.662	167.08	70.0	70.0	0.419	265.28	70.5	70.5	35.46166	6.03	+0.1
TC 1-4	0.760	0.712	0.811	154.77	70.0	70.0	0.452	248.18	70.0	70.0	34.10000	7.13	-0.39
TC 1-5	0.697	0.743	0.748	146.49	70.0	70.0	0.478	248.90	70.5	70.5	33.95600	7.25	-0.48
TC 1	0.721	0.732	0.785	162.78	70.0	70.0	0.430	262.50	70.0	70.0	35.38833	6.59	+0.75
TC 2	0.652	0.766	0.720	191.06	70.0	70.0	0.366	253.96	70.0	70.0	34.60000	6.77	+0.26
TC 3	0.649	0.768	0.706	148.91	70.0	70.0	0.470	255.96	70.0	70.0	33.10000	7.60	+0.03
TC 4	0.402	0.890	0.487	159.88	70.0	70.0	0.563	230.68	70.0	70.0	32.30250	9.89	-5.77
TC 5	0.434	0.874	0.541	153.91	70.0	70.0	0.455	218.58	70.0	70.0	30.98833	8.84	-1.17
TC 6	0.305	0.938	0.398	141.13	70.0	70.0	0.496	223.10	70.0	70.0	31.49000	9.79	-1.95
TC 7	0.379	0.902	0.493	128.86	70.0	70.0	0.543	224.62	70.0	70.0	31.65333	13.24	-4.07
TC 8	0.875	0.655	0.917	146.44	70.0	70.0	0.478	282.91	71.0	71.0	36.78333	0.660	+0.03
TC-11	0.416	0.883	0.561	223.34	110.0	110.0	0.493	345.94	110.0	110.0	31.1666	12.22	-4.62
TC-12	0.669	0.757	0.785	246.44	110.0	110.0	0.446	382.69	110.0	110.0	33.6000	9.00	-2.29
TC-13	0.5285	0.8273	0.708	213.14	110.0	110.0	0.516	340.61	110.0	110.0	30.7834	11.31	-3.28
TC-14	0.659	0.762	0.753	237.04	110.0	110.0	0.464	379.00	110.0	110.0	33.37000	10.69	-2.67
TC-15	0.838	0.673	0.889	229.38	110.0	110.0	0.480	398.43	110.0	110.0	34.5634	9.27	-1.03
TC-16	0.368	0.907	0.555	225.30	110.0	110.0	0.488	333.18	110.0	110.0	30.3583	11.80	-4.61
TC-17	0.436	0.873	0.588	211.87	110.0	110.0	0.519	334.45	110.0	110.0	30.3250	12.55	-4.95
TC-18	0.887	0.649	0.932	217.33	110.0	110.0	0.506	426.28	110.0	110.0	36.1333	9.30	-1.22

Note: Stresses expressed in pound per square inch

Table 8. Summary of Triaxial Compression Tests on Chattahoochee Sand Consolidated Under Isotropic Condition

Test No.	Initial Property		End of Consolidation					Peak Deviatoric Stress					
	D_r	e	D_r	σ'_1	σ'_2	σ'_3	K_o	σ'_1	σ'_2	σ'_3	ϕ	ϵ_1 %	$\frac{\Delta V}{V}$ %
IC-1	0.83825	0.67339	0.881	72.51	70.0	70.0		284.72	70.0	70.0	37.2500	9.49	-0.49
IC-2	0.63493	0.77444	0.695	70.38	70.0	70.0		234.72	70.0	70.0	32.6000	9.51	-2.63
IC-3	0.84213	0.67146	0.876	72.89	70.0	70.0		290.14	70.0	70.0	37.6833	7.50	+1.01
IC-4	0.40268	0.88987	0.524	72.32	70.0	70.0		237.70	70.0	70.0	33.0250	12.18	-1.87
IC-5	0.43696	0.87283	0.507	70.39	70.0	70.0		235.90	70.0	70.0	32.8416	14.5	-2.9
IC-6	0.87213	0.65655	0.910	72.35	70.0	70.0		292.49	70.0	70.0	37.8667	7.42	+ .59
IC-7	0.93559	0.62501	0.994	70.79	70.0	70.0		292.59	70.0	70.0	37.8716	9.49	- .55
IC 1-1	0.73587	0.72427	0.793	70.40	70.0	70.0		276.57	70.50	70.50	36.4250	12.58	- .78
IC 1-2	0.68992	0.74711	0.747	72.65	70.0	70.0		255.34	70.50	70.50	34.5617	10.42	-1.48
IC 1-3	0.44022	0.87121	0.545	71.27	70.0	70.0		229.26	70.50	70.50	31.9800	12.62	-4.0
IC 1-4	0.36155	0.91031	0.407	72.42	70.0	70.0		233.18	70.50	70.50	32.3900	14.00	-3.69
IC 1-5	0.77362	0.70551	0.820	72.89	70.0	70.0		266.45	71.00	71.00	35.3950	8.16	-0.69
IC 1-6	0.71967	0.73235	0.771	74.31	70.0	70.0		264.12	70.0	70.0	35.5167	8.98	-0.84
IC 1-7	0.82960	0.67769	0.870	73.03	71.0	71.0		282.83	70.0	70.0	37.1000	7.1	+0.55
IC-11	0.695	0.745	0.794	111.06	110.0	110.0		373.99	110.0	110.0	33	12.9	-2.35
IC-12	0.7500	0.715	0.829	110.64	110.0	110.0		372.16	110.0	110.0	33.2	0.43	-1.15
IC-13	0.5488	0.888	0.634	110.93	110.0	110.0		353.25	110.0	110.0	31.8	10.21	-1.95
IC-14	0.518	0.764	0.612	111.23	110.0	110.0		347.99	110.0	110.0	31.3	11.68	-2.64
IC-15	0.4045	0.837	0.531	110.66	110.0	110.0		337.50	110.0	110.0	30.5	12.89	-3.87
IC-16	0.8428	0.67113	0.895	111.75	110.0	110.0		422.91	110.0	110.0	36.0	9.30	-0.21
IC-17	0.8994	0.643	0.950	112.53	110.0	110.0		411.08	110.0	110.0	35.3	7.77	-0.38
ITC-1	0.9205	0.6325	1.017	287.40	286.00	286.00		945	275	275	33.31	18.2	
ITC-2	0.8274	0.67876	0.996	294.98	289.00	289.00		980	289	289	33.00	20.3	
ITC-3	0.8942	0.6456	0.995	328.70	282.00	282.00		921.41	279	279	32.40	18.1	
ITC-4	0.91589	0.6348	1.007	317.21	288.00	288.00		995	288	288	33.45	18	

Table 8. (Continued)

Test No.	Initial Property		End of Consolidation					Peak Deviatoric Stress					
	D_r	e	D_r	σ'_1	σ'_2	σ'_3	K_o	σ'_1	σ'_2	σ'_3	ϕ	ϵ_1 %	$\frac{\Delta V}{V}$ %
ITC-5	0.9818	0.602	1.066	286.21	285.00	285.00		950	286	286	32.50	19	
ITC-6	0.7153	0.7345	0.791	324.57	284.00	284.00		992.23	286.5	286.5	33.50	(14.57)	
ITC-7	0.5463	0.81848	0.695	342.92	288.00	288.00		925	287.0	287.0	31.73	20	
ITC-8	0.54125	0.812	0.670	372.74	294.00	294.00		905	292	292	30.80	21	
ITC-9	0.5942	0.7947	0.677	347.31	292.00	292.00		921.51	297	297	30.85	15.68	

Note: Stresses expressed in pound per square inch

APPENDIX II

SUPPLEMENTARY TEST, CALIBRATION CHARTS FOR LOAD CELLS, AND EVALUATION OF END PLATE FRICTION

Evaluation of the Coefficient of Friction

Prior to the design of the plane strain apparatus, several tests were performed to obtain the minimum coefficient of friction between the sand used in the test and different materials. Among the materials used were brass, aluminum, lucite, chromium, and steel.

The direct shear box was used in conducting two types of tests. In the first type of test the polished surface of the material was used as a base on which the upper part of the shear box rests. The box was filled with sand and covered with a rigid cap. Normal force was applied at the top of the cap, then shear force was applied until it started to move. Readings of both normal force and shear force were taken. The normal force was then increased and the process was repeated. Several readings were taken and a curve of the shearing stress versus the normal stress was plotted. The coefficient of friction was considered to be equal to the average slope of that curve. Figure 57 shows the coefficient of friction between Chattahoochee sand and the different materials used in the test.

In the second type of test, the same procedure of loading was followed except that a rubber membrane was attached to the bottom of the shear box with the sand resting on it. The polished surface of material to be tested was smeared with a thin film of silicone grease prior to the test. Curves for shearing stress versus normal stress for different material are shown in Figure 58. The results of the test show that the minimum coefficient of friction was between the rubber membrane and polished stainless steel covered with silicone grease.

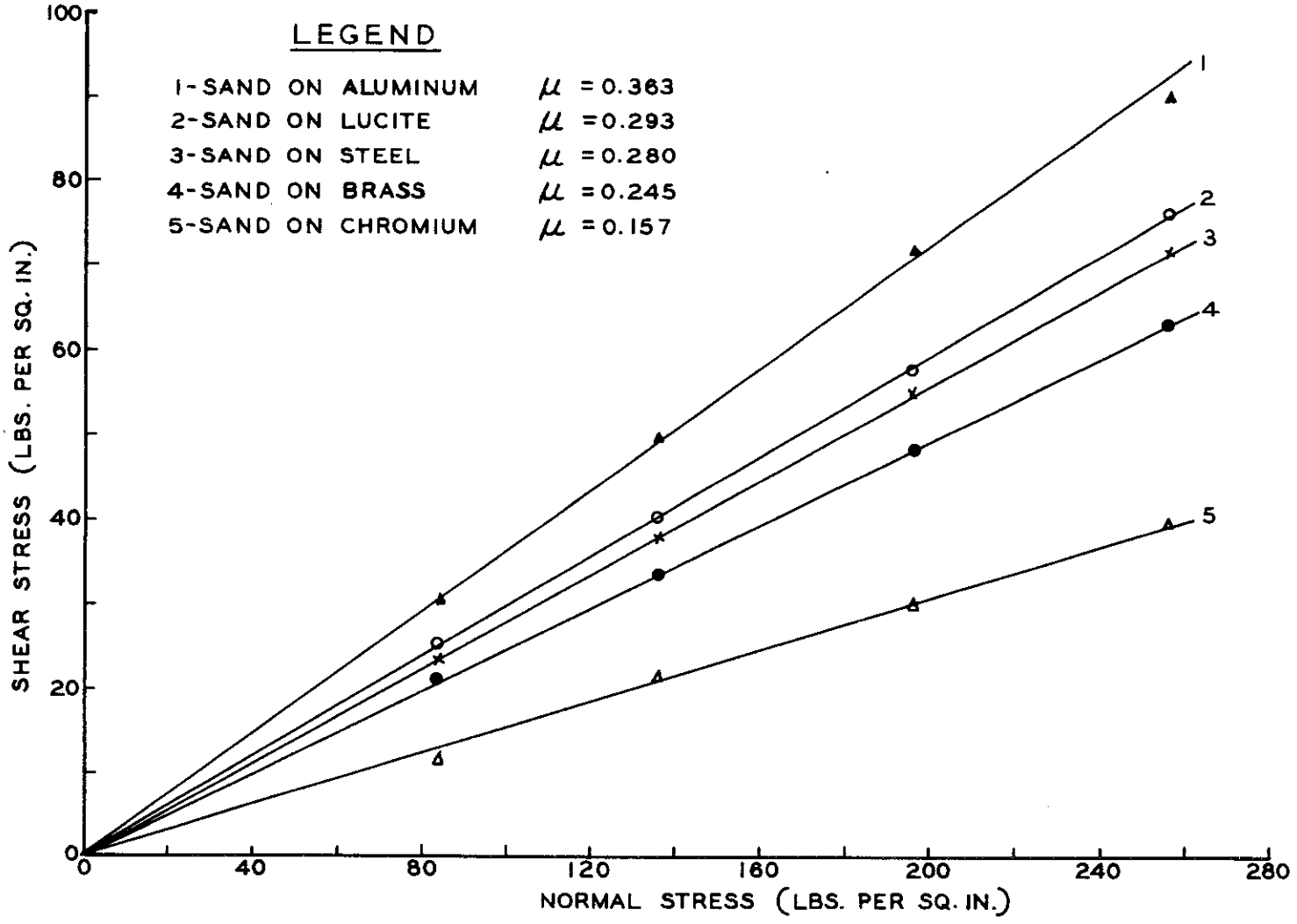

Figure 57. Coefficient of Friction Between Sand and Polished Materials

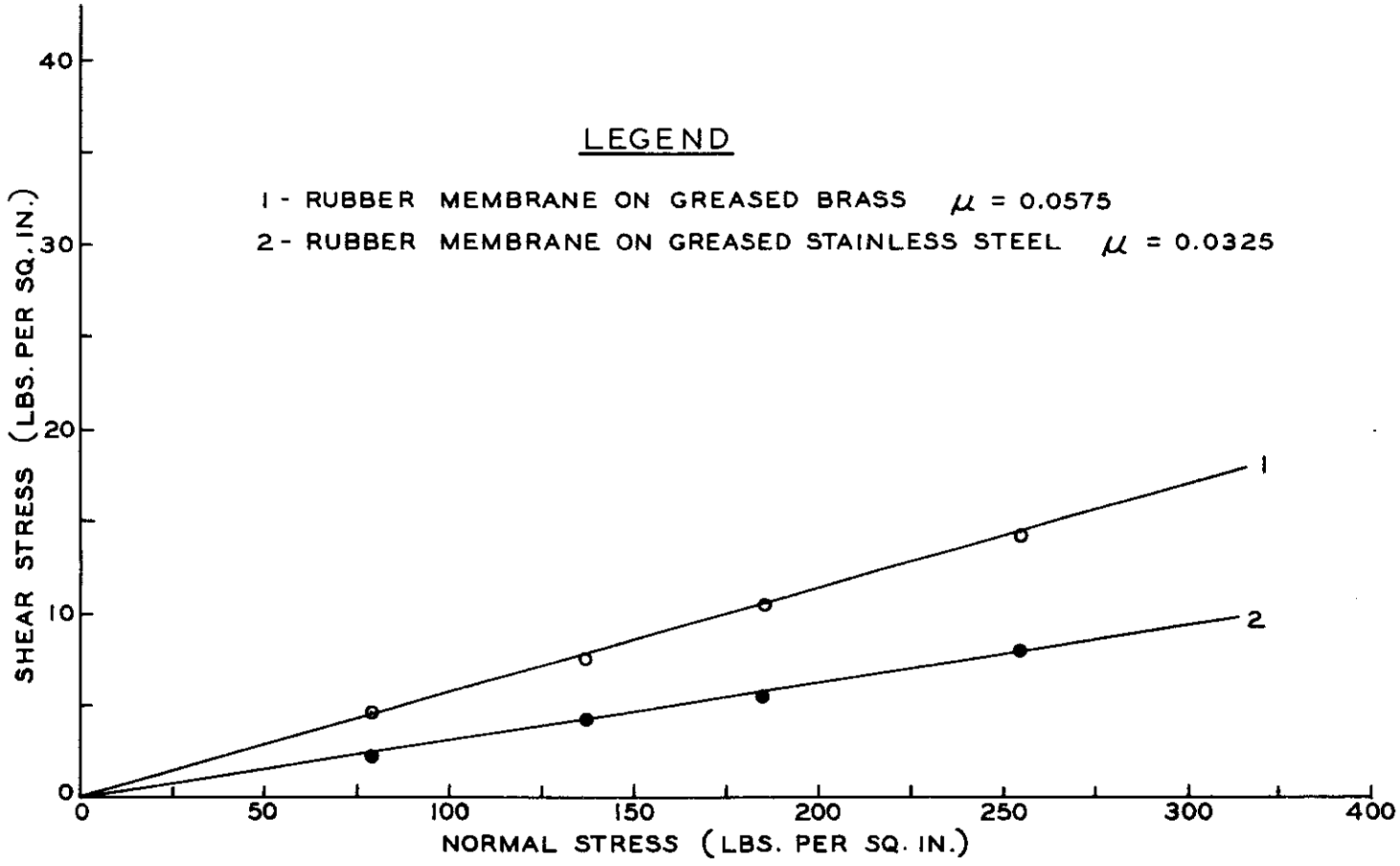

Figure 58. Coefficient of Friction Between Rubber Membrane and Greased Metals

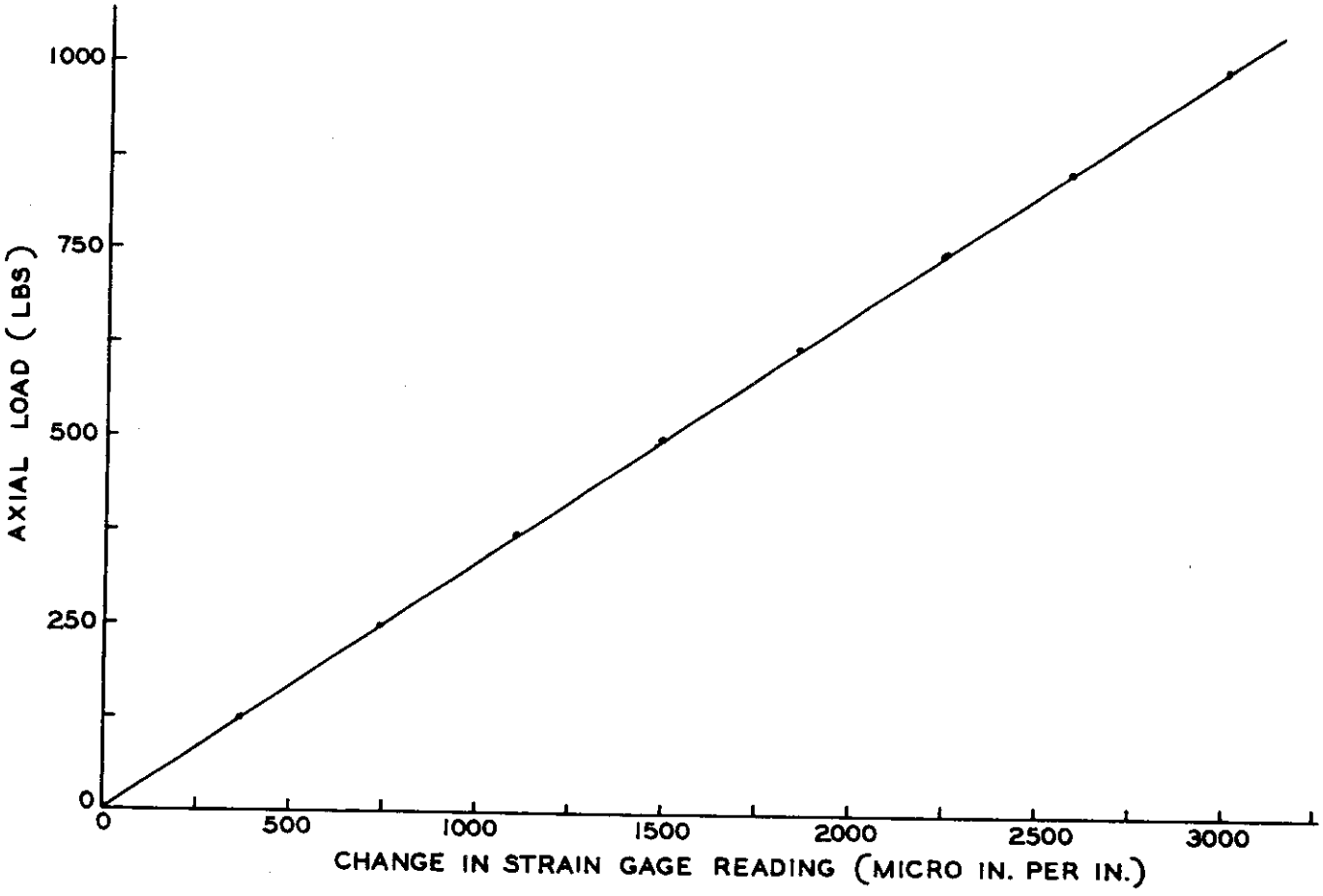

Figure 59. Calibration Chart for 1000 Pounds Load Cell

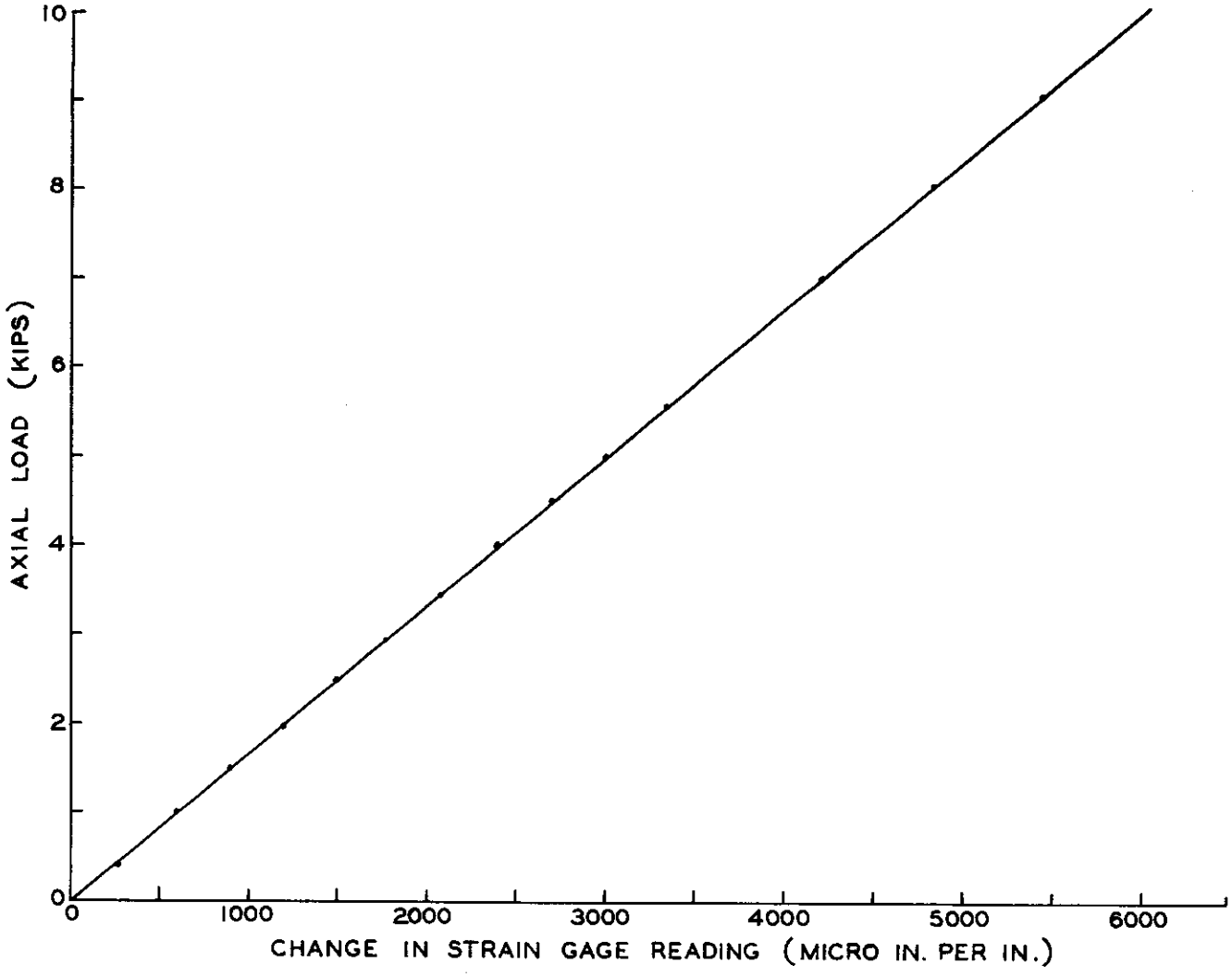

Figure 60. Calibration Chart for 10^{k} Load Cell

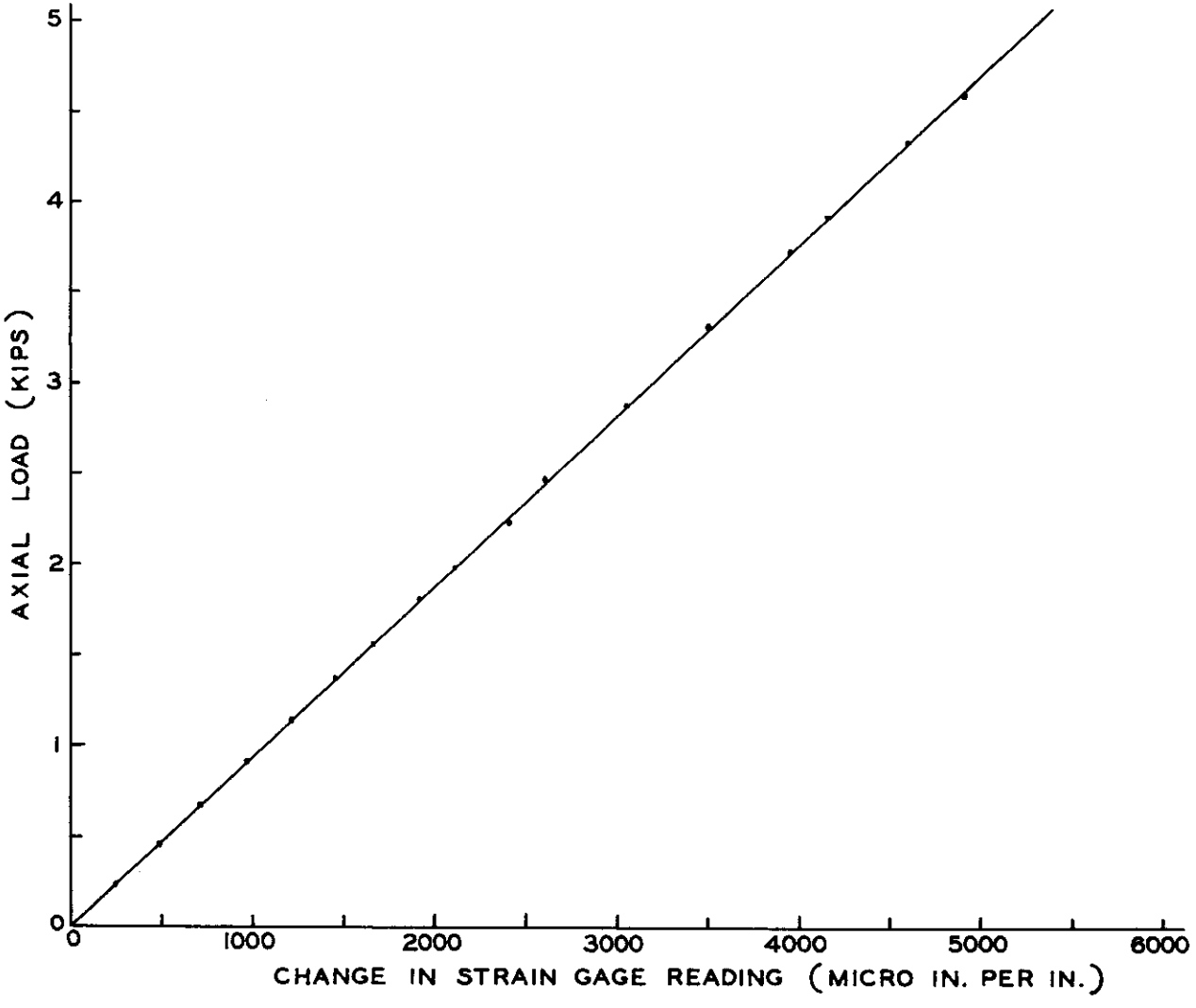

Figure 61. Calibration Chart for 5 Kips Load Cell

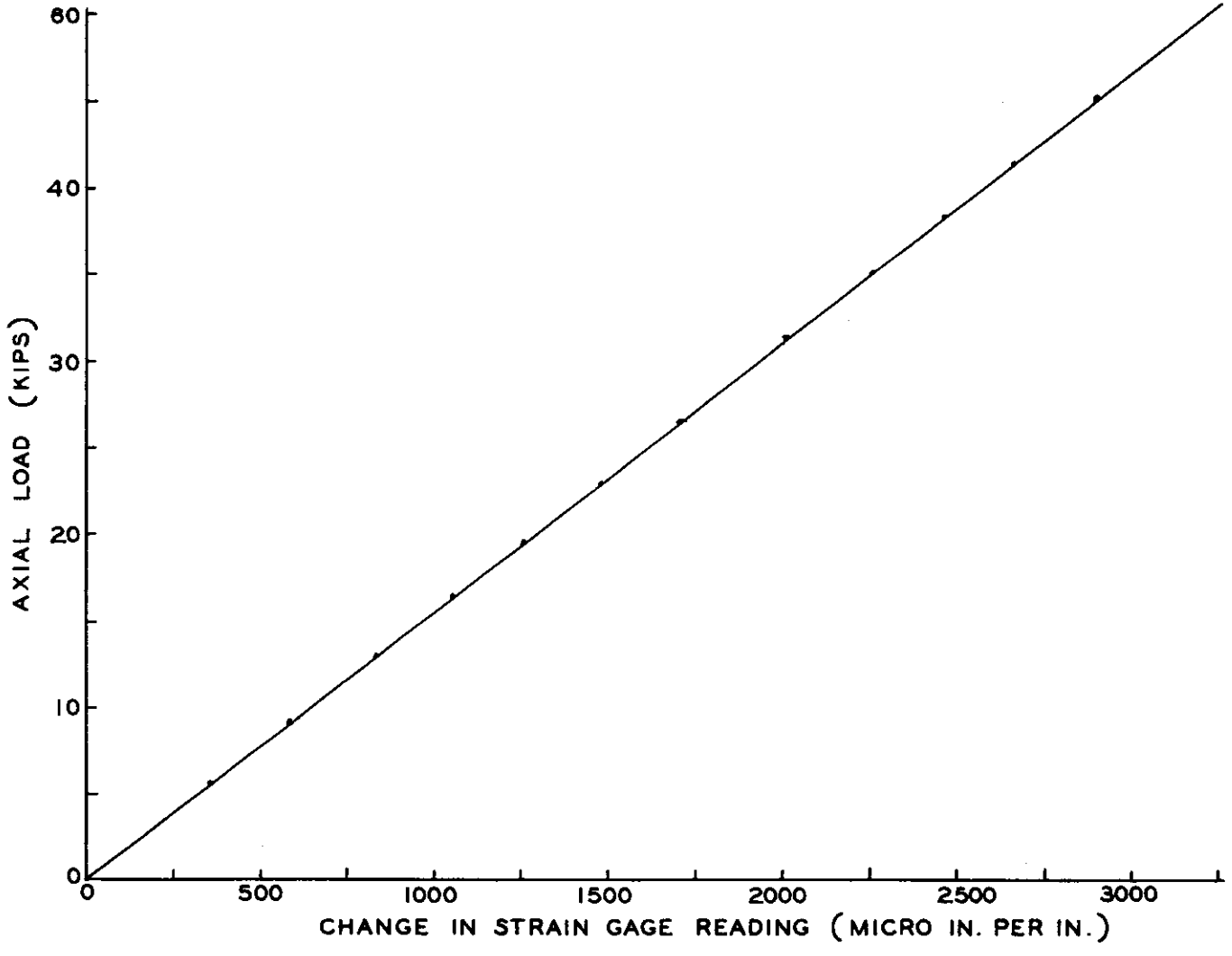

Figure 62. Calibration Chart for 50 Kips Load Cell

Evaluation of End Plate Friction

A plane strain specimen is entirely surrounded by a rubber membrane and is in contact with two end plates. The end plates insure that the specimen will deform under a plane strain condition. During a test, part of the axial load is used to overcome friction developed between the rubber membrane and the end plates. Therefore, the end friction introduces an error in the total axial load apparently carried by the specimen. In some cases the end friction can amount to a significant part of the total axial load applied. Unless a correction is made to eliminate the load resulting from the end friction the measured soil strength will be in error.

Due to the complexity of factors contributing to the friction, a rigorous analytical solution is difficult to obtain. However, by using some simplifying assumptions a semi-empirical solution can be derived. The main assumptions necessary for a mathematical formulation are as follows:

1. The intermediate principal stress, σ_2, is uniformly distributed over the area of contact between the rubber membrane and the plates.

2. The coefficient of friction between the rubber membrane and the end plates is constant.

3. The friction due to strain between the rubber membrane and the end plates during consolidation is neglected.

Other secondary assumptions will be made during the development of the mathematical formulation.

Consider point A on the end of a specimen in x, y coordinates, the position of which is defined by r, θ in polar coordinates, as shown in Figure 63, displaced to a position B. Then from the geometry the following relations are obtained:

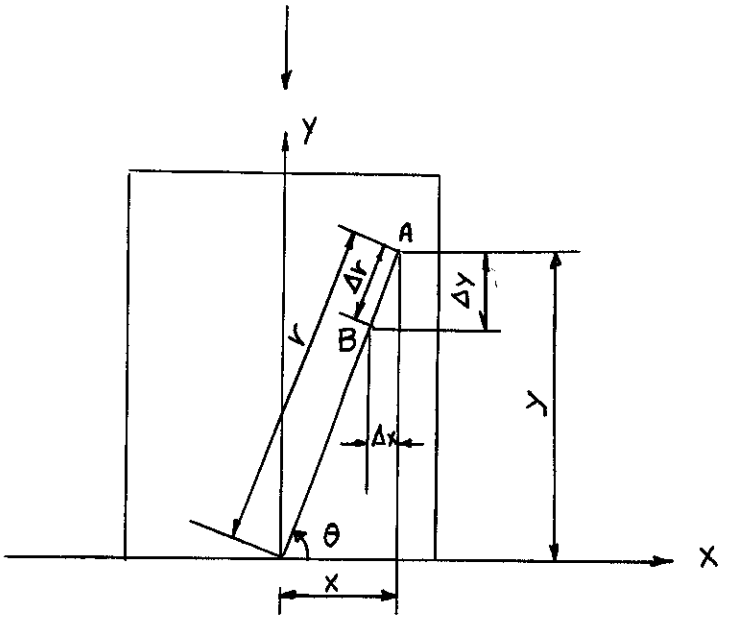

Figure 63. Soil Element on the End of Specimen

$$\frac{\Delta x}{x} = \frac{\Delta y}{y} = \frac{\Delta r}{r} \quad . \tag{35}$$

But

$$\frac{\Delta y}{y} = \epsilon y \quad . \tag{36}$$

Therefore,

$$\Delta r = \epsilon y \cdot r \quad . \tag{37}$$

Now if it is assumed that a small element of area r dr dθ in the plane r, θ is acted upon by σ_2, then the total friction force in the direction of motion will be $\mu\ \sigma_2\ r\ dr\ d\theta$, where μ is the coefficient of friction. The work done $d\ W_i$, in small distance Δr, is

$$d W_i = \mu \sigma_2 \, r \, dr \, d\theta \; . \; \epsilon y \, r \quad , \tag{38}$$

or

$$W_i = \mu \sigma_2 \, \epsilon y \int \int r^2 \, dr \, d\theta \quad . \tag{39}$$

The double integral can be evaluated easily by taking half the area of contact and dividing each half into four zones, as shown below in Figure 64.

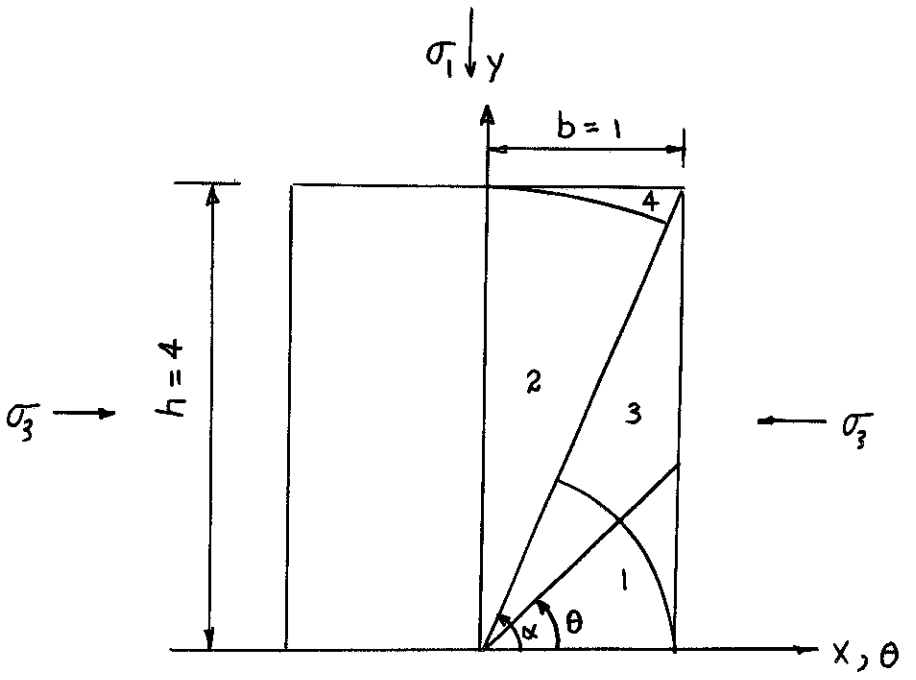

Figure 64. Area of Contact Between the Rubber Membrane and the End Plate

Solving the integration and collecting terms, the result is:

$$W_i = \mu \sigma_2 \, \epsilon y \left[\frac{b^3}{G} \left\{ \frac{\sin \alpha}{\cos^2 \alpha} - \ln \tan \left(\frac{\alpha}{2} + \frac{\pi}{4} \right) \right\} + \frac{h^3}{G} \left\{ \frac{\sin \alpha}{\cos^2 \alpha} - \ln \tan \frac{\alpha}{2} \right\} \right] \tag{40}$$

Substituting the numerical value of b = 1 unit, h = 4 units, and $\alpha = \tan^{-1}\frac{h}{b}$, the expression reduced to $W_i = 7.77\ \sigma_2\ \mu\ \epsilon y$.

The total work done on both ends is

$$W_i = 4 \times 7.77\ \sigma_2\ \mu\ \epsilon y = 31.08\ \sigma_2\ \mu\ \epsilon y.$$

Now if it is assumed that the input work due to the deviatoric stress $(\sigma_1-\sigma_3)$ in overcoming the effect of end friction is W_e, then:

$$W_e = L.W.\ (\sigma_1-\sigma_3) \times \epsilon y.H \quad , \tag{41}$$

where

L = length of the specimen = 16 units

W = width of the specimen = 2 units

H = height of the specimen = 4 units

$(\sigma_1-\sigma_3)$ = extra deviatoric stress to overcome end friction.

Substituting the numerical values in equation (41) the expression becomes:

$$W_e = 128\ (\sigma_1-\sigma_3)\ \epsilon y \quad . \tag{42}$$

Since $W_i = W_e$, then

$$(\sigma_1-\sigma_3) = 0.243\ \mu\ \sigma_2 \quad . \tag{43}$$

The above expression can be used only for the case of consolidated undrained test.

APPENDIX III

COMPUTER PROGRAM

```
GEORGIA TECH REC 8-5500 ALGOL COMPILER     TUESDAY,   6/20/67,  7:02 PM.

 BEGIN COMMENT ANALYSIS OF PLANE STRAIN TEST OF SAND                                    0000
                                                          START OF SEGMENT **********   2
             DURING    SHEAR                                                          0000
 END OF COMMENT ;                                                                     0000
 REAL LO, DO, HO, VO, WT, W, SG, EO, A10, WETDEN, DRYDEN, VS, DR,A20,                 0000
 DELTAVO, SR1ZERO, SR2ZERO, SR3ZERO,DELTAHO, UO, S1MINUSS30 ;                         0000
 INTEGER I,N ;                                                                        0000
 ALPHA SAMPLENO, TESTDATE, MONTH, YEAR;                                               0000
 FILE IN CARD"QYSFR" (2,10);                                                          0000
 FILE OUT PRINT 6(2,15);                                                              0003
 LABEL L1,L2;                                                                         0007
 FORMAT FMT1(X3,A6,X8,A2,X1,A4,X1,A4), FMT0(I5),                                      0007
                                                          START OF SEGMENT **********   3
 FMT2(5F7.3,3I7),                                                                     0007
 FMT3( X2,"SAMPLENO",X6 ,"TEST COMPLETED"//),                                         0007
FMT4(3I6,4F8.3),                                                                      0007
FMT5(X3,"S1",X5,"S2"X5,"S3",X2,"S1MINUSS3",X2,"E1",X4,"S2S1RATIO",                    0007
 X1,"S3S1RATIO",X2,"MS",X4,"OCTS",X2,"CELLPR",X2,"U"/),                               0007
 FMT6(3F7.2, F8.2, F8.4, F8.3, F10.3, 4F7.1),                                         0007
FMT7(///X1,"DELTAH",X1,"DELTAV",X3,"E1",X5,"VOLSTRAIN",X2,"OCTSTRAIN"                 0007
 X3,"E3",X3,"OCTSRATIO",X3,"F1",X5,"F2",X4,"PPPA"/),                                  0007
 FMT8 ( F7.3,F8.3,F8.4,F9.4,F10.4,2F9.4,2I7,F8.3 ),                                   0007
 FMT9(//X3,"SHEAR",X1,"STAGE"//);                                                     0007
                                                    3 IS  127 LONG, NEXT SEG    2
 LIST LST1(SAMPLENO, TESTDATE, MONTH, YEAR),                                          0007
 LST2(LO, DO, HO,DELTAVO,DELTAHO,SR1ZERO,SR2ZERO,SR3ZERO);                            0016
WRITE (PRINTER0);                                                                     0030
 L2:READ (CARD,FMT1,LST1)[L1];                                                        0033
 READ (CARD,FMT2,LST2);                                                               0038
 READ (CARD,FMT0,N);                                                                  0042
 BEGIN                                                                                0050
 REAL ARRAY                                                                           0050
                                                          START OF SEGMENT **********   4
 A1, SR1, SR2, SR3, F1, F2, DELTAH, U, S1, S2, S3, A2, E1,DELTAV,PPPA,                0000
OCTSRATIO, VRDG, MS, OCTS, OCTSTRAIN, VOLSTRAIN, HRDG, BP, X, DELTAU,                 0004
 E2, E3, E, CELLPR, S1MINUSS3, S2S1RATIO, S3S1RATIO[0:N];                             0006
 LIST LST3(FOR I:=1 STEP 1 UNTIL N DO[SR1[I],SR2[I],SR3[I],  HRDG[I],                 0010
   VRDG[I],CELLPR[I],BP[I]]),                                                         0019
 LST4(S1[I], S2[I],S3[I],S1MINUSS3[I],E1[I],S2S1RATIO[I],S3S1RATIO[I] ,               0028
 MS[I],OCTS[I],CELLPR[I],U[I]),                                                       0040
 LST5(DELTAH[I],DELTAV[I],E1[I],VOLSTRAIN[I],OCTSTRAIN[I],E3[I],                      0049
 OCTSRATIO[I],F1[I],F2[I],PPPA[I]);                                                   0059
 READ (CARD,FMT0,LST3);                                                               0068
 VO:=LO×HO×DO ;                                                                       0072
 WRITE (PRINTER,FMT3);                                                                0074
 WRITE (PRINTER,FMT1,LST1);                                                           0077
 WRITE (PRINTER,FMT9);                                                                0080
 FOR I :=1 STEP 1 UNTIL N DO BEGIN                                                    0083
 F1[I] := 15.5 × (SR1[I] - SR1ZERO ) ;                                                0084
 F2[I] := 2.011814 × (SR2[I] - SR2ZERO ) ;                                            0086
 U[I] := 0.022901×(SR3[I] - SR3ZERO ) + BP[I] ;                                       0089
  IF I=1 THEN UO := U[I] ;                                                            0092
 DELTAU[I] := U[I] - UO ;                                                             0094
 DELTAH[I]:= HRDG[I] +DELTAHO ;                                                       0096
 E1[I]:= DELTAH[I]/HO ;                                                               0098
DELTAV[I]:= (VRDG[I]-DELTAVO)/16.39 ;                                                 0100
 VOLSTRAIN[I]:= DELTAV[I]/VO ;                                                        0103
 E3[I]:= VOLSTRAIN[I] + E1[I] ;                                                       0105
 A1[I]:= LO×DO×(1+DELTAV[I]/VO)/(1-E1[I]) ;                                           0107
 A2[I]:= HO×DO×(1+DELTAV[I]/VO);                                                      0112
```

```
                S3[I]← CELLPR[I]*U[I]};                                                                    0115
                S2[I]←       F2[I]/A2[I] +S3[I] };                                                         0118
                S1[I]←       F1[I]/A1[I] +S3[I] };                                                         0121
                S1MINUSS3[I] ← S1[I]-S3[I] };                                                              0124
                 IF I=1 THEN S1MINUSS30 ← S1MINUSS3[I] };                                                  0126
                X[I] ← S1MINUSS3[I] - S1MINUSS30 };                                                        0128
                IF ABS(X[I]) < 0-10 THEN PPPA[I] ← 050 ELSE                                                0130
                PPPA[I] ←  DELTAU[I]/X[I] };                                                               0133
                S2S1RATIO[I] ← S2[I]/S1[I] };                                                              0142
                S3S1RATIO[I] ← S3[I]/S1[I] };                                                              0144
                OCTSTRAIN[I]←0.6667×((E1[I])*2+(E3[I])*2+(E1[I]-E3[I])*2)*0.5 };                           0146
                MS[I]← 0.3334×(S1[I] + S2[I] + S3[I])};                                                    0154
                OCTS[I]←0.3333×((S1[I]-S2[I])*2+(S2[I]-S3[I])*2+(S3[I]-S1[I])*2)*0.5 };                    0158
                OCTSRATIO[I]← OCTS[I]/MS[I] };                                                             0167
                END };                                                                                     0169
                WRITE (PRINT,FMT5)};                                                                       0171
                FOR I ←1 STEP 1 UNTIL N DO WRITE (PRINT,FMT6,LST4)};                                       0174
                WRITE (PRINT,FMT7)};                                                                       0185
                FOR I ←1 STEP 1 UNTIL N DO WRITE (PRINT,FMT8 ,LST5)};                                      0188
                END};                                                                                      0195
                                                                                  4 IS   199 LONG, NEXT SEG    2
                WRITE(PRINT[PAGE])}; GO TO L2};                                                            0052
                L1: END.                                                                                   0055
                                                                                  2 IS    59 LONG, NEXT SEG    1
      EXP IS SEGMENT NUMBER 0005,PRT ADDRESS IS 0140
      LN IS SEGMENT NUMBER 0006,PRT ADDRESS IS 0137
      OUTPUT(W) IS SEGMENT NUMBER 0007,PRT ADDRESS IS 0066
      BLOCK CONTROL IS SEGMENT NUMBER 0008,PRT ADDRESS IS 0005
      INPUT(W) IS SEGMENT NUMBER 0009,PRT ADDRESS IS 0071
      X TO THE I IS SEGMENT NUMBER 0010,PRT ADDRESS IS 0141
      GO TO SOLVER  IS SEGMENT NUMBER 0011,PRT ADDRESS IS 0070
      ALGOL WRITE   IS SEGMENT NUMBER 0012,PRT ADDRESS IS 0014
      ALGOL READ    IS SEGMENT NUMBER 0013,PRT ADDRESS IS 0015
      ALGOL SELECT  IS SEGMENT NUMBER 0014,PRT ADDRESS IS 0016
                                                                                  1 IS     2 LONG, NEXT SEG    0
                                                                                 15 IS    69 LONG, NEXT SEG    0
NUMBER OF ERRORS DETECTED =   0;  COMPILATION TIME =   33 SECONDS.
PRT SIZE =  99; TOTAL SEGMENT SIZE =   456 WORDS; DISK SIZE =  25 SEGS; NO. PGM. SEGS =  15
ESTIMATED CORE STORAGE REQUIREMENT =  6202 WORDS.
```

BIBLIOGRAPHY

1. Sowers, G. F., "Strength Testing of Soils," Special Technical Publication No. 361, American Society for Testing and Materials, Symposium on the Laboratory Shear Testing of Soils, 1963, pp. 3-21.

2. Kjellman, W., "Report on Apparatus Consummate Investigation of the Mechanical Properties of Soil," Proceedings, First International Conference Soil Mechanics and Foundation Engineering, Vol. II, 1936, pp. 16-20.

3. Bjerrum, L. and Kummencje, O., "Shearing Resistance of Sand Samples of Circular and Rectangular Cross-Section," Norwegian Geotechnical Institute, No. 44, 1961.

4. Christensen, N. H., "Model Tests on Plane Active Earth Pressure in Sand," The Danish Geotechnical Institute, Bulletin No. 10, 1961.

5. Whitman, R. V. and Luscher, U., "Basic Experiments Into Soil Structure Interaction," Journal Soil Mechanics and Foundation Division, ASCE, SM6, Vol. 88, 1962, pp. 135-167.

6. Roscoe, K. H., Arther, J. R. F., and James, R. G., "The Determination of Strain in Soils by an X-ray Method," Civil Engineering and Public Work Review, Vol. 58, 1963, pp. 873-876 and pp. 1009-1012.

7. Leussink, H. and Wittke, W., "Difference in Triaxial and Plane Strain Shear Strength," S.T.P. No. 361, ASTM, Symposium on Laboratory Shear Testing of Soils, 1964, p. 88.

8. Marsal, R. J., "Discussion on Shear Strength on Consolidation," Sixth International Conference Soil Mechanics, Vol. III, 1965, pp. 310-312.

9. Duncan, J. M. and Seed, H. B., "Strength Variation Along Failure Surface in Clay," Journal Soil Mechanics, Vol. 92, No. SM6, 1966, pp. 102-104.

10. Cornforth, D. H. "Some Experiments on the Influence of Strain Conditions on the Strength of Sand," Geotechnique, Vol. 14, No. 2, 1964, pp. 143-166.

11. Bishop, A. W. and Henkel, D. J., "The Measurement of Soil Properties in Triaxial Test," Edward Arnold, London, 1957.

12. Wade, N. H., "Plane Strain Failure Characteristics of a Saturated Clay," Ph.D. Thesis, University of London, 1963.

13. Shibata, T. and Karube, D., "Influence of the Variation of the Intermediate Principal Stress on the Mechanical Properties of Normally Consolidated Clays," Sixth International Conference Soil Mechanics, Vol. I, 1965, pp. 359-363.

14. Nadi, A., "Theory of Flow and Fracture," McGraw-Hill Company, Inc., New York, 1950.

15. Terzaghi, K., "Theoretical Soil Mechanics," John Wiley & Sons, Inc., New York, 1963, 11th Printing.

16. Sowers, G. B. and Sowers, G. F., "Introductory Soil Mechanics and Foundation," The Macmillan Company, 1961, 2nd Edition.

17. Terzaghi, K., "A Fundamental Fallacy in Earth Pressure Computation," from contribution to Soil Mechanics, 1925-1940, Boston Society of Civil Engineers, pp. 277-294.

18. Bishop, A. W., "Test Requirements for Measuring the Coefficients of Earth Pressure at Rest," Proceedings Brussels Conference on Earth Pressure Problems, Vol. I, 1958, pp. 11-14.

19. Simons, N. E., "Discussion," Proceedings Brussels Conference on Earth Pressure Problems, Vol. III, 1958, pp. 50-53.

20. Elmer, W. O. and Herbert, O. I., "Earth Pressures at Rest Related to Stress History," Canadian Geotechnical Journal, Vol. II, February, 1965, pp. 1-15.

21. Jacky, J., "The Coefficient of Earth Pressure at Rest," Journal of the Society of Hungarian Architects and Engineers, Budapest, 1944, pp. 355-358.

22. Clough, G. W., "An Investigation of the Shear Strength of Sand at High Pressure," Master Science Thesis, Georgia Institute of Technology, 1965.

23. Domaschuk, L., "A Study of the Static Stress-Deformation Characteristics of Sand," Ph.D. Thesis, Georgia Institute of Technology, 1965.

24. Kondner, R. L. and Zelasko, J. S., "A Hyperabolic Stress-Strain Formulation for Sand," Proceedings Second Pan American Conference on Soil Mechanics and Foundation Engineering, Vol. I, 1963, pp. 289-333.

25. Kondner, R. L. and Zelasko, J. S., "Void Ratio Effect on the Hyperabolic Stress-Strain Response of Soil," Special Technical Publication No. 361, ASTM, Symposium on Laboratory Shear Testing of Soils, 1964, pp. 250-257.

26. Wroth, C. P. and Basset, R. E., "A Stress-Strain Relationship for the Shearing Behavior of a Sand," Geotechnique, Vol. XV, No. 1, 1965, pp. 32-56.

27. Duffy, J. and Mindlin, R. D., "Stress-Strain Relation of Granular Media," Transactions, ASME Journal of Applied Mechanics, Vol. 24, 1957, p. 585.

28. Sowers, G. F., "Modulus of Elasticity of Sand," Unpublished data.

29. Timoshinko, S. and Goodier, J. N., "Theory of Elasticity," McGraw-Hill Company, Inc., New York, 1951, p. 366.

30. De Merchant, D. P., "An Investigation of the Shear Strength of Sand in Triaxial Extension," Master Science Thesis, Georgia Institute of Technology, 1967.

31. Taylor, D. W., "Fundamentals of Soil Mechanics," John Wiley & Sons, Inc., 1948, pp. 346 and 373.

32. Bishop, A. W., Correspondence on "Shear Characteristics of a Saturated Silt, Measured in Triaxial Compression," by Penman, A. M., Geotechnique, Vol. 4, 1954, pp. 43-45.

33. Poorooshasb, H. B. and Roscoe, K. H., "The Correlation of the Result of Shear Tests with Varying Degree of Dilatation," Fifth International Conference of Soil Mechanics and Foundation, Vol. I, 1961, pp. 297-300.

34. De Wet, J. A., "The Use of the Energy Concept in Soils Mechanics," Fifth International Conference of Soil Mechanics and Foundation, Vol. I, 1961, pp. 403-405.

35. Bridgman, P. W., "Physics of High Pressure," The Macmillan Company, New York, 1931, p. 1931.

36. Rowe, P. W., "Stress, Dialatancy, Earth Pressure and Slopes," Journal Soil Mechanics and Foundation A.S.C.E., Vol. 89, No. SM3, pp. 37-42.

37. Vesic, A. B. and Barksdale, R. D., "Discussion Test Methods and New Equipment," Special Technical Publication No. 361, American Society for Testing and Materials, Symposium on the Laboratory Shear Testing of Soils, 1963, pp. 301-305.

38. Hirschfeld, R. C. and Poulos, S. J., "High-Pressure Triaxial Tests on a Compacted Sand and an Undisturbed Silt," Special Technical Publication No. 361, American Society for Testing and Materials, Symposium on the Laboratory Shear Testing of Soils, 1963, pp. 329-338.

39. Hall, E. B. and Gordon, B. B., "Triaxial Testing with Large-Scale High Pressure Equipment," Special Technical Publication No. 361, American Society for Testing and Materials, Symposium on the Laboratory Shear Testing of Soils, 1963, pp. 315-328.

VITA

Mosaid Al-Hussaini was born January 31, 1937 in Mosul, Iraq. He graduated from Adadeah High School in 1954. In the same year he entered Baghdad University and in 1958 received a Bachelor of Civil Engineering degree. After a short period of practice he entered the Reserve Officer College, Iraq Army, Corps of Engineers and served with it until September, 1959. In October, 1959 he left the Army and joined the Department of Housing and Development in the capacity of an assistant to the resident engineer. After serving two years he left for the United States to enroll at the Virginia Polytechnic Institute, Blacksburg, Virginia, to pursue graduate study. In 1963 he received a Master of Science degree in Structural Engineering. Following graduation he left the school to work with the State Board Commission of Maryland at the Bureau of Bridges. Six months later he entered the Georgia Institute of Technology in pursuit of a Doctor of Philosophy degree. At the present time he is working in the Soils Division of the U. S. Army Engineer Waterways Experiment Station in Vicksburg, Mississippi.